# Investigation of the Piezoelectric Functionalization Potential of Aeronautical Composite Parts

Rogers Kipkoech Langat

▶ **To cite this version:**

Rogers Kipkoech Langat. Investigation of the Piezoelectric Functionalization Potential of Aeronautical Composite Parts. Embedded Systems. Université de Toulouse, 2024. English. NNT : 2024TLSEP097 . tel-04801784

**HAL Id: tel-04801784**

**https://theses.hal.science/tel-04801784v1**

Submitted on 25 Nov 2024

**HAL** is a multi-disciplinary open access archive for the deposit and dissemination of scientific research documents, whether they are published or not. The documents may come from teaching and research institutions in France or abroad, or from public or private research centers.

L'archive ouverte pluridisciplinaire **HAL**, est destinée au dépôt et à la diffusion de documents scientifiques de niveau recherche, publiés ou non, émanant des établissements d'enseignement et de recherche français ou étrangers, des laboratoires publics ou privés.

RÉPUBLIQUE FRANÇAISE
*Liberté Égalité Fraternité*

Université de Toulouse

# Doctorat de l'Université de Toulouse

**préparé à Toulouse INP**

## Investigation du potentiel de Fonctionnalisation Piézoélectrique de pièces Aéronautiques Composites

Thèse présentée et soutenue, le 14 octobre 2024 par

**Rogers Kipkoech LANGAT**

**École doctorale**
AA - Aéronautique, Astronautique

**Spécialité**
Systèmes embarqués

**Unité de recherche**
LGP - Laboratoire Génie de Production

**Thèse dirigée par**
Micky RAKOTONDRABE et Arthur CANTAREL

**Composition du jury**
M. Franck RUFFIER, Président, CNRS Côte d'Azur
Mme Viviane PASQUI, Rapporteuse, Sorbonne Université Paris
M. Morvan OUISSE, Rapporteur, SUPMICROTECH-ENSMM
M. Micky RAKOTONDRABE, Directeur de thèse, UTTOP
M. Arthur CANTAREL, Co-directeur de thèse, UTTOP

**Membres invités**
M. Mohammad AL JANAIDEH, Guelph University Toronto Canada
M. Emmanuel DE LUYCKER, UTTOP

*Everything is theoretically impossible, until it is done.*

*ROBERT A. HEINLEIN*

# Acknowledgment

I am deeply grateful to my supervisors, Prof. Micky Rakotondrabe, Dr. Arthur Cantarel, and Dr. Emmanuel De Luycker, for their invaluable guidance and support throughout this journey. Their expertise and encouragement have been instrumental in the completion of this thesis. The three-year journey would not have been as fulfilling without their dedication, patience, and flexibility in teaching me how to conduct scientific and engineering research with autonomy. Thank you for your insightful comments, suggestions, and motivation that kept me going. Your mentorship has instilled in me lifelong skills, for which I am deeply grateful.

I extend my heartfelt thanks to my thesis reviewers, Prof. Marvan Ouisse and Dr. Viviane Pasqui, for accepting to review my thesis. Your insightful remarks and relevant questions have been immensely helpful in making me view my thesis from a different perspective. I am grateful for the time you took to carefully review my work. A special mention goes to Prof. Franck Ruffier, the president of the jury. The defense was well coordinated, thanks to your professionalism and expertise. I would also like to thank Prof. Mohammad Al Janaideh for honoring the invitation and participating in the thesis defense with great questions and encouraging remarks. To the entire jury, your support and extensive expertise across multidisciplinary fields made the defense an engaging and enriching experience. Your insights have inspired me and fostered a deep sense of curiosity. I am sincerely grateful for your valuable contributions, which have significantly helped in improving my final manuscript.

I also extend my sincere gratitude to École Doctorale Aéronautique et Astronautique (EDAA) and Campus France at the French Embassy in Nairobi for providing me with the scholarship funding that made this research possible. Your financial support was crucial in enabling me to pursue my thesis. My special appreciation goes to the University of Technology of Tarbes Occitanie Pyrénées for hosting me within its research units at LGP and ICA laboratories. My memory of the staff at these two laboratories will forever be inscribed in my heart for their kindness and support at all times. You became my family and made me feel at home while living in Tarbes. I also wish to acknowledge my colleagues both within and beyond the lab. Your collaboration, friendship, and intellectual exchanges enriched my research experience in countless ways. Every moment spent together, both inside and outside the lab, was invaluable, and I will miss it greatly. I wish you all continued success!

My profound gratitude goes to my family for their unwavering support and understanding during these three years. Your love and encouragement have been my greatest source of strength. I particularly wish to thank and dedicate this thesis to my lovely parents, Mr. Anthony Kilel and Mrs. Ruth Kilel, as well as my loving fiancé Karen and my wonderful siblings, Albert, Kevin, Ronald, and Mercy.

Lastly, I thank God for granting me the grace and perseverance to see this journey through. Your guidance and blessings have been my constant companions.

To everyone who has contributed to this thesis, I extend my deepest gratitude. Thank you.

# Résumé

Cette thèse porte sur l'intégration de matériaux piézoélectriques dans des structures composites renforcées de fibres longues afin de développer des composites intelligents dotés de fonctionnalités avancées pour des applications aéronautiques et spatiales. La recherche vise à améliorer la surveillance de l'intégrité structurelle (SHM) et les capacités de récupération d'énergie grâce aux propriétés des matériaux piézoélectriques pour la détection, l'actionnement et la récupération d'énergie. L'étude couvre de manière exhaustive la sélection des matériaux, les processus de fabrication, la caractérisation expérimentale de ces composites multifonctionnels et l'exploration de leurs applications potentielles. La motivation provient de la transition de l'industrie aéronautique vers des matériaux composites tels que les polymères renforcés de fibres de carbone (PRFC) pour leurs propriétés mécaniques spécifiques supérieures et leur rentabilité. Malgré ces avantages, les composites sont susceptibles d'être endommagés par des défauts de fabrication et des conditions d'exploitation ou de service, ce qui nécessite des techniques de surveillance innovantes. L'introduction de méthodes de contrôle non destructif (CND) a amélioré la détection des défauts, mais ces techniques ont des limites, ce qui incite à explorer des stratégies SHM. Cette thèse contribue au domaine en développant en validant des structures composites intelligentes incorporant du fluorure de polyvinylidène (PVDF) comme matériau piézoélectrique. La recherche démontre l'intégration réussie du PVDF avec un impact minimal sur l'intégrité mécanique des structures composites. La plage d'utilisation de ces composites intelligents avec des performances thermoélectromécaniques stables, ce qui est crucial pour les applications pratiques en SHM et en récupération d'énergie à également été déterminée. Le potentiel des fibres naturelles dans les structures aérospatiales secondaires est également exploré, en soulignant leurs avantages fonctionnels malgré leurs propriétés mécaniques inférieures à celles des fibres de carbone. Les applications avancées de ces composites intelligents sont étudiées, notamment leurs capacités de récupération d'énergie et leurs performances SHM dans des conditions de charge dynamique. Des analyses empiriques et numériques confirment l'efficacité des capteurs PVDF intégrés dans la détection des anomalies structurelles, offrant ainsi une solution potentielle durable pour les systèmes SHM autonomes. Une étude de cas utilisant des techniques d'apprentissage automatique pour la détection et l'identification des défauts démontre en outre le potentiel de ces composites intelligents dans l'amélioration de la fiabilité et de la performance des systèmes SHM via une approche de détection in situ. Par conséquent, cette thèse établit une base solide pour le développement de composites intelligents avec des capteurs piézoélectriques intégrés, mettant en évidence leur potentiel de transformation pour améliorer la sécurité, l'efficacité et la durabilité des aérostructures modernes. Les résultats ouvrent la voie à de futures recherches sur l'optimisation des dimensions et du positionnement des éléments actifs, l'évaluation de la durabilité à long terme et l'amélioration des systèmes SHM grâce à des réseaux de capteurs distribués et à des capacités de transmission de données sans fil.

# Abstract

This thesis investigates integrating piezoelectric materials into long fiber-reinforced composite structures to develop smart composites with advanced functionalities for aeronautics and space applications. The research aims to enhance structural health monitoring (SHM) and energy harvesting capabilities through piezoelectric materials' direct and inverse properties for sensing, actuation, and energy recovery. The study comprehensively covers material selection, manufacturing processes, the experimental characterization of these multifunctional composites, and the exploration of their potential applications. The motivation stems from the aviation industry's transition to composite materials like carbon fiber reinforced polymers (CFRP) for their superior mechanical properties and cost effectiveness. Despite these advantages, composites are prone to damage from fabrication flaws and operation/service conditions, necessitating innovative monitoring techniques. Introducing non-destructive testing (NDT) methods have improved defect detection, but these techniques have limitations, prompting exploring SHM strategies. The thesis contributes to the field by developing and validating smart composite structures incorporating polyvinylidene fluoride (PVDF) as the piezoelectric material. The research demonstrates the successful integration of PVDF with minimal impact on the mechanical integrity of the composites. The usage range of these smart composites with stable thermoelectromechanical performance, which is crucial for practical applications in SHM and energy harvesting, was also determined. The potential for natural fibers in secondary aerospace structures is also explored, emphasizing their functional benefits despite their lower mechanical properties compared to carbon fibers. Advanced applications of these smart composites are investigated, including their energy harvesting capabilities and SHM performance under dynamic loading conditions. Empirical and numerical analyses confirm the effectiveness of embedded PVDF sensors in detecting structural anomalies, offering a sustainable potential solution for autonomous SHM systems. A case study employing machine learning techniques for fault detection and identification further demonstrates the potential of smart composites in enhancing the reliability and performance of SHM systems via an in-situ sensing approach. Therefore, this thesis establishes a robust foundation for developing smart composites with embedded piezoelectric sensors, highlighting their transformative potential in improving modern aerostructure safety, efficiency, and sustainability. The findings pave the way for future research into optimizing the dimensions and positioning of active embeds, assessing long-term durability, and advancing SHM systems through distributed sensor networks and wireless data streaming capabilities.

# Contents

# List of Figures

# List of Tables

# Chapter 1

# Introduction

## Contents



## 1.1 Context

This thesis is framed within the context of long fiber-reinforced composite parts, which are extensively used in aeronautics and are being developed for space applications. The study begins by investigating various types of fibers used in composite structures, composite production techniques, and several piezoelectric active materials to determine which are best suited for the

intended applications. The goal is to establish how these composite structures could be functionalized by integrating piezoelectric active materials. Due to their direct and inverse piezoelectric properties, these active materials can perform sensing, actuation, and energy recovery. Therefore, the main emphasis of this study is on the development and research of structures combining both composite and piezoelectric materials.

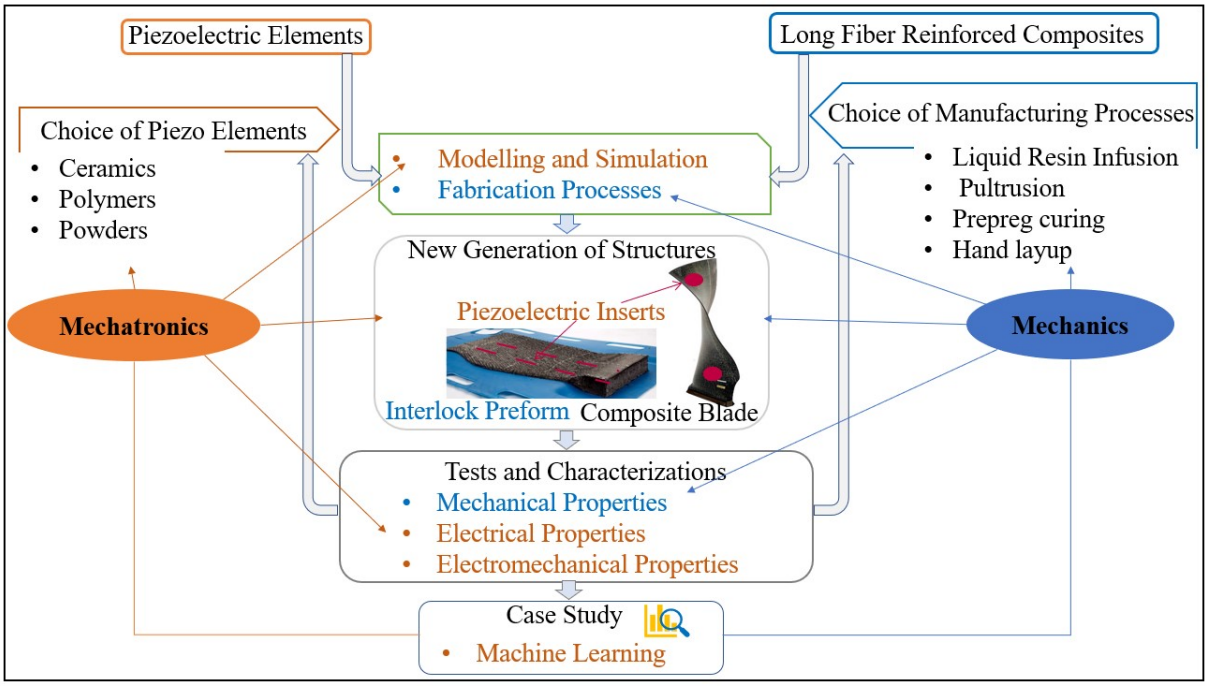


Figure 1.1: Research Architecture.

Figure 1.1 illustrates the research architecture, summarizing the steps and multidisciplinary nature of the thesis. It outlines the selection of materials and manufacturing processes, the integration of piezoelectric inserts into composite structures, and the subsequent testing and characterization of these new structures. This comprehensive approach highlights the intersection of mechatronics and mechanics in achieving structural functionalities such as sensing, actuation, and energy harvesting.

## 1.2 Motivation

### 1.2.1 Smart Materials

The emergence of smart materials has revolutionized modern engineering by enabling the development of smart structures capable of sensing, actuating, and energy harvesting. Defined as materials capable of receiving, transmitting, or processing stimuli to yield advantageous outcomes [1, 2], these smart materials are invaluable in diagnosing material damage by altering their properties in response to such stimuli [3]. Often referred to as intelligent or active materials, they can be integrated into structures or bonded to surfaces, providing not only structural functionality but also logic control, signal conditioning, and power amplification for electronic signals [3]. An exemplary illustration of such materials is found in piezoelectric materials, which generate an internal electric field when subjected to mechanical stress or strain and, conversely, undergo mechanical deformation when an electric field is applied. This unique capability allows for the integration of measurement [4, 5], actuation [6, 7], and energy harvesting functionalities [8, 9, 10, 11, 12], into a single material, significantly enhancing the efficiency and functionality of modern engineering applications.

The development and application of smart materials have revolutionized various fields, from aerospace and civil engineering to biomedical devices and robotics. The ability of smart materials to accurately sense and respond to environmental changes enables the creation of advanced systems with unprecedented levels of precision and adaptability. For example, piezoelectric materials have been extensively used for high-resolution sensors and actuators [13], providing precise control and real-time monitoring capabilities. Furthermore, the versatility of smart materials offers a wide range of design solutions to meet diverse performance requirements and operating conditions [14], making them indispensable in the pursuit of innovative and sustainable technological advancements. Indeed, to gain a competitive edge in the twenty-first century, the fabrication of smart structures has become a pivotal endeavor. These materials are continually explored to achieve damage diagnosis in aerostructures. With the combination of these promising benefits, incorporating them into aerostructures could lead to improved structural health management and the establishment of energy-efficient structural systems.

### 1.2.2 Composite Structures in Aeronautics

Over the years, the aviation industry has experienced a significant shift from traditional materials to composite materials in various engineering and structural applications [3, 15, 16]. A prime example of this transformation is the Airbus A350, where 53% of the components are made from carbon fiber reinforced polymers (CFRP), as illustrated in Figure 1.2 [17]. This transition is primarily driven by the superior mechanical properties of composites, including high tensile strength, low density, and exceptional structural durability [18, 19]. These attributes create lighter and more robust aircraft components, enhancing fuel efficiency and reducing operational costs [20]. Additionally, composites exhibit remarkable resistance to environmental factors such as corrosion, UV radiation, and chemical exposure, ensuring longer life spans and reduced maintenance needs [21]. The cost-effectiveness of composites, bolstered by advancements in manufacturing technologies, makes them an economically viable option, improving performance, efficiency, and safety in modern aircraft design and manufacture.

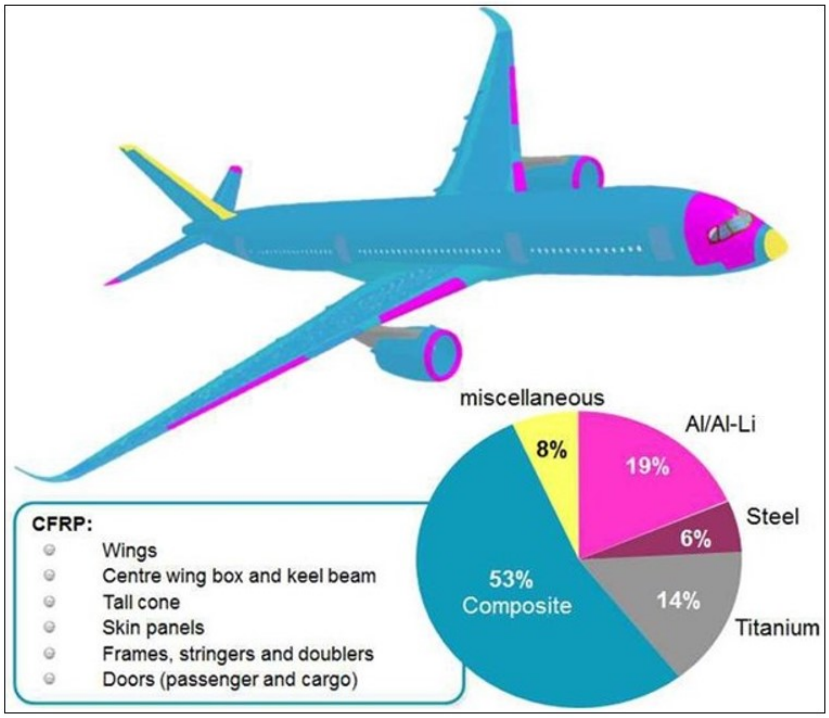


Figure 1.2: Illustration of the materials used in the design and manufacture of modern aircraft, specifically highlighting the extensive use of composite materials [17].

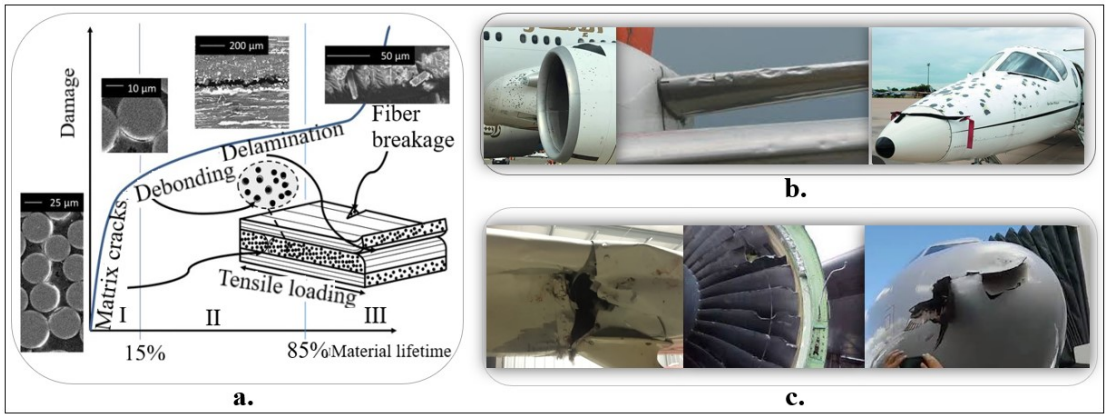


Figure 1.3: Illustration of common defect types experienced in the aviation industry, depicting: **a.)** the evolution of damages sustained from fabrication and minor impacts over the material lifetime [22], **b.)** defect types resulting from hailstone hits, and **c.)** effects of bird strikes.

Despite their advantages, composite materials have significant drawbacks due to their susceptibility to various types of damage from fabrication flaws and service conditions [23]. Typical defects from the fabrication process, such as microcracks and voids, create stress concentration regions that lead to delamination and debonding under continuous loading as depicted in Figure 1.3a. If not monitored, these failures can cause catastrophic damage to critical load-bearing structures, leading to losses and accidents [24]. Additionally, composite materials are vulnerable to environmental conditions, particularly moisture content and temperature variations, affecting their mechanical performance. Their low damping ratio, inability to yield, and difficulties in refurbishment further limit their application. Certainly, the operational environment subjects aircraft to various types of structural damage. Lightning strikes, for instance, can cause hole-like damage and surface scorch marks [25], while hailstone impacts contribute to punctures, dents, and sometimes penetrative scratches presented in Figure 1.3b. Bird strikes [26] can severely damage engine fan blades or the plane's radome and other vital parts of the plane structure as illustrated in 1.3c. Additionally, debris encountered during takeoff can create scratches, potentially initiating delamination and ply separation if not detected early. Consequently, it is crucial to thoroughly characterize and monitor the behavior of composite materials under operational conditions, particularly in extreme loading scenarios and adverse environmental factors like thermal degradation. Managing damage from fabrication ensures it remains within allowable limits, while early detection of operational damage enables timely repairs, preventing

catastrophic failures.


Figure 1.4: Illustration of NDT techniques currently applied in damage diagnosis of aerostructures, adapted from www.makepartsfast.com and www.gom.com.

In recent years, innovative methods for monitoring and detecting failures have emerged through non-destructive testing (NDT) techniques [22]. Figure 1.4 illustrates various NDT technologies, including but not limited to ultrasonic testing (Figure 1.4a), eddy current array tests (Figure 1.4b), ATOS compact scan for surface damage inspection (Figure 1.4c), and infrared thermography (Figure 1.4d). These techniques enhance routine maintenance by providing detailed structural insights, facilitating the optimization of maintenance schedules, and significantly improving the safety and efficiency of aeronautic maintenance practices [22]. However, these benefits come with challenges: high initial costs for equipment and training, the need for specialized personnel, increased inspection times, and the potential for human error in interpreting results. Despite advancements in development and optimization for accurate defect detection, NDT techniques still rely heavily on human intervention. This reliance leads to high labor costs, as devices must access structural parts using external equipment [3].

Furthermore, they are limited to scheduled-based maintenance, which means defects might be identified after they have evolved to a severe stage, potentially impacting other structural parts due to non-uniform stress distribution. Therefore, it is crucial to explore other methods to enhance condition-based maintenance.

Therefore, a significant paradigm shift in the aerospace sector will result from the "structural health monitoring" (SHM) strategy, referring to a new technology that utilizes embedded sensors inside the structure to continuously and autonomously monitor the physical status of a structure with as little operator intervention as possible [27].

This strategy is realized based on the smart-material-based structural systems employing sensor technology with an integrated intelligent algorithm to assist in the collection and analysis of data on the health status of structures, thereby improving life-cycle management [28]. Moreover, the critical need for smart system deployment in the aeronautical sector necessitates the development of active composite structures. Indeed, the development of these smart structures is made possible by the high-quality features of active piezoelectric materials: their ease of integration/co-fabrication with fiber-reinforced composite structures and their capacity to be used as sensors, actuators and as energy harvesters [29, 30, 31]. The combination of smart materials, specifically piezoelectric ones, with algorithms aims to leverage the unique strengths of both tools for enhanced performance in SHM. Additionally, the technologies and processes used to produce these active materials with integrated functionalities continue to gain interest among researchers and industrial players [32, 33, 34, 35, 36]. Thanks to the existence of thin film piezoelectric materials, integration is facilitated with minimal mechanical impacts on the structure, all while boasting enhanced sensing capabilities. It is evident that composite structures with embedded sensors enable real-time monitoring, which can be used to collect useful information about the functionality and structural integrity of the composite parts during service [35, 37].

Furthermore, embedded sensors allow for the monitoring of some critical and inaccessible structural parts, as well as the identification and monitoring of barely visible impact damages (BVID) in composite structures [24]. Certainly, the SHM strategy is desirable in the aeronautics industry because vital information about the health of plane structures can be established before the development of critical damages, leading to the avoidance of accidents [38, 39]. SHM technology provides numerous benefits, such as increased security as a result of updates on the state

of critical structures, the enhancement of condition-based maintenance (normally, the schedule maintenance technique would be applied when using the conventional NDTs, which necessitates that the plane is grounded to run scheduled maintenance checks) and thus a reduction in delays in airplane maintenance, and the lowering of repair costs, which contributes to low life-cycle costs [40, 41, 42]. Nonetheless, commercial full-scale SHM systems are still being investigated [43], with the researchers' main concern being the limited battery lifespan required to power these sensors, which impedes monitoring autonomy. Additionally, since these sensors are primarily intended for use inside structures, replacing their batteries could be difficult. Thus, the integration and use of active piezoelectric materials, which are essentially transducing elements, is foreseen to eliminate the need for external powering systems, resulting in the implementation of the desired monitoring autonomy.

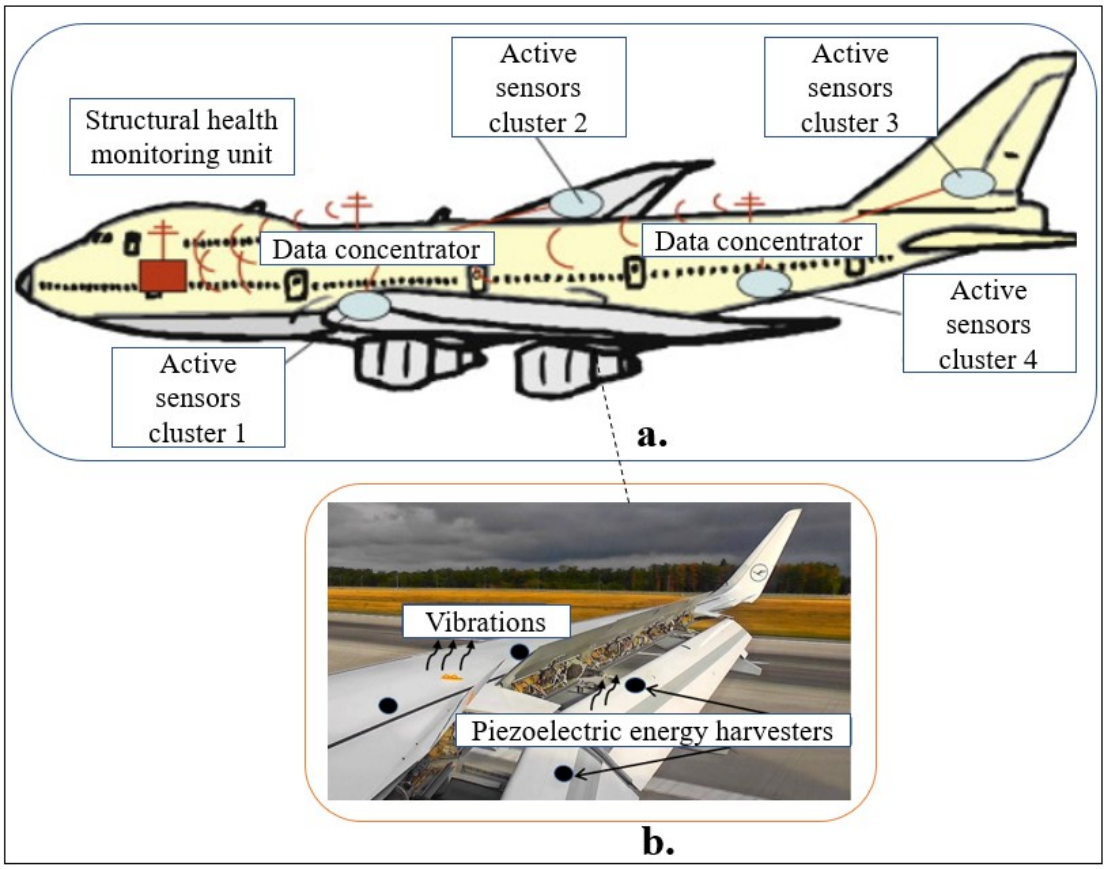


Figure 1.5: Illustration of structural health monitoring with integrated active sensor nodes [44] and energy harvesting through wing vibrations.

Figure 1.5 illustrates the feasibility of these solutions, depicting Figure 1.5a, which shows distributed sensor nodes that can channel real-time data on the health state of the structure, and Figure 1.5b, which presents the possibility of leveraging ambient vibrations to harness energy from integrated piezo elements for powering SHM sensor nodes.

## 1.3 Contribution

This exploratory thesis aimed to investigate the development of smart composite structures by leveraging the integration technology to fully embed piezoelectric materials within the classical fiber-reinforced composite materials without compromising their mechanical integrity. The primary contributions of this research are as follows:

- Material selection for functionalized fiber-reinforced composites, presented at the 23rd International Conference on Composite Materials (ICCM23). This work is presented in Chapter 2.

- Development and characterization of advanced composite structures. This study was published in the journal *Mechanics of Advanced Materials and Structures* by Taylor and Francis and is extensively discussed in Chapter 3.

- Exploration of the thermo-electromechanical characteristics of the developed smart composite materials. This work was presented at the 21st European Conference on Composite Materials (ECCM21) and is addressed within the composite characterization topics in Chapter 3.

- Exploration of harnessing energy from smart composite structures to power SHM sensor nodes for autonomous monitoring of aerostructures' health status. This work, presented at the SAGIP Congress in Marseille 2023, is developed in Chapter 4.

- Investigation of prospective applications in SHM technology, with several techniques and findings published in the *Micromachines* Journal of MDPI. This work, which delves into the potential applications of the proposed structures, is developed in Chapter 4.

- Implementation of simplified machine learning models for damage detection and recognition in aeronautic composite structures, featuring common defects found in aircraft structures during service. This work, discussed in Chapter 5, was submitted to the *IFAC Mechatronics Journal*.

In summary, this research has significantly contributed to the field of smart composite structures through multiple publications and presentations.
The key publications disseminating these findings are:

1. Langat, Rogers K., Emmanuel De Luycker, Arthur Cantarel and Micky Rakotondrabe, *"Material Selection for Functionalized Fiber-reinforced Composite Structures"*, ICCM, (International Conference on Composite Materials), Belfast Ireland, July-August 2023.

2. Langat, Rogers K., Emmanuel De Luycker, Arthur Cantarel, and Micky Rakotondrabe. *"Toward the development of a new smart composite structure based on piezoelectric polymer and flax fiber materials: Manufacturing and experimental characterization."* Mechanics of Advanced Materials and Structures (2023): 1-15.

3. Langat, Rogers K., Emmanuel De Luycker, Arthur Cantarel, and Micky Rakotondrabe. *"Integration Technology with Thin Films Co-Fabricated in Laminated Composite Structures for Defect Detection and Damage Monitoring."* Micromachines 15, no. 2 (2024): 274.

4. Langat, Rogers K., Emmanuel De Luycker, Arthur Cantarel and Micky Rakotondrabe, *"Characterization of Thermo-Electromechanical Properties in Smart Composite Structures under Dynamic Loading and Temperature Variations"*, ECCM, (European Conference on Composite Materials), Accepted, Nantes France, July 2024.

5. Langat, Rogers K., Emmanuel De Luycker, Arthur Cantarel, and Micky Rakotondrabe. *"Improving Structural Health Monitoring in Aeronautical Composite Materials: Leveraging Embedded Sensor Data for Enhanced Performance and Simplified Machine Learning-Based Fault Detection and Identification"*, Submitted, IFAC Mechatronics Journal.

## 1.4 Thesis Organization

This thesis is structured as follows:

Chapter 1: This introductory chapter provides the context of the thesis, discussing the motivation for using composites in the aeronautic field, the associated challenges, and the urgent necessity for advancements in structural health monitoring. It also outlines the thesis's contributions.

Chapter 2: This chapter introduces the fundamentals of fiber-reinforced composite materials, including fabrication techniques, applications, and challenges. It also details piezoelectricity, its historical background, material types, the piezoelectric phenomenon, constitutive equations, and applications. Additionally, it highlights the integration technology for co-fabricating active piezo materials with fiber composites, including the material selection process and relevant considerations.

Chapter 3: This chapter outlines the fabrication steps and considerations involved in creating a smart composite material. It details the assessment of the inserts' impact on the composite structure's mechanical integrity through mechanical characterizations, including X-ray tomography and interlaminar shear strength (ILSS) tests. Additionally, it presents the electromechanical characterization of the developed smart composite materials under dynamic loading and thermal variations to ascertain the sensor's behavior under varying environmental conditions.

Chapter 4: This chapter explores the potential applications of our smart composites. It provides an overview of their energy recovery capabilities and delves into the sensing potential of these functionalized structures. The chapter highlights two significant integrated sensing approaches: passive and active. It proposes damage index and correlation equations through manual feature extraction techniques for structural health monitoring. Additionally, numerical analysis is presented to validate the proposed active sensing approach.

Chapter 5: This chapter details the use of machine learning models for defect detection and damage type recognition in composite structures. It presents an exciting implementation of a simple machine-learning model facilitated by the high-quality data

collected through in-situ sensing via fully embedded sensors. The chapter highlights the potential of combining smart composite structures with intelligent algorithms for real-time monitoring and structural health management, enhancing the safety and reliability of aeronautic composite structures.

Chapter 6: This chapter presents the general conclusion of the thesis and provides detailed future work and perspectives based on our analysis and findings.

# Chapter 2

# Background and Selection: Fiber Reinforced Composites and Piezoelectricity

---

## Contents

## 2.1 Introduction

In the previous chapter, the context and motivation of the study were presented, emphasizing the aim to functionalize classical aeronautical structures by integrating active piezoelectric materials. This chapter delves into the background of fiber-reinforced composites, covering their materials, fabrication techniques, and limitations. It also explores the concept of piezoelectricity, covering its historical background, the piezoelectric phenomenon, constitutive equations, and general applications. Furthermore, the integration technology for embedding piezo materials to create smart composites with enhanced functionality is discussed. The selection criteria for constituent materials in developing these smart composite structures are also detailed in this chapter.

## 2.2 Fiber Reinforced Composites

A composite material is formed by combining two or more non miscible materials in a controlled environment to produce new materials with superior properties that cannot be achieved using the independent constituent materials [45, 46]. Miracle *et al.*, [45] refers to composite materials as those that contain a continuous matrix constituent that binds together and provides a form to an array of a stronger, stiffer reinforcement constituent, noting that the resulting material has a balance of structural properties superior to either of the constituent materials when used independently. This is similar to what Meyer *et al.* [47] noted in their review, referring to composite materials as materials consisting of strong fibers incorporated in a weaker material, generally referred to as a matrix element [48].

The resulting materials possess unique specific properties, making them preferable over conventional materials due to the enhanced characteristics of their base components, which enable their application across various industrial sectors. For instance, the demand for lightweight materials that do not compromise on strength and stiffness for structural applications in the transport industry has significantly driven research and development in composites. This benefit has motivated the use of composite materials in structural parts where high performance is essential at minimized weights, thereby meeting the growing demand for stiff and light materials in aeronautics, space, and sporting applications [47, 49]. Other advantages of composite materials include resistance to fatigue and corrosion, thermal and chemical resistance, electrical insulation properties, and the ability to customize the material for optimal performance in specific applications [45, 46, 47].

To explore the mentioned merits of composite materials and meet the requirements needed for industrial applications, fiber-reinforced composites such as fiber-reinforced polymers have garnered significant research attention aimed to develop cost-effective and durable advanced composites [50]. These materials typically comprise matrix resins and fibers, which can take various forms, as shown in Figure 2.1 [49]. The orientation of these reinforcement materials during the forming process of composite manufacturing in each lamina, as well as the layup sequence, could be selected to achieve desired properties and to obtain the optimal performance of the finished composite product [34, 46].

Nonetheless, as highlighted in the introductory chapter, these composite materials still have significant drawbacks. Notable issues include susceptibility to ply separations and delamination, higher raw material, fabrication, and assembly costs, and mechanical performance influenced by varying environmental conditions. A low damping ratio prevents effective vibration deadening, and refurbishment is challenging. The combustion fumes from these materials are also toxic [34, 47, 51]. Furthermore, composite materials have poor strength in the out-of-plane direction, where the matrix carries the primary load, making them vulnerable to impact damage [46, 51]. These issues limit their widespread use. However, ongoing research and development efforts funded to address these challenges focus on innovative methods and techniques, such as creating new base materials.

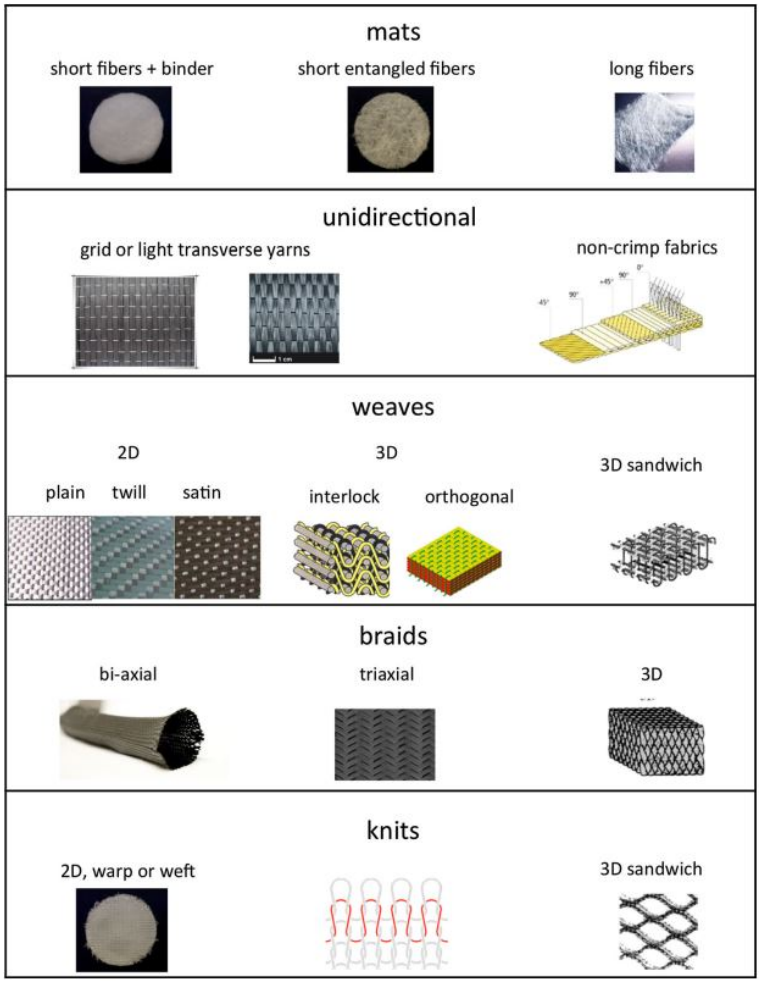


Figure 2.1: Illustration of various fiber forms used as reinforcement materials in composite manufacturing [49].

In the framework of fabrication techniques of fiber-reinforced composite structures, there are two renowned processes; firstly the classical prepreg technologies also referred to as the consolidation process, and secondly the liquid composite molding (LCM) processes [49]. In general, these processes are essential for either impregnating the dry preform by infiltration of liquid matrix or completing the infiltration of the pre-impregnated layups [52]. According to Michaud and Mortensen [53], the consolidation process involves the application of pressure and heat to pre-impregnated resin/fiber assembly to complete infiltration and to squeeze out entrapped air and volatiles released from the polymer during the heating and/or during the chemical reaction stages.

This manufacturing process poses some limiting factors in that it requires high intensive labor and a lot of energy for composite manufacturing which renders it less cost-effective [54]. On the other hand, LCM processes present greater efficiency concerning time and energy utilization in the production of composite products at a cheaper cost [52].

Michaud [49] further highlighted the two forms of LCM, which are the resin transfer molding (RTM) shown in Figure 2.2a and the vacuum-assisted resin transfer molding (VARTM) shown in Figure 2.2b. As presented below, RTM refers to a process with a closed mold, i.e., two-sided rigid mold [52, 55]. The RTM process mold can be patterned to fabricate a complicated shape product. However, it is not suitable for producing large composite structures due to the tooling costs and the difficulties in constructing big closed molds with all the clamping requirements satisfied [34, 55]. In VARTM, the set-up comprises an open mold where the preform is held by a vacuum bag and the resin flow is driven by vacuum [55]. Large parts can be easily fabricated with this type of process since they are made economically feasible due to the reduced tooling costs. It can produce high-quality components [56]. Because of its various advantages, the VARTM process has since been adopted to fabricate industrial and aerospace structures and other large structures such as boat hulls and wind turbines. Compared to other composite manufacturing processes, VARTM produces components with the highest fiber volume fraction desirable to achieve specific mechanical properties for large composite structures in one shot [57]. With the advancement of time, efforts have been made to improve the resin infusion process. As a result, many process variants have been developed to achieve optimal vacuum infusion techniques. In this regard, considerable focus has been given to creating LCM technologies that are more affordable and capable of producing medium to large composite structures [50]. A comprehensive, objective comparison of the standard vacuum-assisted resin infusion processes can be found in the work of Oosterom *et al.*, [56].

In general, all LCM processes, as presented in Figure 2.2, follow a similar sequence: a preform made of dry fibers is placed in a mold, the resin is injected into the mold, and the impregnated fibers are cured for a predetermined amount of time at specific temperatures based on the type of material. After curing, the part is removed from the mold. It is crucial to meticulously control each stage of the fabrication process to ensure that all required parameters and conditions are correctly established [49, 55, 58].

Errors in the fabrication process can lead to defects in the final parts produced through LCM processes, limiting their widespread use. These defects, which can arise at different stages of the fabrication process, are categorized as preform defects, flow-induced defects, and cure defects. The types of defects associated with LCM processes, illustrated in the flowchart in Figure 2.3, are further discussed in the work of Hamidi and Atlan [50].

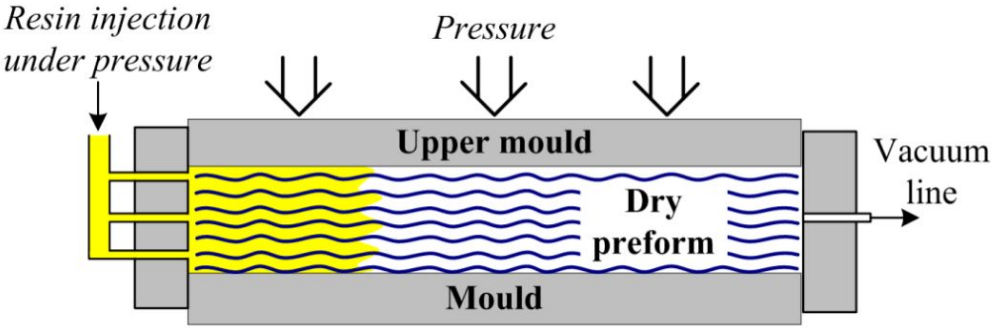


(a) The schematic of the RTM process.

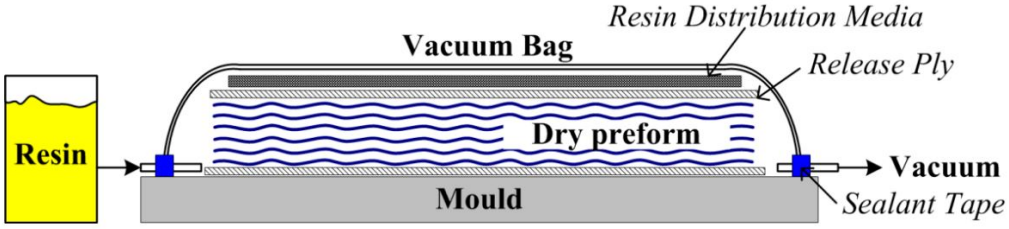


(b) The schematic of the VARTM process.

Figure 2.2: Illustration of liquid composite molding (LCM) forms [52].

The defects compromise the mechanical integrity of composite structures [59]. Preform defects, such as fabric misalignment during the layup stage, typically result in wrinkling due to angle variations between the fibers. Numerous studies are being conducted to establish optimal preform development strategies to address this issue [60, 61]. Flow-induced defects, including dry spots and voids, occur in areas with trapped air or insufficient resin flow. Researchers have proposed various measures to eliminate these flaws. For instance, Qing *et al.* [59] focuses on monitoring the liquid composite molding process using piezo sensors to ensure complete infiltration and reduce flow-induced flaws through effective visualization of the resin flow front

and reaction progression.

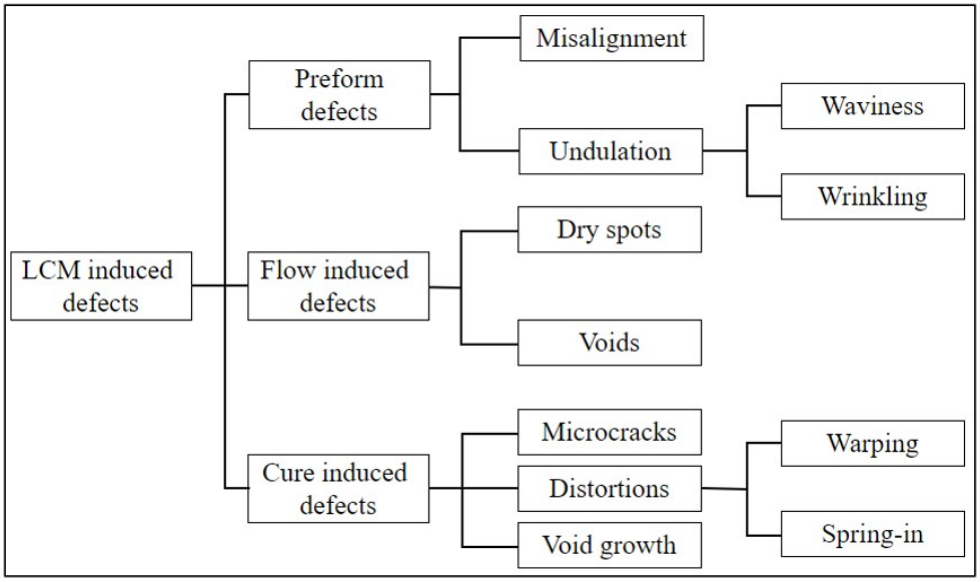


Figure 2.3: Illustration of the process induced defects in LCM [50].

On the other hand, curing process defects, such as micro-cracks and void growth, result from stress concentrations and can be mitigated by controlling curing parameters [50, 59]. Hamidi and Atlan [50] provide a thorough review of LCM-induced defects and the measures taken to produce high-quality structures. Additionally, flaws introduced during the service life of structures, discussed in the previous chapter, are caused by stresses exceeding the maximum allowable stress/strain levels [35]. These imperfections reduce the load-carrying capacity of the structures, often leading to significant structural damage and system failure. In this context, scientists are paying close attention to the development of advanced composite structures in order to attain dependability in terms of physical and mechanical performance. It has also sparked the development of monitoring tools to continuously track the integrity of the structures and foresee the onset of degradation.

In summary, this section introduces fiber-reinforced composite materials, discussing their fabrication techniques, processes, and associated defects. It provides an overview of the challenges faced in composite material fabrication and highlights the necessity of the current focus on developing advanced composite structures to overcome these issues.

## 2.3 Piezoelectricity

### 2.3.1 Definitions and History

Piezoelectricity refers to the ability of certain materials to generate an internal electric field when subjected to mechanical stress or strain. The term "piezo" derives from the Greek word *piezein*, meaning "to press," hence the phenomenon is also known as pressure electricity. This effect can be classified into two categories: the direct piezoelectric effect, which involves the generation of an electric potential difference in some solid materials upon the application of mechanical stress in a suitable direction, and the converse piezoelectric effect, which involves the production of mechanical deformation in the material when an electric field is applied [6, 62, 63].

This phenomenon and the relevant materials that display this effect can be connected to a long history full of occasions that led to the discovery. In 1707, a Dutch man brought tourmaline from the East Indies, a magnificent stone with an observable distinctive feature. When heated, he noticed that the stone attracted other materials, like ashes. Ten years later, in 1717, Louis Lemery observed the same peculiar feature. By 1747, a Swedish botanist and physician, Carl Linnaeus, best known for creating the biological nomenclature, hypothesized that this occurrence might be related to electricity. It was not until 1956 that German physicist Franz Aepinus confirmed the electric nature of the feature. This feature was later named Pyroelectricity; the word *Pyro* comes from a Greek word that means fire. Thus, Pyroelectricity refers to the ability of some materials to generate a temporary voltage when it is being heated or cooled [63].

Finally, understanding the crystal structure responsible for the pyroelectric effect, the Curie brothers, Pierre and Jacques, discovered direct piezoelectricity in 1880 [62]. They found that materials such as quartz, topaz, cane, and tourmaline developed an electric charge proportional to the applied stress under pressure. However, the brothers did not foresee the possibility of the converse effect. Just a year later, in 1881, Gabriel Lippman predicted the converse effect based on the laws of thermodynamics without conducting any tests to support his prediction. This effect was later confirmed experimentally by the Curie brothers [6, 63, 64].

Motivated by events such as the sinking of the Titanic in 1912 due to an iceberg, researchers focused on applying this novel discovery. The onset of World War I in 1914 further intensified the need for ultrasonic sonars to detect German U-boats for the French military. These efforts paid off in 1917 when Paul Langevin successfully transmitted an ultrasonic pulse into the sea, enabling the detection of underwater objects [64].

Today, piezoelectric materials remain a vibrant area of research and innovation. Their high sensitivity, resonant frequency, and remarkable stability make them invaluable for developing precise sensors and actuators. These materials are of great interest and are constantly being investigated for many modern applications, from medical ultrasound imaging and industrial nondestructive testing to innovative energy-harvesting devices and advanced communication systems. Research and technological development efforts have been increasing even further in line with the future needs that piezoelectric materials have to address.

### 2.3.2 Piezoelectric Phenomenon

The piezoelectric effect is closely related to the atomic structure of certain crystal lattices. For a material to exhibit piezoelectricity, it has to be dielectric, meaning it is non-conducting and has to be characterized by an asymmetric crystal structure. The piezoelectric effect occurs due to the specific arrangement of ions within this crystal structure [62]. In an unstressed state, a piezoelectric material remains electrically neutral. This neutrality arises because the positive and negative charges are superimposed and cancel each other out, resulting in zero potential difference. This balance is achieved because the charges are uniformly distributed throughout the structure, maintaining equilibrium across the virtual polar axis [65].

When stress is applied to the material, it disrupts the orientation of the crystal lattice, causing a separation of charges. This separation alters the electric dipole moment, leading to the formation of a surface charge density. Consequently, an electric potential is generated across the material as a direct result of the mechanical stress. Electrodes are used to measure this electric potential, which is proportional to the applied stress. Figure 2.4, which follows, provides a clear illustration of this phenomenon [9, 66]. This also refers to the transversal piezoelectric effect which occurs when mechanical pressure is applied perpendicular to the polar axis $X_1$, as illustrated in Figure 2.5b, causing ions to shift uniformly inward, neutralizing charges on electrodes

B and B′, but displacing the upper silicon and lower oxygen ions outward, generating electric polarization **P** perpendicular to the pressure with reversed charge signs on electrodes A and A′ [67]. In contrast, same apparition of charge occurs when the deformation is applied longitudinally which yields axial piezoelectric effect. This is also referred to longitudinal piezoelectric effect which occurs when mechanical pressure is applied along the polar axis $X_1$ as presented in Figure 2.5a, causing the upper silicon ion to shift between the two upper oxygen ions and the lower oxygen ion to shift between the two lower silicon ions. This ion displacement generates electric polarization **P** along the polar axis $X_1$, aligning with the pressure direction. As a result, positive charges accumulate on the upper electrode A and negative charges on the lower electrode A′, producing an external electric polarization voltage [67].

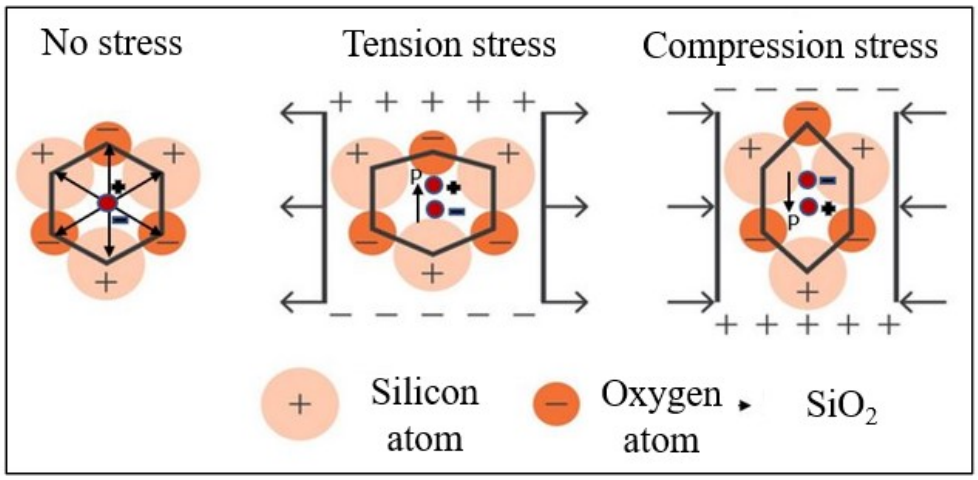


Figure 2.4: Illustration of the piezoelectric effect of a Quartz crystal. Adapted from www.circuitbread.com.

Additionally, this effect depends on the crystal symmetry, the orientation of polarization within the structure, and the strength of the applied stress. There are two configurations regarding crystal symmetry: monocrystalline and polycrystalline structures, as shown in Figure 2.6. In a monocrystalline structure, all of the charge carriers' polar axes point in the same direction, and this orientation is maintained throughout the crystal. This type of crystal is symmetrical because the polar axis would still point in the same direction even if the crystal were split into two halves. On the other hand, a polycrystalline structure is characterized by the presence of polar axes in various regions along the material structure. This structure is

asymmetrical compared to monocrystalline structures because its overall polar axis does not exhibit a consistent pattern upon fragmentation [9, 63, 66].

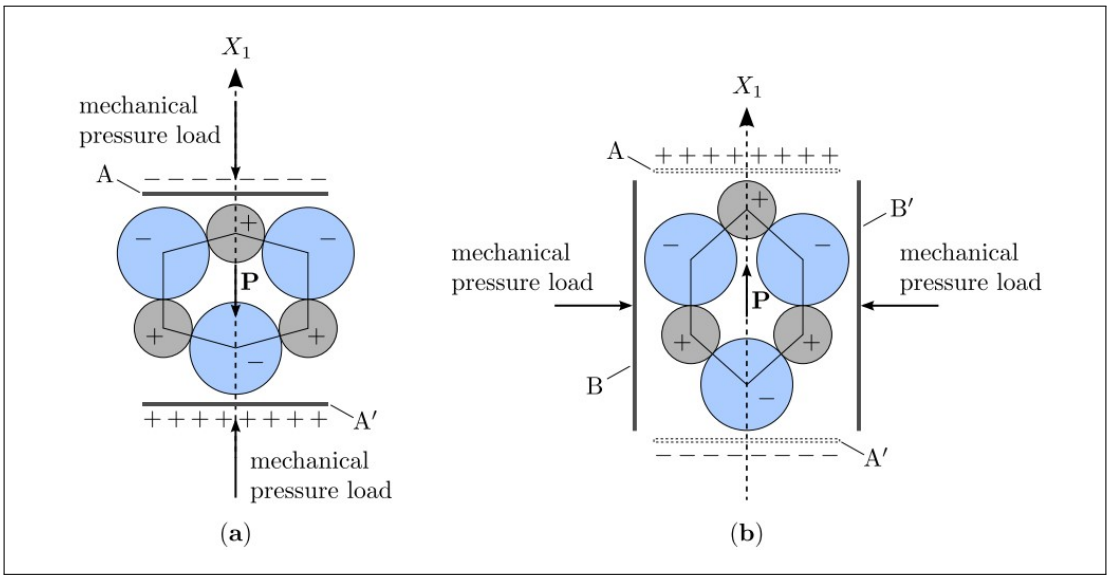


Figure 2.5: Illustration of direct piezoelectric effect. (a) longitudinal piezoelectric effect; (b) transversal piezoelectric effect [67].

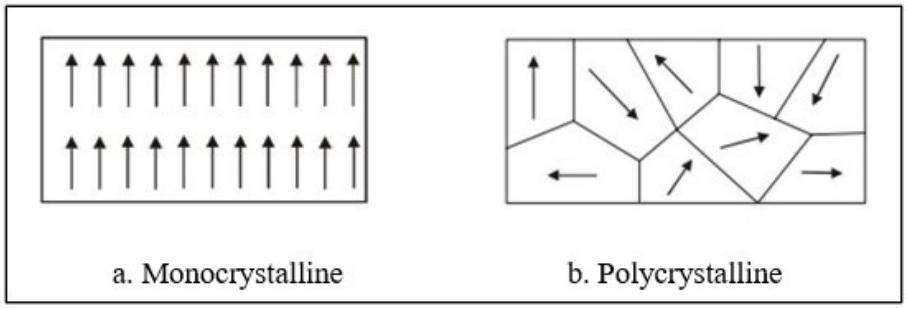


Figure 2.6: Illustration of crystal symmetry: monocrystalline (symmetric) and polycrystalline (asymmetric). Adapted from www.aurelienr.com.

In fact, the orientation of polarization within the crystal plays a vital role in determining whether a material is piezoelectric. In a polycrystalline material structure, for example, the dipoles tend to align in regions called *Weiss domains* (groups of dipoles with parallel orientation), as illustrated in Figure 2.7. These domains are randomly oriented within the crystal, resulting in no net polarization and lack piezoelectric effect. The orientation and alignment of the dipoles

in these domains are essential for enabling a material to exhibit piezoelectric properties. This alignment is achieved through a process called *poling*. Poling involves applying a strong electric field at a high temperature, slightly below the Curie temperature (the temperature above which the material loses its piezoelectric/ferroelectric properties) of the material [9, 66, 68].

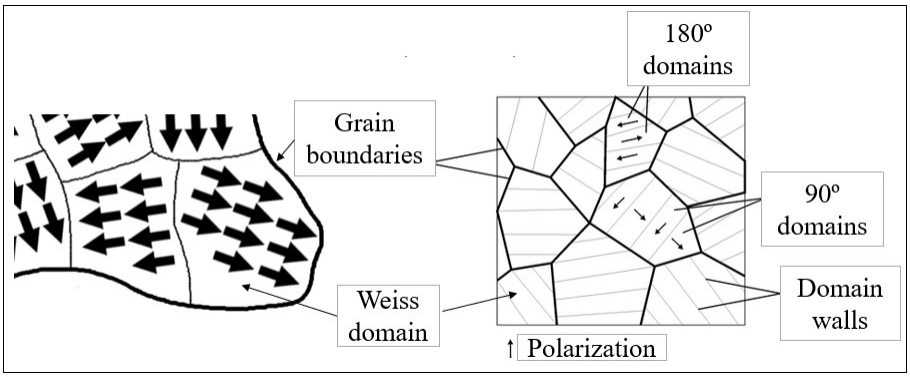


Figure 2.7: Illustration of the grain configuration, subdivided into Weiss domains.

Since the treatment is carried out at high temperatures, the material's molecules can align freely and easily. Consequently, the dipoles align in the direction of the imposed electric field. The electric field is maintained throughout the cooling phase of the poling process to ensure these dipoles do not revert to their original positions. This sustained configuration allows the material to exhibit a piezoelectric effect due to the induced polarization. When the electric field is eventually withdrawn, most dipoles remain aligned in the same direction, though some may revert to their original orientation. Figure 2.8 provides a clear illustration of this process [9, 66, 68].

As shown in Figure 2.9 below, two primary approaches are used in this poling process: contact poling and corona discharge poling. Corona discharge poling polarizes the piezoelectric material by utilizing argon or dry air breakdown. This method exposes a sharp, conductive needle to a high voltage, which ionizes the gas molecules, creating a corona discharge. A metallic grid, positioned just below the needle and operating at a lower voltage of 0.2–3 kV [69], controls the ionized particles as they accelerate toward the piezoelectric material. The applied voltage and the grid's position regulate the electric field, determining the quantity of charge deposited on the material's surface.

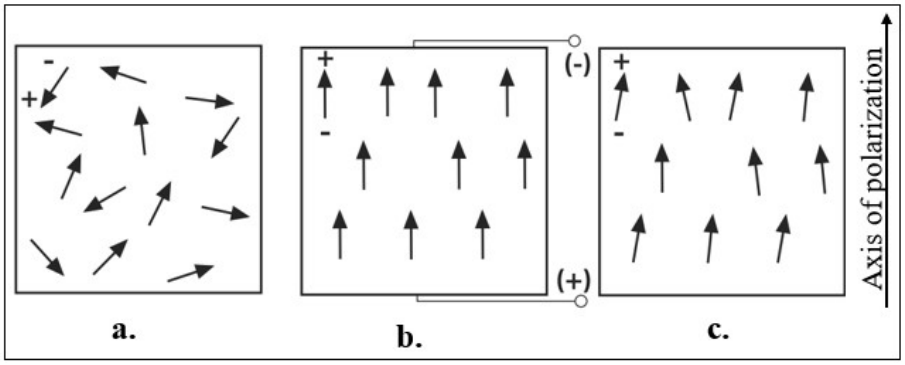


Figure 2.8: Illustration of the polarization effect: a). Randomly oriented dipoles in the crystal, b). Alignment of dipoles during polarization, c). Sustained dipole alignment after cooling and removal of the electric field [66].

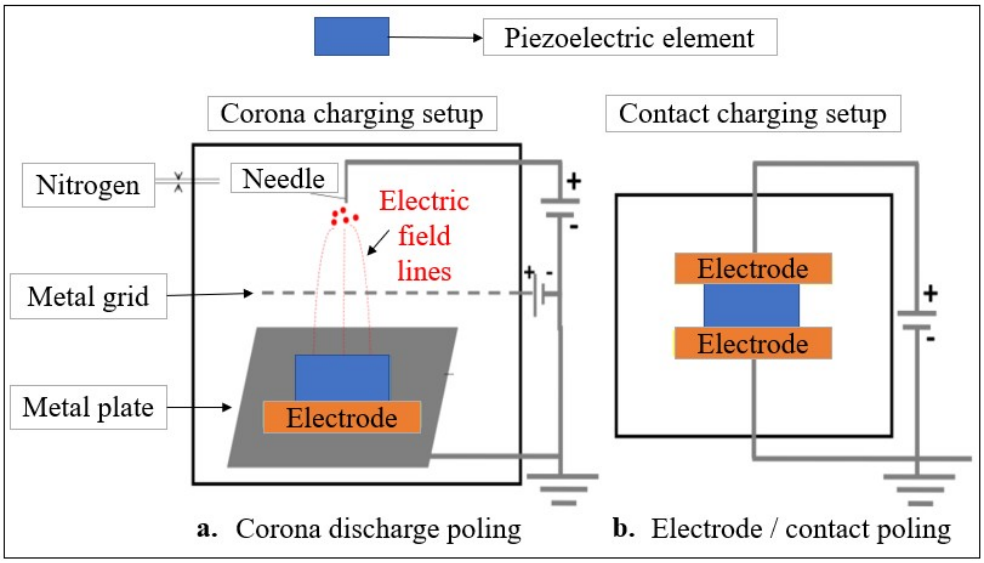


Figure 2.9: Illustration of the piezoelectric poling methods depicting: a). Corona discharge poling and b). Electrode/contact poling approach [69, 66].

On the other hand, in the electrode poling method, metal electrodes are first applied to the piezoelectric material, and then high voltages between 10 and 100 MV/m [66] are imposed. This method is often performed in an insulating medium or vacuum to protect the material from a strong electric field. It is worth noting that several factors influence dipole alignment, including the strength, consistency, and duration of the applied electric field; the magnitude and uniformity of the applied temperature; and the degree of contamination or voids between

the electrodes and the surface of the piezoelectric material [69, 66].

In contrast, corona discharge poling requires the piezoelectric material to be metalized only on one side, whereas electrode poling requires both sides to be metalized. Additionally, corona discharge poling creates an electric field across the entire width of the plate, charging the entire cell, unlike electrode poling, which only polarizes the material in direct contact with the electrode [69].

### 2.3.3 Piezoelectric Materials

Since their discovery, piezoelectric materials have advanced significantly, and these developments are reflected in the materials' properties. The historical evolution, performance, fabrication techniques, and potential applications of these materials are extensively documented by Uchino [64]. These materials can be either naturally occurring or artificially fabricated, designed to possess specific properties, sizes, and shapes tailored to their intended applications [70]. The driving force for the advancement of these materials lies in their potential for industrial and engineering applications. Aabid *et al.* [71] systematically reviews these materials for various industrial use cases.

According to Holterman and Groen [63], these materials could be classified into five distinct categories:

- Piezoelectric Single Crystals
- Piezoelectric Ceramics
- Thin Film Piezoelectrics
- Piezoelectric Polymers
- Piezoelectric Composites

Piezoelectric single crystals are further divided into natural and artificial single crystals. Natural single crystals include Quartz, Rochelle salt, Tourmaline, and Topaz, while artificial single crystals include Lithium Niobate and Lithium Tantalate. Notably, one interesting single crystal that has started to gain traction in research is PMN-PT [72]. These materials are characterized by a near-perfect periodic arrangement of constituent atoms or ions throughout the entire crystal

structure [63]. Piezoelectric ceramics, conversely, consist of numerous grains or single crystals, referred to as "crystallites," which are sintered together to form a solid body. The most widely used ceramics are based on Lead Zirconate Titanate (PZT) and Barium Titanate [63]. These ceramics are favored for their high electromechanical coupling and substantial energy conversion efficiencies [73]. Notably, PZT is widely used in various applications due to its low cost and high force density, making it suitable for sensing, actuation, and energy harvesting. Additionally, the processing of PZT has been well mastered, with substantial literature describing its modeling. Nevertheless, they present challenges such as toxicity [9] and brittleness, making them susceptible to impact damage [73]. However, piezoelectric polymers have been developed to mitigate the issues associated with lead-based ceramics. These polymer-based materials are gaining attention due to their reduced environmental impact, an increasingly important factor for sustainable development [9]. Despite their advantages, piezoelectric polymers exhibit limited electromechanical coupling and low piezoelectric coefficients, which constrain their practical applications, particularly in actuation [73]. On the other hand, piezoelectric composites combine the advantageous properties of ceramics and polymers, optimizing performance characteristics. Furthermore, thin film piezoelectrics are noted for their high sensitivity and low power consumption [63], making them particularly suitable for applications in nano-sized devices where bulk ceramics are impractical.

### 2.3.4 Constitutive Equations

Piezoelectric constitutive equations are associated with their operation modes, specifically the direct and inverse piezoelectric effects. According to the IEEE standard, piezoelectric materials exhibit linear behavior. However, it is essential to note that this linearity is maintained only under low electric fields and low mechanical stress levels [74]. In environments characterized by strong electric fields or high levels of mechanical stress, piezoelectric materials may exhibit significant non-linearity [75].

When a piezoelectric material is mechanically strained or stressed, electrical polarization is induced, and the material deforms accordingly. Due to the linear nature of piezoelectric materials, this electrical polarization effect is directly proportional to the applied stress. This relationship is described by the constitutive equations for piezoelectric materials. The linear

behavior is mathematically represented as:

$$\vec{P} = d\vec{T} \tag{2.1}$$

where, $\vec{P}$: Induced polarization [C/$m^2$] and d: Piezoelectric charge constant [m/V]

At constant electric field, the electric displacement is equal to the piezoelectric polarization:

$$\vec{D}|_{\vec{E}=0} = \vec{P} = d\vec{T} \tag{2.2}$$

where, $\vec{T}$: Stress [N/m2] and $\vec{D}$: The generated electric charge per unit area [C/$m^2$].

In consideration of electrostatics, the relationship between the electric field and the distribution of electric charge is crucial for understanding how an unstressed dielectric material behaves electrically. This description is governed by the equation:

$$\vec{D} = \epsilon\vec{E} \tag{2.3}$$

where, $\epsilon$: The absolute permittivity of the material [F/m] and $\vec{E}$: Electric field [V/m]

Therefore, for non Zero electric fields, total electric displacement is given by:

$$\vec{D} = \epsilon\vec{E} + d\vec{T} \tag{2.4}$$

Equation 2.4 represents the direct piezoelectric effect, which is typically utilized in sensing applications. This effect describes the generation of an electric charge in response to mechanical stress applied to a piezoelectric material.

Similarly, a piezoelectric material experiences electric displacement when an electric field is applied. The resulting stress causes the material to deform. The deformation, or strain, induced by the electric field in the absence of an external load can be described by the inverse piezoelectric effect, as follows:

$$\vec{S}|_{\vec{T}=0} = d^T\vec{E} \tag{2.5}$$

where, $\vec{S}$: Strain - the relative deformation

For a non zero external mechanical stress:

$$\vec{S} = s^E \vec{T} + d^T \vec{E} \tag{2.6}$$

Equation 2.6, represents the inverse piezoelectric effect, which is typically utilized in actuation applications. This effect describes the deformation or strain induced in a piezoelectric material when an electric field is applied.

Equation 2.4 and 2.6, make up the linear constitutive piezoelectric equations and can be re-written in matrix form as:

$$\begin{bmatrix} \vec{S} \\ \vec{D} \end{bmatrix} = \begin{bmatrix} s^E & d^T \\ d & \epsilon^T \end{bmatrix} \begin{bmatrix} \vec{T} \\ \vec{E} \end{bmatrix} \tag{2.7}$$

Since piezoelectric materials are fundamentally anisotropic, that is, exhibiting distinct properties in different directions, the aforementioned characteristics in Equation 2.7 should be seen as tensor quantities to accurately characterize their three-dimensional behavior. The strain $\vec{S}$ and stress $\vec{T}$ are vectors made up of six elements, with the first three elements signifying the normal deformation along the x, y, and z axes and the following three elements signifying the shear deformation in the area surrounding the x, y, and z axes [63]. The electric displacement $\vec{D}$ and electric field $\vec{E}$ are vectors composed of three elements that correspond to the x-, y-, and z-axes, respectively. Figure 2.10, shows the axes of deformation. The description of the electric,

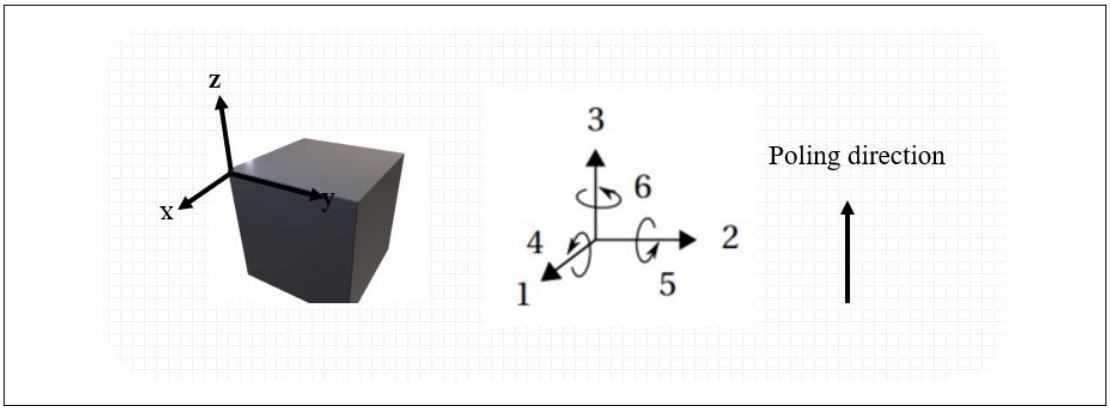


Figure 2.10: The axes of deformation.

elastic, and piezoelectric behavior can be expressed using matrix notations as opposed to the

tensor notations used in the IEEE standard [74]. The linear constitutive piezoelectric equation is thus provided as follows:

$$\begin{bmatrix} S_1 \\ S_2 \\ S_3 \\ S_4 \\ S_5 \\ S_6 \\ D_1 \\ D_2 \\ D_3 \end{bmatrix} = \begin{bmatrix} S_{11}^E & S_{12}^E & S_{13}^E & S_{14}^E & S_{15}^E & S_{16}^E & d_{11} & d_{21} & d_{31} \\ S_{21}^E & S_{22}^E & S_{23}^E & S_{24}^E & S_{25}^E & S_{26}^E & d_{12} & d_{22} & d_{32} \\ S_{31}^E & S_{32}^E & S_{33}^E & S_{34}^E & S_{35}^E & S_{36}^E & d_{13} & d_{23} & d_{33} \\ S_{41}^E & S_{42}^E & S_{43}^E & S_{44}^E & S_{45}^E & S_{46}^E & d_{14} & d_{24} & d_{34} \\ S_{51}^E & S_{52}^E & S_{53}^E & S_{54}^E & S_{55}^E & S_{56}^E & d_{15} & d_{25} & d_{35} \\ S_{61}^E & S_{62}^E & S_{63}^E & S_{64}^E & S_{65}^E & S_{66}^E & d_{16} & d_{26} & d_{36} \\ d_{11} & d_{12} & d_{13} & d_{14} & d_{15} & d_{16} & \epsilon_{11}^T & \epsilon_{12}^T & \epsilon_{13}^T \\ d_{21} & d_{22} & d_{23} & d_{24} & d_{25} & d_{26} & \epsilon_{21}^T & \epsilon_{22}^T & \epsilon_{23}^T \\ d_{31} & d_{32} & d_{33} & d_{34} & d_{35} & d_{36} & \epsilon_{21}^T & \epsilon_{22}^T & \epsilon_{23}^T \end{bmatrix} \begin{bmatrix} T_1 \\ T_2 \\ T_3 \\ T_4 \\ T_5 \\ T_6 \\ E_1 \\ E_2 \\ E_3 \end{bmatrix} \tag{2.8}$$

### 2.3.5 Applications

Piezoelectric materials can be utilized in a wide range of applications, as illustrated in Figure 2.11. One common application is the piezoelectric igniter, such as those used in gas stove lighters. In this device, pressing the button causes a spring-loaded hammer to strike a quartz crystal, generating a spark through the piezoelectric effect.

Another application is in the production of piezoelectric speakers. These speakers operate by applying an electric field to a piezoelectric material, causing it to change size. As charges are introduced or removed by the electric field, the piezoelectric material expands or contracts, leading to elastic deformation perpendicular to the speaker surface. Once the electric field is removed, the material returns to its original shape. This principle is used in the construction of hearing aids [76].

Similarly, piezoelectric materials are employed as transducers in ultrasonic cleaners. In these devices, an electrical signal at an ultrasonic frequency causes the transducer to vibrate, generating compression waves in the cleaning liquid within the tank. These compression waves create cavitation bubbles, providing ultrasonic cleaning power.

Piezoelectric pressure sensors are another critical application. These sensors detect pressure changes by measuring the imbalance of electric charges within the piezoelectric material when pressure is applied. Excessive positive and negative charges appear on opposite sides of the crystal, and this imbalance is transmitted as an electrical current through a circuit, indicating a change in pressure.

Finally, piezoelectric energy harvesting is a promising application wherein the energy generated by applied pressure is stored as electrical energy. This technology is being tested in various contexts, including shoe heels, to generate energy from walking [77].

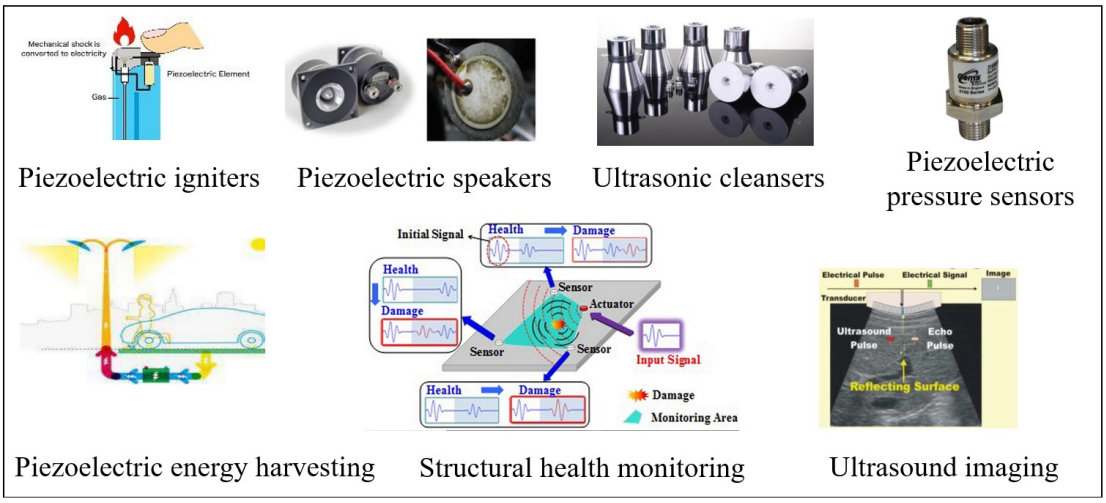


Figure 2.11: General applications of piezoelectric materials [65].

In addition, these materials have demonstrated significant potential for use in structural health monitoring. This application involves embedding a network of piezoelectric sensors within a structure to monitor signals and process results based on changes in the structure under observation [78]. For example, this technology can be employed to monitor the structural integrity of aircraft. Finally, these materials also find applications in the medical field, for example, in ultrasonic imaging.

## 2.4 Integration Technology: Functionalization of Composite Structures

In our context, integration technology refers to the methodologies employed to incorporate active components into composite materials during fabrication. As stated in the introduction, our aim is to explore the potential functionalization of combining piezoelectric active materials with long fiber-reinforced composites. This approach addresses the growing demand for smart, active, and intelligent structures that can adapt to external stimuli, particularly in the aerospace sector. Therefore, this technology is expected to facilitate the establishment of these smart structures. By combining fiber-reinforced composite materials with piezoelectric materials, which have been detailed in previous sections, we seek to fabricate composite structures with additional functionalities such as sensing, actuation, and energy recovery. Indeed, this approach has spurred significant research, with numerous researchers [34, 35, 36, 47, 79, 80, 81, 82, 83, 84, 85] working on investigating these advanced composite structures, leveraging the concept of integration to fully embed active elements within composite laminates.

Meanwhile, two integration techniques have been explored to functionalize composite structures [86]. The first technique, depicted in Figure 2.12, involves directly inserting the piezo element between plies during the layup stage, as demonstrated by Chen *et al.*, Paget *et al.*, and Masmoudi *et al.*, [34, 40, 87]. In this method, the thickness of the piezo element is crucial. According to Meyer *et al.* [47], the embedded element should be relatively thin compared to the ply thickness. This ensures adherence to the host structure's thickness variation limits. Moreover, from the study conducted by Mobaraki *et al.* [88], it was found that for thinner layers of piezoelectric material, the stiffness decreases, and the average strain increases in the material, leading to higher electrical output.

The second method involves the insertion of the active element using a cut-out technique as illustrated in Figure 2.13 [32, 89]. This method requires determining the location of the active element within the plies and then creating a cut-out that precisely matches the element's geometry [32, 87, 90]. By using this technique, the structure's thickness can be effectively controlled, as the cut-out portion compensates for the thickness of the integrated element.

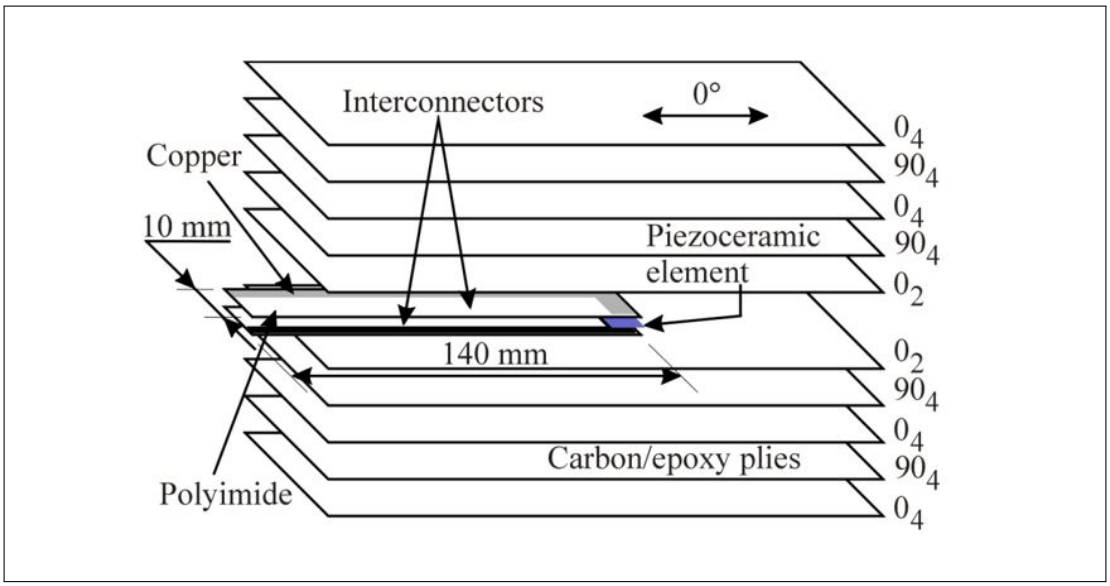


Figure 2.12: Illustration of a direct embedding approach of a piezoceramic element into a CFRP laminates [87].

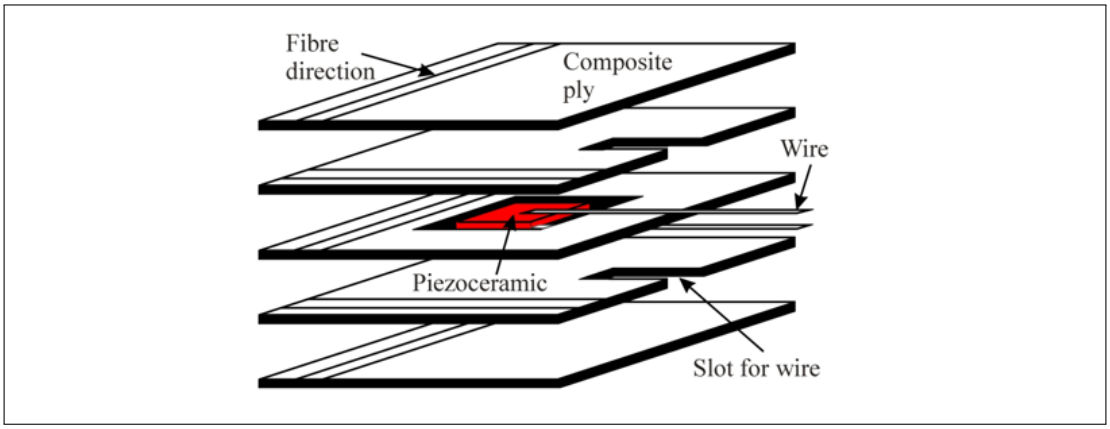


Figure 2.13: Illustration of embedding approach with a cut-out technique [87].

There are, however, challenges associated with these embedding techniques, as illustrated in Figure 2.14. According to Paradies *et al.*, [32], directly inserting a piezoelectric element between the plies leads to thickness variation, resulting in the formation of resin pockets near the embedded component. These resin pockets, depicted in Figure 2.14a, weaken the structure and can initiate delamination, compromising the mechanical integrity of the fabricated structure

[50, 91]. On the other hand, when the embedded element is positioned directly between plies, the continuity of the plies and fibers is preserved. However, in the case of cut-outs, discontinuities occur at the fiber layers, as shown in Figure 2.14b, due to the cutting required to accommodate the inserts. Therefore, investigation and material selection are necessary to choose materials that minimize the detrimental effects of inserts on the structural integrity and physical conformity of the structure while ensuring desired functional characteristics.

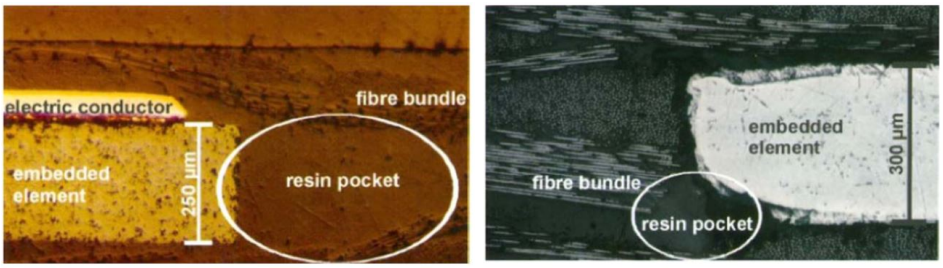


(a) Cross-section of a fully embedded bulk piezoelectric element without a cut-out.

(b) Cross-section of a fully embedded bulk piezoelectric element with a cut-out.

Figure 2.14: Effects of embedded piezoelectric materials on the host structures [32, 47].

It is evident that the selection of manufacturing procedures or rather the integration technology and processes is intricately linked to the choice of materials. Therefore, selecting suitable materials is essential for maintaining the mechanical properties of host structures when active materials are added. Additionally, it is crucial to ensure that the host structures do not compromise the functional properties of the embedded materials. Striking this balance is vital for smart composites to preserve their structural integrity and optimal functionality.

## 2.5 Materials Selection

### 2.5.1 Overview

Selecting appropriate materials for functionalized structures is challenging due to the vast array of fiber-reinforced composites for host structures and various available piezoelectric materials. This material selection process is a crucial step in designing and producing smart composite structures that utilize piezoelectric and fiber-reinforced composite materials. The choice of ma-

terials directly impacts the performance and functionality of the fabricated composite structure [92].

For piezoelectric materials, considerations such as piezoelectric coefficients, mechanical properties, temperature stability, and environmental impact are important factors to be considered. The selection of appropriate piezoelectric materials is essential to ensure efficient energy harvesting, sensing, or actuation capabilities in the smart composite structure [93].

Similarly, for fiber-reinforced composites, properties such as fiber type, orientation, volume fraction, matrix material, and manufacturing process significantly affect the composite structure's mechanical, thermal, and electrical properties [94]. It is, therefore, imperative to pick a combination that will improve performance and preserve the ideal physical, mechanical, and chemical qualities of the respective constituent materials.

The selection of these materials, for developing a smart structure, involves a meticulous process focusing on their intended functionality. The primary factors considered encompasses the capacity of the host fiber-reinforced composite material to provide adequate insulation for the embedded sensor, the curing temperature, ensuring that it remained below the Curie temperature of the chosen piezoelectric material, and the manufacturing process of the smart composite. These criteria are of utmost importance in ensuring the feasibility and viability of the resulting smart material structure for future deployment in aerospace applications. Furthermore, the high preference for eco-friendly materials and the strict environmental controls put into place are also factored into the primary considerations when choosing materials [95]. Thanks to the development of natural fibers for technical applications and the accessibility of eco-friendly piezoelectric materials [96, 97], the material selection process must also consider the lifecycle performance and sustainability aspects of the smart composite structure.

Environmental considerations such as recyclability, energy consumption during manufacturing, and end-of-life disposal should be considered. Additionally, the long-term durability and reliability of the selected materials in the operational environment of the smart composite structure, including temperature, humidity, and mechanical loading conditions, should be evaluated. It is, therefore, essential to note that proper material selection can contribute to the smart composite structure's overall sustainability and lifecycle performance, ensuring its functionality and durability throughout its service life.

In this thesis, material selection was conducted using a systematic approach that included a comprehensive literature review and experimentation to identify the most suitable materials for the intended application. Various factors were considered, such as functional requirements, manufacturing constraints, and lifecycle performance. To begin our exploration into the development of smart composite materials, flax fiber and PVDF (Polyvinylidene fluoride) were chosen as the optimal materials. The selection of flax fiber and PVDF piezoelectric material for producing smart composite materials holds promising potential for various applications, including sensing and energy harvesting.

Flax fiber is an attractive alternative to carbon or glass fibers thanks to its inherent sustainability, low environmental impact, good electrical insulation properties, and excellent mechanical properties, such as a high strength-to-weight ratio and good damping characteristics. In piezoelectric materials, PVDF emerges as a favorable choice over materials like PZT (Lead Zirconate Titanate) due to its flexibility, elasticity, and resistance to brittleness under mechanical stress [98]. Furthermore, PVDF offers the advantage of being non-toxic, alleviating concerns associated with the presence of lead in PZT, and ensuring the safety and a lower environmental impact of the composite material. By combining the mechanical properties of flax fiber with the flexibility and non-toxic nature of PVDF, the resulting smart composites achieve an optimal balance between structural functionality, performance, and environmental sustainability, making them highly suitable for sensing, actuation, self-sensing, and energy harvesting applications [4, 98, 99, 100].

The utilization and practicality of flax fiber-reinforced composites have garnered significant interest as an alternative to synthetic materials within the aviation and transportation industries. While carbon fiber reinforced polymers (CFRP) have been extensively employed due to their exceptional mechanical properties, their energy-intensive production necessitates the exploration of bio-based alternatives. Flax fibers possess cost-effectiveness and widespread availability, rendering them highly appealing for industrial applications [101]. Indeed, by reducing reliance on energy-intensive materials and promoting sustainability, flax fiber composites have the potential to substantially impact modern aircraft and transportation systems. Although their use is primarily limited to secondary parts, their utilization in primary load-bearing components remains constrained [102]. Nonetheless, certain research studies have highlighted their suit-

ability for hybrid composite development, particularly in combination with carbon fibers [103]. This approach proves advantageous in manufacturing smart composite materials, as flax fibers can provide desired electrical insulation for sensors while carbon fibers contribute significant mechanical strength.

In the next section, we explored the selection of PVDF, a polymer-based piezoelectric material, and pre-impregnated unidirectional flax fiber for their potential in developing smart composite materials. Laminated composite samples were fabricated using a symmetrical lamination scheme $[0°/90°/0°]_s$, with PVDF embedded in different layer positions for each sample. Vibration tests with magnetic excitation were conducted on the developed smart composite materials to explore their functional properties and sensitivity. Additionally, the electrical insulation properties of the fiber-reinforced materials were investigated during the material selection phase.

### 2.5.2 Materials Assessment and Experimental Methods for Effective Selection

The materials utilized in this assessment included flax fiber prepregs, carbon fiber prepregs, glass fiber prepregs, mu-copper tape, bronze wire mesh, aluminum foil, and PVDF. Experimental samples were produced using the consolidation fabrication method, as illustrated in Figure 2.15. The smart composite samples were rectangular, each measuring 50 mm by 92 mm, and incorporated a PVDF piezo film measuring 12 mm by 52 mm, oriented at a 45° angle.

The laminated smart composite plate consisted of six lamina layers based on unidirectional flax fiber prepregs as illustrated in Figure 2.15. The piezo patch was embedded directly between the plies of the composite, with its thickness of 52 $\mu$m exerting minimal impact on the overall thickness of the sample. Specifically, the PVDF layer was centrally located within the composite structure. Three samples were investigated where PVDF was positioned at the midplane, between layers 4 and 5, and between layers 5 and 6.

Continuity tests and resistance measurements were performed on the carbon and flax fiber samples explicitly fabricated for evaluation of the electrical conductivity and insulation property, as illustrated in Figure 2.16b. The actual smart composite samples were then subjected to

vibration tests with sinusoidal electromagnetic excitations. The smart composite beams were clamped, and excitation of constant strength with varying frequencies was implemented to check on the response and sensitivity of the PVDF at different layers.

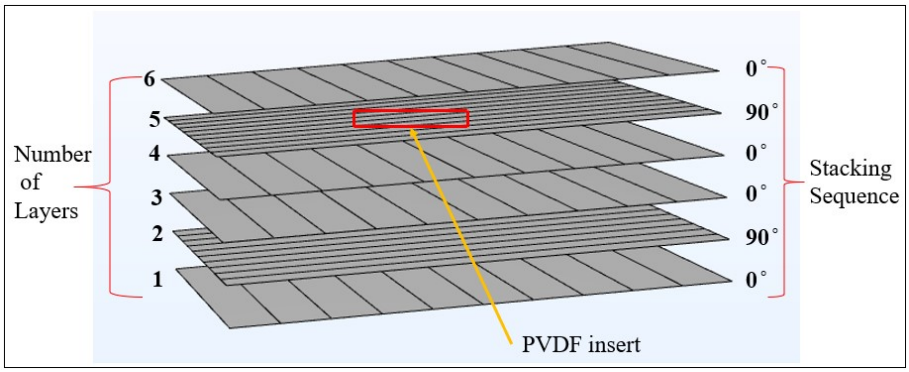


Figure 2.15: Fiber orientation and embedded piezoelectric material position in the laminated smart composite structure.

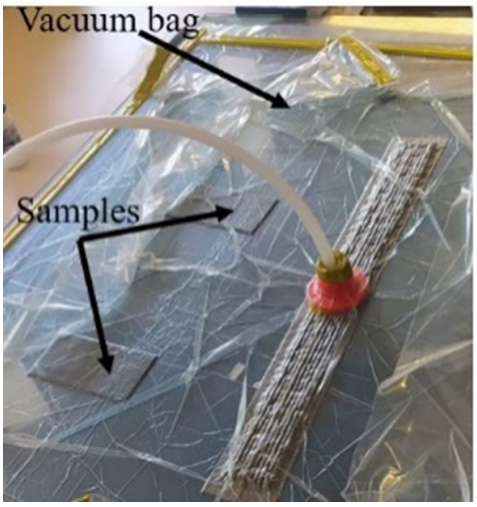


(a) Samples fabrication based on consolidation molding process.

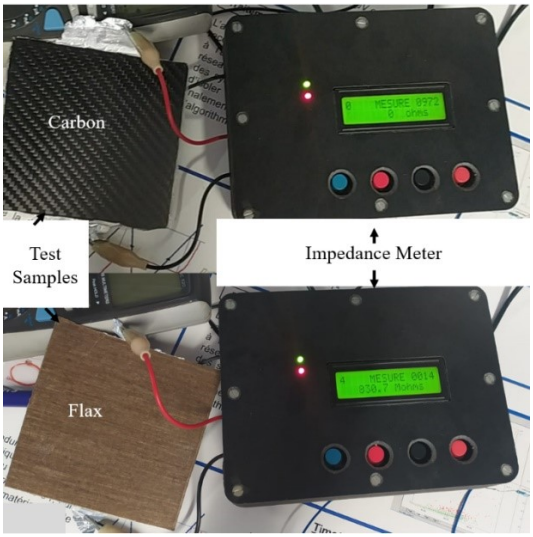


(b) Samples conductivity test.

Figure 2.16: Illustration of the fabrication and experimental tests on material selection.

## 2.6 Discussions

The environmental aspect helped to narrow down the material selection. Other technical considerations regarding the end product, particularly the thickness variation and sensitivity of the smart composite structure, have also been beneficial. Another important consideration was the non-planar nature of aerospace structures, which necessitated flexible, easy-to-fabricate, and customizable materials. These factors ultimately led to choosing a polymer-based piezoelectric material, specifically PVDF. The continuity test on the new materials revealed that the carbon fiber-based samples had low electrical resistance and thus poor insulation compared to the Flax fiber pre-impregnated ones (Table 2.1). This provided valuable insight into the feasibility of using flax fiber to prevent short-circuiting of the embedded sensor.

Table 2.1: Electrical conductivity test results.

| **Composite's Fiber Type** | **Electrical Continuity** | **Resistance** |
|---|---|---|
| Carbon | Yes | 0Ω |
| Flax | No | 830.7 MΩ |

Within the framework of sensitivity analysis, three distinct samples were examined. The first sample involved a PVDF piezo patch embedded in the midplane of the laminate structure. The second sample featured a piezo patch between layers 4 and 5, while the third sample had a piezo patch between layers 5 and 6 of the smart composite beam. All three pieces were subjected to dynamic bending induced by magnetic excitation. This investigation aimed to evaluate the impact of inter-lamina stresses on the piezo patches and assess their feasibility for practical sensing applications. The voltage responses were recorded using a PicoScope 2000 series and presented graphically in Figure 2.17a. Furthermore, the voltage responses at various frequencies were analyzed, resulting in identifying resonance frequencies presented in Figure 2.17b.To enhance the resolution of the frequency response data, especially given the low-frequency vibration behavior involving bending modes, one can consider using a smaller frequency step and a logarithmic scale for the ordinates. This approach would provide a more detailed and accurate depiction of the frequency characteristics, facilitating better interpretation and comparison of the results.

The obtained results were compiled and presented in Table 2.2.

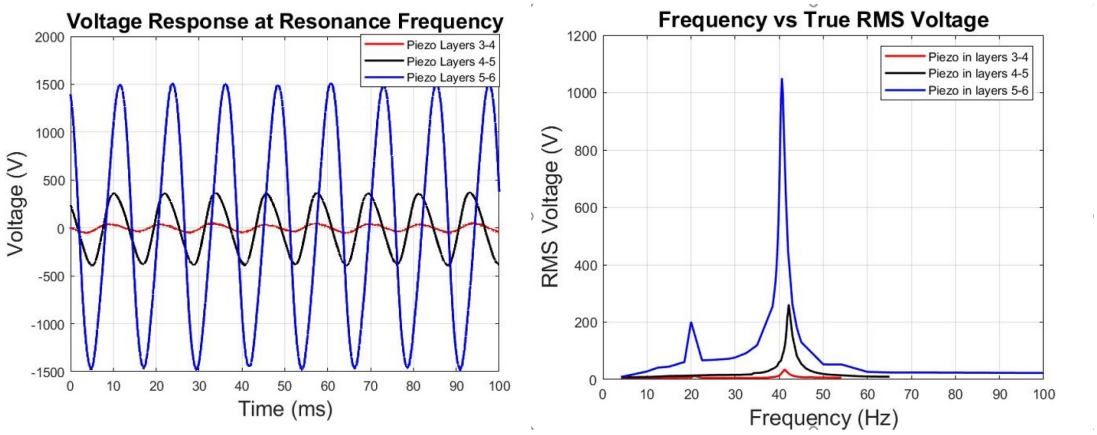


(a) Voltage response for the test samples with PVDF placed in different laminate layers.

(b) Frequency response for the test samples with PVDF placed in different laminate layers.

Figure 2.17: Illustration of the sensitivity test response conducted to validate the selected materials

Table 2.2: The sensitivity test results from dynamic loading of the smart composite laminates based on FlaxPregs and PVDF. The peak to peak and the true RMS voltages were measured at resonance.

| **Composite Number** | **Position of Piezo Layer** | **Pk-Pk Voltage (mV)** | **RMS Voltage (mV)** | **Resonance Frequency (Hz)** |
|---|---|---|---|---|
| Sample 1 | Layers 3-4 | 108.93 | 34.67 | 41.21 |
| Sample 2 | Layers 4-5 | 770.30 | 261.6 | 42.15 |
| Sample 3 | Layers 5-6 | 3017.60 | 1048 | 40.60 |

From the results presented in Figure 2.17, the voltage response of the smart composite structure with the sensor embedded in the midplane exhibits a small peak-to-peak voltage. This can be attributed to the unique stresses experienced by the midplane of the laminate during dynamic bending. As the beam bends, the midplane undergoes both tensile and compressive stresses. At the neutral axis, where the bending moment is zero, the midplane experiences minimal stress, resulting in relatively small strains approaching zero. This explains the observed signal to a large extent.

Furthermore, the presence of the piezo layer in the midplane slightly shifts the neutral axis, which can influence changes in stresses and strain distribution. Additionally, imperfections such as voids and resin pockets may cause non-linear stress distribution, leading to deformation

of the PVDF piezo layer in this position. It is important to note that the stresses and strains experienced in this laminate region during dynamic bending through thickness are critical factors in determining the structural behavior and integrity of the composite laminate beam. Accurate analysis and understanding of these stress and strain distributions provide valuable insights for designing resilient and reliable composite structures capable of withstanding the demands of dynamic bending loads.

Nevertheless, strains progressively increase towards the outer layers, reaching their maximum magnitudes. This observation aligns with the voltage response evolution concerning the sensor's positioning in our test samples, as presented in Table 2.2. Based on these findings, it can be inferred that incorporating PVDF within electrically insulating bio-composite material, it retains its remarkable sensitivity. Thus, it holds promising potential for critical applications, including non-destructive health monitoring strategies currently under investigation within the aerospace industry.

## 2.7 Summary and Conclusions

In this chapter, the background on fiber-reinforced composites and the piezoelectric effect is detailed. The integration strategies proposed in the literature, aimed at combining these materials for advanced functionality, are also briefly highlighted. Additionally, a brief illustration of the material selection process and considerations is provided, accompanied by relevant discussions.

In the context of smart composite structures, selecting appropriate constituent materials is critical. For instance, precise dimensional control necessitates the use of relatively thin inserts compared to the ply thickness. Based on our observations, utilizing PVDF has proven to be highly beneficial, effectively reducing thickness variation and preventing fiber cutting. Furthermore, dynamic vibration tests have confirmed the feasibility of implementing PVDF in aeronautical structures, considering the natural frequency range, voltage response, and the material's sensitivity. This establishes its reliability for applications requiring embedded sensors.

Appropriate integration technology is also crucial in the development of these structures. For instance, given the prior knowledge that dipole retention in piezoelectric materials is temperature-dependent, the design and fabrication of smart composite materials must be conducted within

reasonable limits to avoid risking the loss of piezoelectric capability.

Moving forward, the next chapter aims to explore diverse fabrication methodologies that align with the selected materials. It will also investigate the mechanical integrity aspects, the electromechanical response, and the thermoelectromechanical effect on these structures.

# Chapter 3

# Development of Smart Composite Structures: Fabrication Processes, Tests, and Characterization

---

## Contents

## 3.1 Introduction

Although integration technologies and processes for creating smart composite structures have been established, significant limitations still necessitate additional research to overcome, as illustrated in the previous chapter. This chapter introduces a novel perspective, offering innovative insights and valuable contributions to the existing knowledge. The primary contribution lies in addressing the critical need to integrate active materials seamlessly within composite structures. Experimental analysis is considered to evaluate the influence of these embedded elements on the structure's mechanical performance and assess the resulting functional properties. X-ray micro-computed tomography and an additional strength-of-material test approach, Interlaminar Shear

Strength (ILSS), are performed to explore the impact of the insertion on the integrity of the laminate structure and vibration tests are conducted to assess the electromechanical properties. In addition, an evaluation of the thermal stability of the produced smart composite material is presented in detail. Therefore, this chapter also presents a significant study of the thermo-electromechanical performance of smart composite materials subjected to dynamic loading and temperature variations.

## 3.2 Related Literature

In the existing literature, research in smart composite materials is on the rise, with many researchers exploring different fabrication techniques focusing on integrating these active elements within classical composite structures while proposing novel application possibilities. These include structural health monitoring, active noise suppression and vibration control, and energy harvesting [34, 35, 36, 79, 80, 82, 83, 85, 104, 105, 106, 107, 108].

It is envisaged that using this integration/co-fabrication technique would lead to a significant change in the development of functional composite structures within the context of scientific research and the industrial sector. However, embedding active elements within a composite poses a challenge compared to the classical method of attaching active components to the surface of a pre-existing structure. This results from some constraints imposed by the design and fabrication processes and the influence of the material choice. For instance, numerous investigations on developing smart composite structures in the literature are still centered on integrating lead-based active materials, primarily Lead Zirconate Titanate (PZT) [10, 40, 78, 86, 87, 109, 110, 111, 112]. Its high energy conversion efficiency and strong electromechanical coupling indicate its preference [73]. Nonetheless, there are certain disadvantages to these lead-based piezoceramics, including their toxicity [9] and brittleness, which renders them susceptible to impact damage and directly affects the structural integrity of the resulting structures. Consequently, there is still a need to investigate the most effective and environmentally friendly materials for smart composites as mentioned in the previous chapter. One alternative to PZT is using piezoelectric polymers to develop these smart structures.

These polymer-based materials have recently received attention from researchers as eco-friendly materials are becoming more crucial for environmental sustainability [9]. In contrast to their counterparts, they are also considered for their flexibility [106], which enables the fabrication of non-planar smart structures. Similarly, the choice of fabrication processes and optimal process parameters should be examined appropriately to address issues such as delamination and depolarization of the active element.

Indeed, one approach to developing smart composite structures involves incorporating active materials into their design to enhance their capabilities. Within this context, a crucial concern revolves around the seamless integration of these materials throughout the manufacturing process. Meyer *et al.* 2019 [47] provide an extensive review of the manufacturing techniques of smart composite structures with embedded piezoelectric transducers. The same methods and procedures used to create traditional fiber-reinforced composites, such as liquid composite molding techniques and prepreg technologies [49, 52, 53, 54, 55, 56, 57, 58, 59], are used to create these structures. The layup process remains similar but involves adding smart materials within the ply layers at the forming phase [113]. Nevertheless, there arises a necessity for certain technical adjustments in these processes. This requirement is driven by several notable challenges that significantly affect the manufacturing process when an insert is introduced. Thus, the ultimate goal is to successfully manage these modifications while preserving the geometrical and material attributes of the host structures and to ensure the effective operation of the embedded piezoelectric transducer [34, 35].

Therefore, when designing a smart composite structure using techniques such as the consolidation molding process (applying pressure and heat to complete the infiltration) or vacuum-assisted resin transfer molding, it is crucial to consider several technical factors. These include the curing temperature, the type of reinforcement materials used, the type of piezoelectric material utilized, and the compaction pressure applied during the manufacturing process. It is imperative to carefully consider these factors as they can significantly impact the final composite material's structural integrity and overall performance. The curing temperature, for instance, is critical in accelerating the hardening of the resins [114] and, thus, the process in general.

Consequently, evaluating the maximum curing temperature of the concerned materials is crucial to ascertain whether the integrated piezoelectric material will withstand the set thermal conditions during the manufacturing phase. This is because depolarization will occur when the temperatures are above the piezoelectric material's Curie temperature as described in Chapter 2, rendering the embedded patch non-piezoelectric. This will necessitate re-polarization after the process to ensure the functioning of the embedded piezoelectric material [32, 115]. Nevertheless, it is crucial to recognize that re-polarizing smart composites with embedded piezoelectric materials poses a formidable challenge. Therefore, a proper selection of materials and fabrication processes could aid in eliminating the need for this extra step. Compaction pressure also plays a crucial role. Optimal pressure helps ensure that all the entrapped air is drained from the part and that the bonding between the fibers, the matrix, and the embedded transducers is not compromised. This also helps to guarantee a higher fiber volume ratio and reduce the amount of voids and imperfections in the material [57]. On the other hand, an appropriate piezoelectric material should be selected where high compression pressures are applied since bending is more likely to break brittle components. Piezoelectric ceramic materials, for example, can become brittle under pressure and require compliance with the maximum allowable pressure [34].

Moreover, the wiring framework is yet another crucial component in the fabrication of these smart structures. An essential step is the electrical connection between the wires and the embedded piezoelectric transducers. This is due to the fact that the reliability of smart composite structures depends significantly on the connection's quality. This connection framework must be designed in such a way as to withstand the manufacturing process and the operational conditions of the finished structure. Paget *et al.* [87] suggests that when in use, the interface between the piezo element and inter-connectors (which could be wires, strips, coaxial cables, and/or conductive plies) must have dependable electrical conduction and bonding. This can be achieved by either soldering, use of conductive adhesive, or through co-cured conductive plies. The soldering technique is the easiest to implement, however, it finds some drawbacks when the solder spot volume is large enough to create a wedge shape that could break the embedded element during the compaction or even creates regions of weakness that compromises the effectiveness of the fabricated structure. Additionaly, conventional soldering cannot be implemented for thin films and polymers.

In this cases one has to employ other soldering techniques like diffusion soldering which requires specialized equipment and skills to realize [116]. One of the possible solutions to these issues is to use the conductive adhesive to bond wires on the surface of the transducers or lay up the plies and the conductive layers together and then co-cure it with the rest of the plies. In some cases, the choice of the reinforcement materials may also affect the electrical connection of the transducer, for instance, carbon fibers have electrical conductivity, which causes short-circuit, making it necessary to use insulators such the polyamides (Kapton tapes) [32, 117]. Ghasemi *et al.* [118] investigated the techniques on which wires could be taken out of the composite laminates, their findings indicated good results where the connectors were co-cured by the embedding approach. However, there is still a need to evaluate a proper wiring technique that ensures good connection and minimal combined thickness variation.

In this chapter, contrary to the classical functionalization techniques, which involve attaching sensors, actuators, or energy recuperators to pre-existing structures, this current work proposes to investigate fabrication processes that allow for the integration of desired functionalities from the manufacturing stage. Therefore, the first contribution of this study lies in addressing the vital requirements of seamlessly embedding active materials within composite structures. Secondly, it emphasizes the versatility of piezoelectric polymers, particularly Polyvinylidene Fluoride (PVDF), which is durable and flexible, easily conforming to irregular surfaces, making them versatile for embedded applications. Thirdly, it investigates the electrothermomechanical behaviour and proposes the optimal operating conditions for smart composites with fully embedded, polymer-based piezoelectric material for the first time in the literature.

## 3.3 Materials and Methods for the New Smart Composite Structure

### 3.3.1 Material Selection

The initial stage in designing a fabrication process involves the selection of suitable materials, as illustrated in the flowchart depicted in Figure 3.1. To facilitate this process, a multi-criteria decision analysis (MCDA) method was utilized in this investigation.

The MCDA method allowed for the consideration of critical factors such as material cost, performance, and environmental impact during the material selection process.

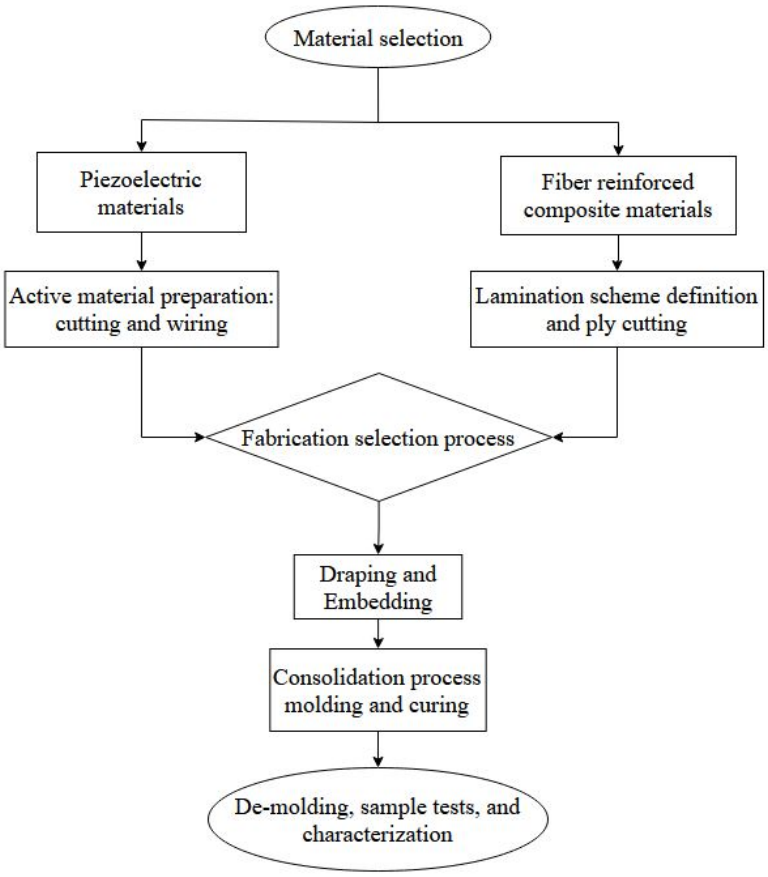


Figure 3.1: Sequential stages in the creation of smart composite structures: From material selection to sample characterization.

By adopting this approach, the best material choices for the fabrication process considered in this study are; FlaxPreg T-UD 110, a pre-impregnated material made of an epoxy resin and reinforced with unidirectional flax fibers with a fiber volume fraction of 51 % developed by LINEO, a conductive-adhesive coated copper foil tape, and FV30-MZ-000145 Polyvinylidene fluoride (PVDF) a polymer-based piezoelectric material developed by Kynar, Goodfellow.

Table 3.1: Material properties of unidirectional flax prepregs.

| Material | Density | Area weight | Fiber volume fraction | Thickness | Curing temperature | Young's modulus | Poisson's ratio |
|---|---|---|---|---|---|---|---|
| FlaxPreg T-UD 110-5, LINEO | 1.3 [g/cm$^3$] | 110 [g/m$^2$] | 51 [%] | 0.2 [mm] | 80 [°C] for 30 minutes and 120 [°C] for 1 hour | 35 [GPa] | 0.35 |

Flax fibers require less energy in their production process as compared to carbon and glass fibers. Moreover, as eco-friendly materials become more and more important in achieving sustainable development goals, a natural fiber, specifically UD-prepreg flax fibers (Table 3.1.), was proposed for investigation in this study. Additionally, this material was chosen for its excellent qualities, including its low density, good electrical insulation, and ease of use.

Another composite material utilized in this research was the Epoxy E-Glass Woven prepreg (HexPly® M34/41%/300H8/G), selected for its excellent insulation capabilities and favorable curing temperatures for the embedded sensor. It consists of a pre-impregnated glass fiber material with 41% M34 resin content and 55% fiber volume, sourced from Hexcel Corporation, Stamford, CT, USA (Table 3.2). The epoxy resin matrix in this material has a glass transition temperature of 80 °C.

Table 3.2: Material properties of epoxy E-Glass woven prepreg (HexPly® M34/41%/300H8/G).

| Material | Density | Area Weight | Fiber Volume Fraction | Young's Modulus | Curing Temperature |
|---|---|---|---|---|---|
| E-Glass Woven prepreg | 1800 [kg/m$^3$] | 300 [g/m$^2$] | 55 [%] | 21 [GPa] | 90 [°C] for 90 min |

Furthermore, a polymer-based piezoelectric material has been suggested for integration as an active element. In particular, a PVDF film with the properties shown in Table 3.3. This ensures that the toxicity and brittleness issues that other active materials may introduce are addressed. Moreover, this choice provides straightforward fabrication through the use of direct embedding. This is possible because its thickness is significantly less than that of the prepreg

flax fiber lamina. This material undergoes a glass transition at -40 °C, signifying a transition from a rigid to a more flexible state as the temperature increases.

It exhibits a Curie temperature of 195°C, indicating the temperature at which it shifts from a ferroelectric to a paraelectric state due to thermal agitation. Above 110 °C, the material experiences a reduction in its piezoelectric properties, referred to as depolarization onset, though it still maintains sufficiently valuable piezoelectric characteristics [119]. It is worth noting that it is recommended to use this material at temperatures below 100 °C for optimal performance in various applications [120].

Table 3.3: Material properties of Polyvinylidene fluoride (PVDF), a polymer-based piezoelectric material.

| **Material** | **Density** | **Max Operating temperature** | **Piezo strain constant** | **Youngs modulus** | **thickness** | **Sample size** | **Curie Temperature** |
|---|---|---|---|---|---|---|---|
| PVDF Film | 1780 [kg/m$^3$] | 100 [°C] | $d_{31}$= 23<br>$d_{33}$= -33 [($10^{-12}$) C/N] | 2-4 [GPa] | 0.052 [mm] | 12 [mm] X 60 [mm] | 195 [°C] |

In establishing the electrical connection, we opted for an adhesive-based conductor in the form of a copper foil tape coated with a conductive adhesive layer on one side (ADVANCE AT526), with a thickness of 35 $\mu$m, with an operating temperature range of -20 °C to 155 °C, and an electrical resistance through the adhesive of 0.003 Ω. This choice precluded the utilization of soldering due to the associated risk of wedge formation at solder points, a phenomenon that, as elaborated upon in the related literature section, has the potential to initiate the formation of structural cracks when subjected to external loading.

### 3.3.2 Proposed Design and Fabrication Processes

The general preparation of these materials follows the selection procedure (see Figure 3.1). Cutting the pieces to the required sizes and attaching copper tape conductors to the top and bottom surfaces of the piezoelectric material are two essential steps in the preparation of active piezoelectric materials. This active material (PVDF piezoelectric film) was cut into a rectangle

measuring 12 mm by 60 mm.

On the other hand, upon successful selection of reinforcement material (pre-impregnated flax fibers). The lamination scheme was defined. A cross-ply symmetric lamination scheme of $[0°/90°/0°]_s$ presented in Figure 3.2, was adopted in this study. Six pieces of UD-preg flax fibers were then cut into a rectangular shape of 50 mm by 250 mm while respecting the predefined orientation of fibers. This was followed by the selection of the fabrication process. At this stage, the vacuum-assisted consolidation molding process shown in Figure 3.3, was selected. This process is essential for completing the infiltration of the pre-impregnated layups [52]. It involves the application of pressure and heat to the pre-impregnated resin/fiber assembly to complete infiltration and squeeze out entrapped air during the heating/curing stage [53]. The draping of the plies was then performed following the stacking sequence depicted in Figure 3.2. The wired active element was embedded between lamina 5 and 6, 30 mm from the edge of the plies.

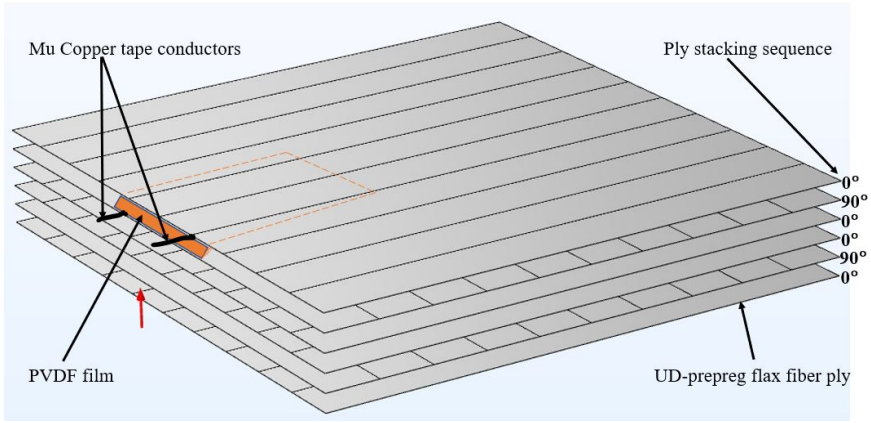


Figure 3.2: Exploded view of ply stacking sequence and PVDF placement layout for cross-ply symmetric lamination scheme $[0°/90°/0°]_s$ with cut UD-Preg Flax fiber samples (50 mm x 250 mm).

Figure 3.3 presents the fabrication process setup. Initially, the mold plate was prepared by applying a release/de-molding agent (Cirex Si 111). Next, a peel-ply fabric was applied onto the base plate, and subsequently, the composite preform was positioned on top of it. This fabric was essentially placed to achieve a smooth consistent surface and to prevent the vacuum bag from sticking onto the formed composite. It also aids to absorb a small amount of the excess resin during the curing process.

As for the conductors, to avoid excess resin from covering them (rendering the tape non-conductive) a masking tape was wrapped around it. A second peel-ply fabric was then added to the top of the preform samples to ensure a consistent surface finish of the composite structures. After this, a vacuum bag was attached to the mold making a hole on top for the vacuum pump tube. The vacuum creates a compression pressure which ensures a perfect bonding and the desired fiber volume fraction.

Following this, the mold was placed in an oven under vacuum pressure. The oven temperatures was set to 80 °C for 30 minutes, then raised to 120 °C for another 60 minutes. At the end of this curing cycle, the oven was switched off and left to cool to allow the safe removal of the mold assembly. De-molding began, and the produced samples were collected for testing and characterization.

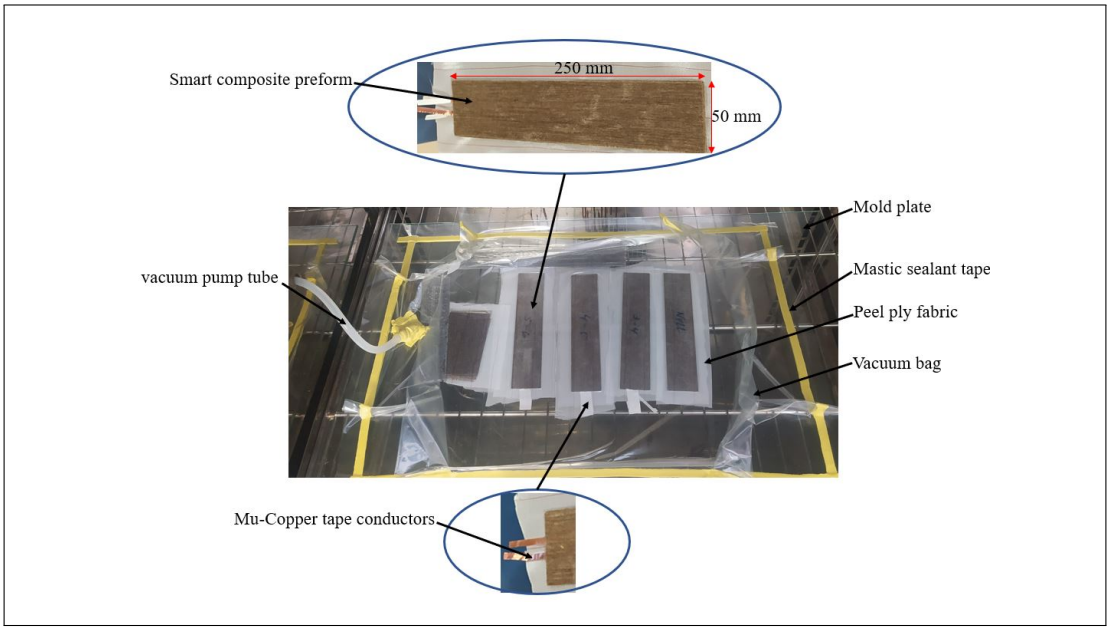


Figure 3.3: Vacuum bagging consolidation and curing process for smart composite preform - initial cure at 80°C for 30 minutes, then an elevation to 120°C for 60 minutes.

### 3.3.3 Assessment of the Active Material Inserts Impact on the Structure

#### 3.3.3.1 X-ray Micro-computed Tomography Scan Test

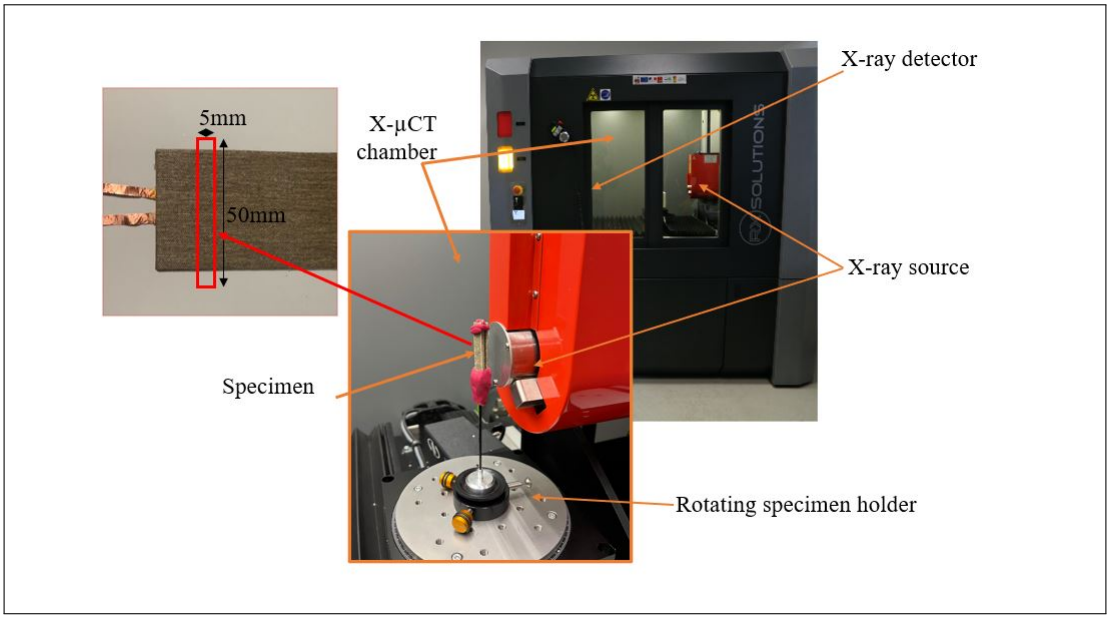


Figure 3.4: The X-ray micro-computed tomography test configuration with an acquisition voltage of 140 kV, a current intensity of 71 $\mu$A, and a resolution of 7 $\mu$m.

A sample with a wired piezoelectric element embedded between layers 5 and 6 was prepared for an X-ray micro-computed tomography scan. The specimens for tests were cut using a rotating diamond disc saw into 5 mm by 50 mm samples at the region with the wiring and PVDF film. The volume images were then generated by a laboratory tomography device (Easytom RXSolution) shown in Figure 3.4, with a voxel size of 7 $\mu$m. The acquisition parameters utilized were a voltage of 140 kV and a current intensity of 71 $\mu$A. The specimen was positioned on a rotation stage, and 1440 projections of transmitted X-ray absorption intensity field were recorded at each angular step of 0.25° by a flat panel detector (1920 x 1536 pixels) through an X-ray detector. Each projection was obtained by averaging ten images recorded at the same angular position. The images were reconstructed with the same voxel size of 7 $\mu$m using Avizo software.

#### 3.3.3.2 Inter-laminar Shear Strength (ILSS) Test

To determine the embedded elements' impact on the apparent interlaminar shear strength of the fabricated smart composite material. A sample consisting of a wired PVDF film embedded within the midplane of the structure was prepared for interlaminar shear strength (ILSS) testing. Four variants of specimens measuring 10 mm by 20 mm were obtained from the samples: i) Pure FlaxPreg based composite, ii) FlaxPreg with embedded PVDF film patch, iii) FlaxPreg with wired embedded PVDF film patch, and iv) FlaxPreg with embedded copper tape wires.

Following ISO 14130, these specimens were subjected to an interlaminar shear strength (ILSS) test assessed through a short beam shear (SBS) test. The experiments utilized an INSTRON 33R4204 tensile testing machine depicted in Figure 3.5 below, employing a 3-point bending configuration with a 1 mm/min testing speed.

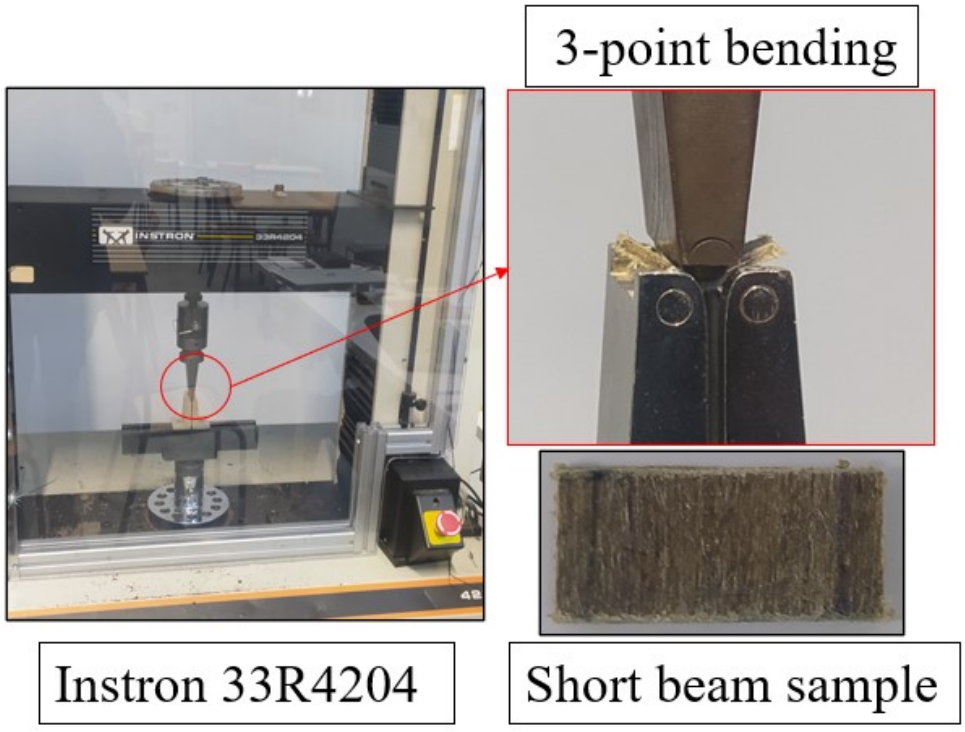


Figure 3.5: Short Beam Shear (SBS) test using an INSTRON 33R4204 testing machine.

### 3.3.4 Proposed Electromechanical Tests Experimentation and Data Acquisition Set-up

Figure 3.6, shows the experimental setup for assessing the electromechanical characteristics of the created smart composite structure. The smart composite plate was clamped on one end, 30 mm from the edge, and a magnetic material plate was clipped on the other end. Subsequently, it was subjected to vibration tests with sinusoidal electromagnetic excitations. An impulse response was also evaluated by displacing the free end of the clamped smart structure.

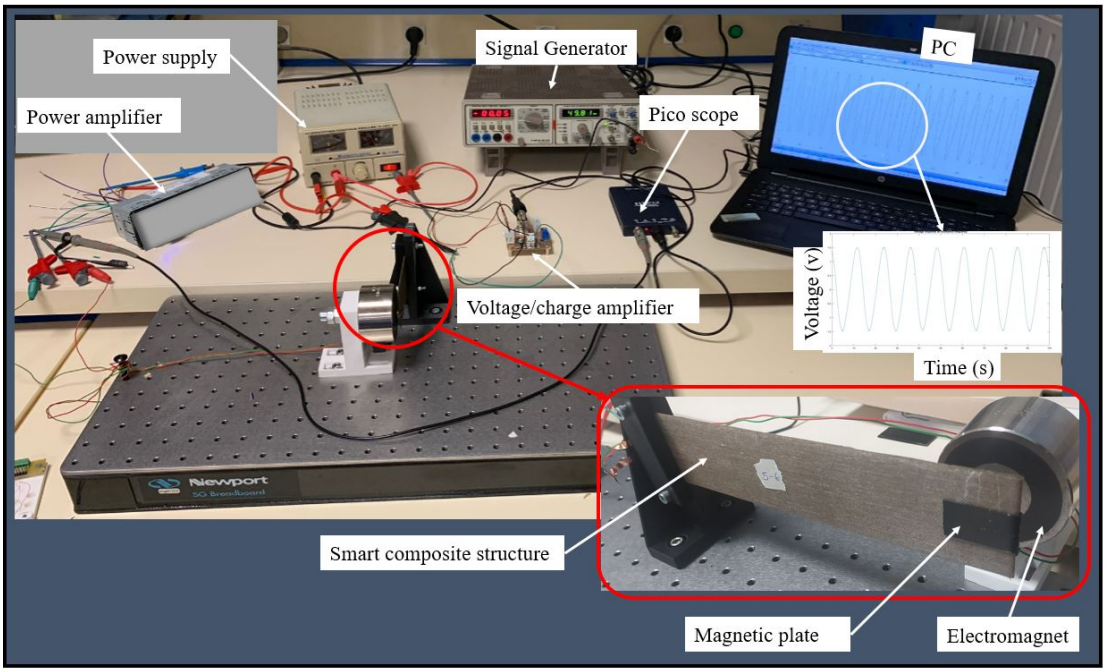


Figure 3.6: Experimental setup for electromechanical characterization of smart composite structure under sinusoidal electromagnetic excitations and impulse response evaluation.

The block diagram presented in Figure 3.7, describes the experiments' equipment, connection, data flow, and acquisition. A function generator (HAMEG HM 8030-3) was utilized to produce a sine waveform. The generated signal was amplified and fed into an electromagnet (RS PRO EM65-12V-DC). This generates a magnetic field resulting in a relative sinusoidal motion of the clamped smart composite plate, causing it to vibrate due to magnetic induction. During this stage, the function generator frequencies were adjusted gradually until the resonance frequency of the structure was reached.

The data were collected using the PicoScope (PICOSCOPE 2204A) series device connected to a computer for analysis and visualization.

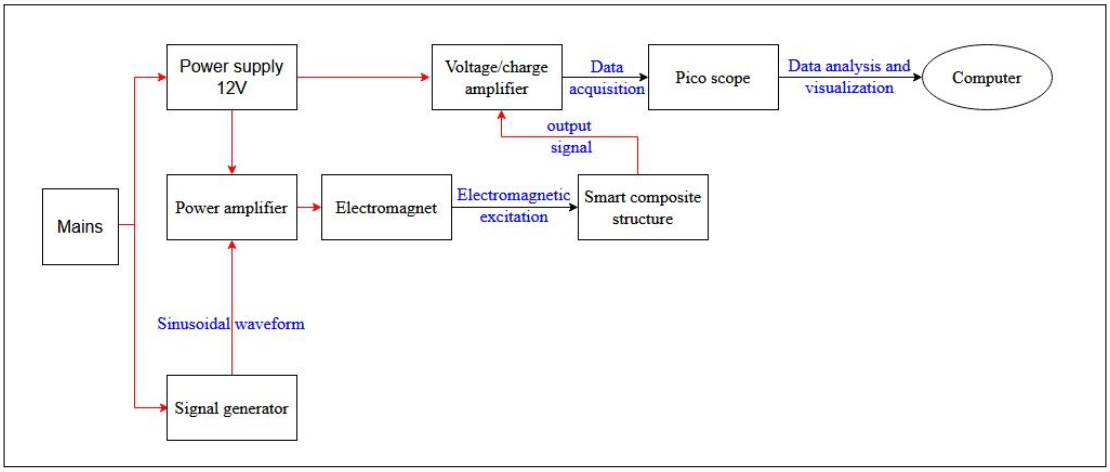


Figure 3.7: A block diagram illustrating the experimental setup's equipment, connection, data flow, and acquisition.

### 3.3.5 Assessment of Thermo-Electromechanical Properties in Smart Composite Structures

To explore the effects of temperature (variations) and mechanical strains on the electrical properties of a fully embedded sensor. Short beams of 12.5 mm X 50 mm smart composite materials were produced through the consolidation molding process, incorporating glass fiber-reinforced composite materials and embedded piezoelectric elements, specifically Polyvinylidene fluoride (PVDF). Thermo-mechanical tests were then conducted on the obtained samples using a DMA test procedure. This allowed a thorough evaluation of their electromechanical behavior amidst changing temperature conditions and dynamic mechanical loading. The impact of the induced thermo-mechanical stresses was assessed experimentally using a rheometer DHR – 1, as illustrated in Figure 3.8. The specifications and the descriptions of the DMA tests are presented in Table 3.4.

Table 3.4: Descriptions of the DMA tests parameters.

| DHR Specifications | Description |
|---|---|
| DHR Geometry | Dual clamp cantilever |
| Temperature Ramp | 23 °C to 165 °C |
| DMA Mode | 3-point bending |
| Ramp Rate | 5 °C/min |
| Frequency | 1 Hz |
| Sample Dimension | (50 × 12.5 × 1.6) $mm^3$ |
| Strain $\epsilon$ | 0.15% |

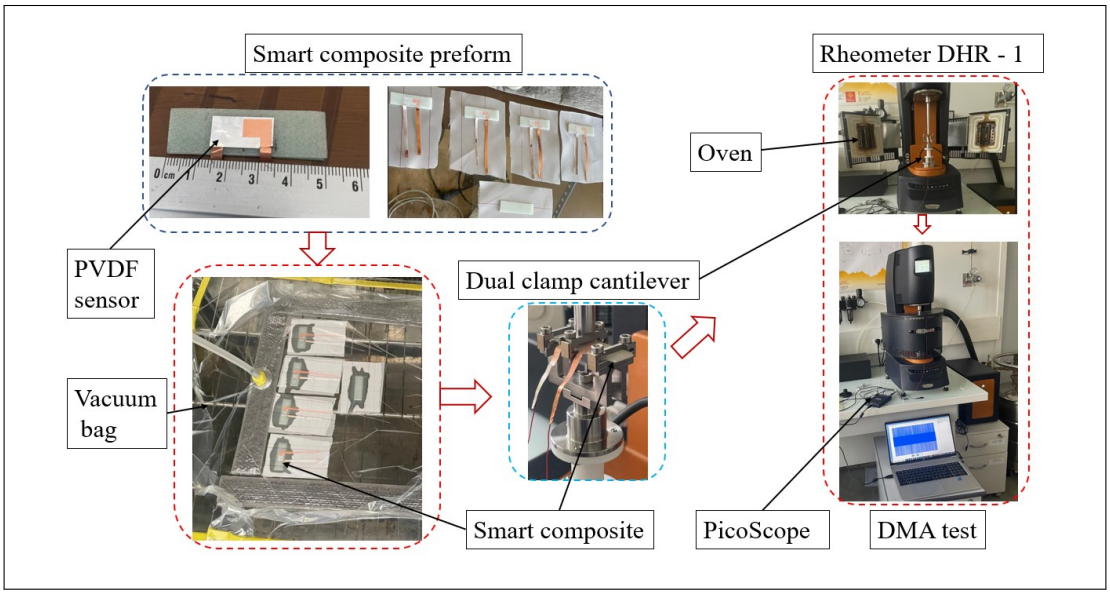


Figure 3.8: Illustration depicting the fabrication process of smart composites integrated with piezoelectric material (PVDF) and the DMA testing experiment setup. The setup features a dual clamp cantilever for a three-point bending test to assess the mechanical properties and functional capabilities of the composites.

## 3.4 Results and Discussions

### 3.4.1 Smart Composite Structure

Figure 3.9, depicts the resulting smart composite structure based on the selected materials and the manufacturing process. Covering the conductors during the curing process was observed to help ensure that the conductors were free of resin which guarantees good electrical connection. Moreover, the peel-ply fabric also delivered a uniform and smooth surface finish.

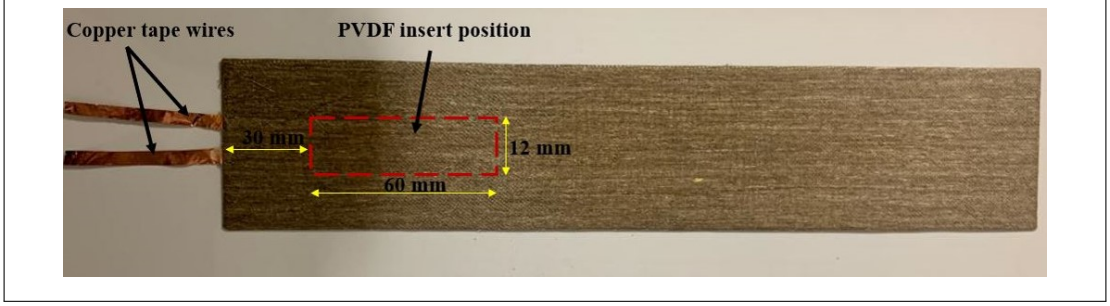


Figure 3.9: The resulting laminate smart composite structure with an integrated wired PVDF film measuring 60 mm ×12 mm × 0.052 mm.

### 3.4.2 Impact of the Active Material Inserts on the Mechanical Integrity of the Structure

#### 3.4.2.1 X-ray Micro-computed Tomography Test Results

To investigate the effect of the manufacturing process and material choices, as well as analyze the consequences of incorporating piezoelectric materials inside classic laminate composite materials. The manufactured specimen was subjected to X-ray micro-computed tomography. The results of the tomographs show excellent bonding between the co-cured conductors and the PVDF film as shown in Figure 3.10. It can also be seen from this tomography image that fiber continuity is preserved due to the use of the direct embedding technique [32].

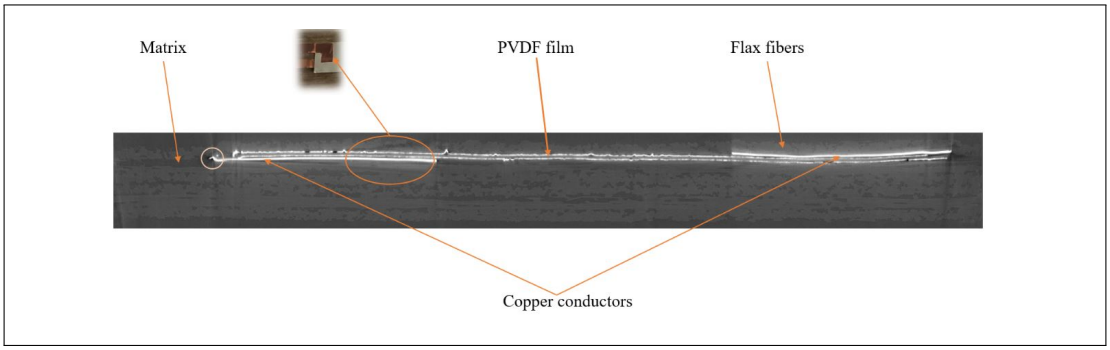


Figure 3.10: X-ray micrograph of a smart composite structure's cross-section obtained at 140 kV from a 5 mm by 50 mm sample containing PVDF film, conductive copper tape, and flax-preg host plies.

Nonetheless, it is practically impossible to fabricate a flawless composite structure. The tomography results show evidence of defects within the structure. From defect observation and analysis, two types of defects were identified, those induced by flaws in the raw materials, and those arising from the fabrication process.

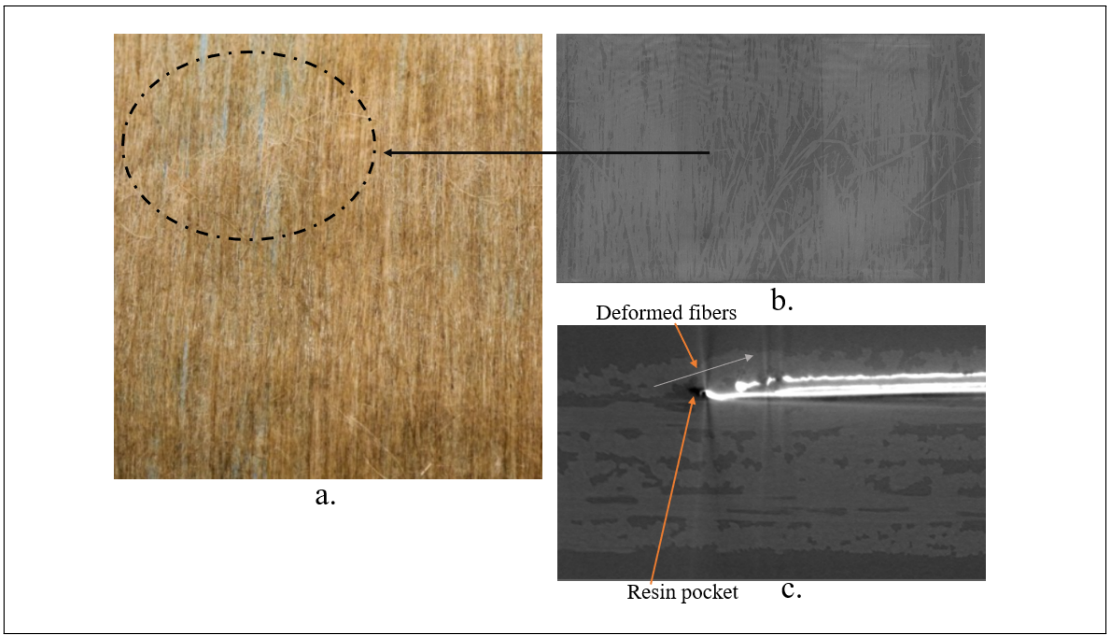


Figure 3.11: Defects; **(a)** presents the UD-preg flax fiber showing the variational density of the fibers, **(b)** presents a tomography image of the fibers in the structure with misaligned fibers sustained from the raw material, and **(c)** presents the tomography image showing the flaws within the edges of the embedded structure i.e resin pockets and shape distortion of the fibers.

In Figure 3.11(a), a picture is shown of the UD-preg flax fiber material, depicting a variation in the density of fibers. Additionally, some fibers appear to be misaligned in a random arrangement. This misalignment may have been caused by vibrations of the machinery or electrostatic repulsion during the fiber coating phase of the fiber manufacturing process [121]. It should also be noted that flax fibers are shorter and not continuous as compared to glass and carbon fibers, so the end of the elementary fibers may move a few centimeters, causing a shift in the primary direction. Indeed it is evident that natural fibers present some variability. However, our chosen fabrication process still delivered a good quality structure for tests and characterization with the initial orientation of fibers in the plies being preserved in the finished structure. This is illustrated in the tomography image presented in Figure 3.11(b).

Furthermore, the presence of the embedded piezoelectric material locally modifies the orientations of the fibers. The fibers' direction was distorted, particularly where the copper tape conductors were attached to the piezo. This could be attributed to the significant thickness variation in this region, as opposed to areas with only PVDF film insert, which show little fiber shape variation. Figure 3.11(c) shows this kind of flaw, and it also shows a formed resin pocket at the edge of the embedded element. It is undoubtedly difficult to create a completely void-free composite. We could, however, report that with proper host and embedded element selection, we were able to achieve a tolerable void content in comparison to the occurrence of huge resin pockets and voids reported in [32, 122].

#### 3.4.2.2 Inter-laminar Shear Strength (ILSS)

Using the short beam shear (SBS) test, we assessed how incorporating copper tape connectors and integrating PVDF film piezoelectric material within the flax fiber reinforced composite materials impacted their mechanical integrity. This assessment involved determining and comparing the apparent inter-laminar shear stresses using a three-point bending method. The inter-laminar shear strength was calculated using the formula provided below:

$$\sigma, ILSS = \frac{3}{4} \cdot \frac{F_{max}}{b \cdot h}$$

where $F_{max}$ is the maximum load-bearing of the specimen before fracture, b is its width, and h is the thickness of the specimen. The determined ILSS values and their variation concerning the embedded patch specimen type is summarized and presented in Table 3.5.

Table 3.5: Specimens' inter-laminar shear stress and their impact on the strength of the host material.

| **Sample test specimen** | **ILSS [MPa]** | **Material strength impact[%]** |
|---|---|---|
| Pure FlaxPreg | 4.1705 | reference |
| FlaxPreg + PVDF | 4.1416 | -0.69 |
| FlaxPreg + PVDF +Copper Tape | 3.8739 | -7.11 |
| FlaxPreg + Copper Tape | 3.9428 | -5.46 |

Figure 3.12 presents the resulting load-displacement curves of the tested specimens. Here, a notable observation emerges, where the inclusion of embedded wired PVDF films leads to increased composite rigidity, potentially yielding at higher loads than the pure material, as depicted in the figure. This phenomenon implies an overall improvement in the material's load-bearing capacity, attributed to the enhanced rigidity resulting from integrating these elements. However, an intriguing contrast surfaces when evaluating Interlaminar Shear Strength (ILSS), which assesses explicitly the interlaminar shear behaviour and interfacial bonding, revealing that the pure FlaxPreg composite material exhibits significantly higher values compared to the composite with embedded copper tape wires and PVDF film as depicted in Table 3.5. This divergence can be attributed to the presence of embedded elements that may introduce stress concentrations and weaken the bonding between layers.

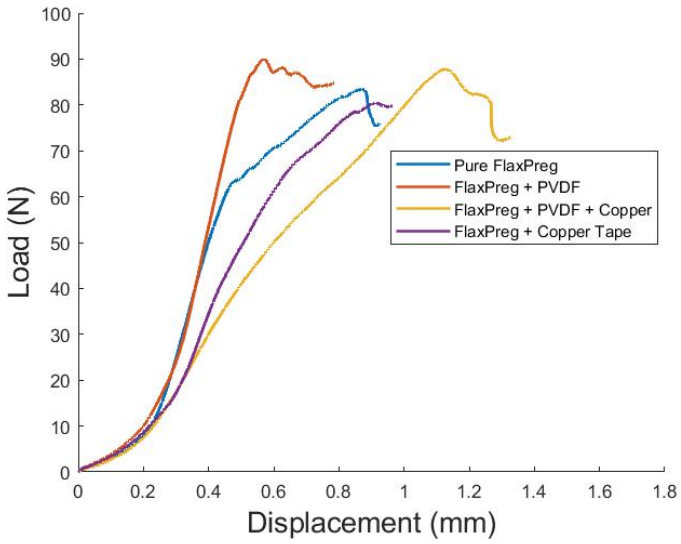


Figure 3.12: Mechanical performance tests through short beam shear (SBS): The load vs displacement curves of the 4 samples subjected to 3-point bending test.

The primary objective of this study was to investigate the influence of integrated thin film piezoelectric materials on the strength of laminated composite materials. It is essential to acknowledge that the embedded elements did not encompass the entire midplane dimensions of the specimens; instead, they covered approximately half of the midplane area, measuring 12 mm by 10 mm.

Nevertheless, the results obtained remain substantially indicative of the material's strength, particularly as evaluated through ILSS. Consequently, the short beam strength observed can be directly correlated with the interfacial bonding strength between the fibers, matrix, and the embedded structure. Notably, the failure mechanism in this type of test predominantly involves shear rather than tensile yield. From the results, we can see that the integration of PVDF films alone leads to a reduced strength by 0.69%, the wires alone copper foil reduced by 5.46%, and that of the wired PVDF by 7.11%. It is essential to underline that our selection of materials and the integration process have effectively mitigated the impact on strength compared to previously reported findings in the literature, as summarized in Table 3.6.

Table 3.6: Comparing influence on the mechanical properties with other works featuring fully embedded active materials.

| **Reference** | **Host Material** | **Embedded Element** | **ILSS Impact [%]** | **Void Content** | **Resin Pockets** |
|---|---|---|---|---|---|
| Current Work | FlaxPreg | PVDF | -0.69 | none | none |
| Current Work | FlaxPreg | PVDF+Copper | -7.11 | none | low |
| [106] | GFRP | Pt-coated PVDF | -0.73 | - | - |
| [106] | GFRP | PVDF+Copper | -8.15 | - | - |
| [123] | CFRP | P(VDF-TrFE) | 8 | - | - |
| [124] | GFRP | MFC | 7.71 | - | - |
| [124] | GFRP | PZT | 15 | - | - |
| [32] | GFRP | PZT | - | - | high |

In summary, the data presented in Table 3.6, drawn from previous research on composites with fully embedded piezoelectric elements, highlights the minimal impact of PVDF material on mechanical performance, showcasing a mere 0.69% degradation. This degradation is comparable to Pt-coated PVDF, demonstrating a 0.73% degradation. These findings emphasize PVDF film as a reliable choice for integration into composite materials. Compared to PZT, our utilization of copper-wired PVDF film demonstrated a superior ability to maintain material strength with a 7.11% impact against 15%. Furthermore, our assessment of resin pockets resulting from integration showed only minor resin pockets at the edges of the embedded element, particularly compared to composites with embedded bulk ceramics. A smart composite material's effectiveness depends on material selection and fabrication procedures.

The substantial improvements observed validate our chosen piezoelectric material as an effective and worthwhile option for integration into embedded sensors or energy harvesters for structural health monitoring. It's essential to recognize that these strength impact results serve as approximate guidelines for design purposes. The embedded active element did not cover the entire mid-plane of the test samples; its dimensions were 12 mm by 10 mm. In real-world applications, the ratio of the embedded element's area to that of the host material would typically be significantly larger, resulting in more realistic values.

### 3.4.3 Electro-mechanical Properties

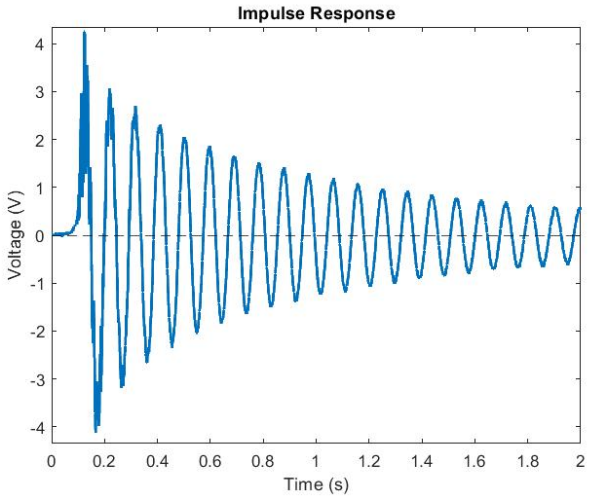


Figure 3.13: Impulse response of the smart composite structure obtained by displacing the clamped sample's tip by approximately 40 mm.

Figure 3.13 depicts the impulse response for the manufactured smart composite structure. This was obtained by displacing the clamped sample's tip by approximately 40 mm and releasing it to oscillate freely. Using the PicoScope 2000 series, we monitored and recorded the output signal. This gave a clear indication of the fact that the piezoelectric properties of the embedded PVDF film were preserved throughout the entire fabrication process. This was demonstrated by its sensitivity to displacement stimuli. The maximum peak voltage measured was 4 V with an amplification factor of 4, and it was observed that with larger displacements, this voltage response could be raised further. The signal frequency was determined to be 10.53 Hz from the

free vibration of the structure.

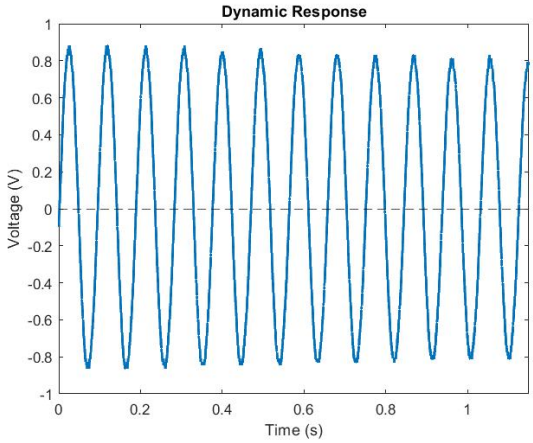


Figure 3.14: The smart composite vibration tests voltage response obtained at the structure's resonance frequency with a recorded peak-to-peak voltage of approximately 1.8 V.

The structure's response to dynamic loading was then examined using the experimental setup shown in Figure 3.6. In this case, when the magnetic field is created, it induces a dynamic interaction force between the magnetic plate clip attached to the tip of the test structure and the electromagnet itself. Vibrations are therefore created in the structure resulting in the response shown in Figure 3.14. The analysis of this voltage output response provided significant insight into the sensitivity of the structure to varying frequencies under dynamic loading. Thus, it is clear that our composite structure has added functionalities that could be exploited for sensing or energy harvesting purposes.

A Fast Fourier Transform (FFT) was also used to process the data based on the voltage response values recorded during the vibration tests. This was done to assess the constructed composite structure's natural frequencies. The extracted characteristic frequencies from the FFT analysis are presented in Figure 3.15. It was determined that the resonance frequency was 10.43 Hz. The determination of this frequency is very crucial in smart composite structures as it can be utilized in the detection of the changes in the structure's stiffness which may be indicative of damage or degradation. However, it is important to recognize that this frequency is influenced by multiple factors, including the thickness of the plate, material properties such as the modulus of elasticity and fiber orientation, as well as the boundary conditions that are set.

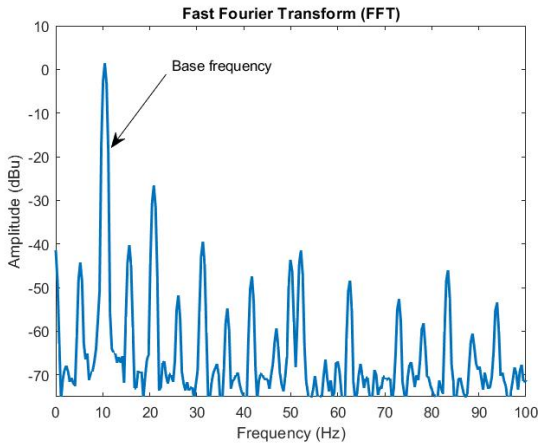


Figure 3.15: Extracted characteristic frequencies from a fast Fourier transform(FFT) analysis.

### 3.4.4 Thermo-Electromechanical Properties Results

Indeed, smart composite materials have been proposed in the literature for fascinating applications aimed at enhancing the autonomous health monitoring of aeronautic structures through structural health monitoring technology [125, 44]. These applications rely on electromechanical response signals recorded from embedded sensors, described in the previous section, to track and provide insightful data regarding the health status of the material. The baseline, often referred to as the damage indicator base, is typically compared with the actual signal, and any deviations would indicate the presence of anomalies within the structure [126]. Nevertheless, if the materials' behavior under operational conditions is not thoroughly characterized, diurnal environmental changes can severely impair the accuracy of these diagnostic thresholds. Temperature fluctuations, for instance, critically influence structural behavior, potentially distorting diagnostic signals. This is because both the mechanical and viscoelastic properties of composites are functions of temperature, as temperature activates the thermal transitions in the polymer chains of the matrix [127]. Therefore, it becomes necessary to conduct electro-thermomechanical tests to ascertain stable operation ranges before these new smart composites are deployed in aeronautical parts. The findings of these investigations are presented in the following sections.

#### 3.4.4.1 Linear Field Range

The initial step was identifying the strain range where the material exhibited linear viscoelastic behavior. A strain sweep revealed consistent storage modulus values up to about 0.15% strain, beyond which non-linear behavior began. Concurrently, a frequency sweep from 1 Hz to 16 Hz confirmed a stable material response. The results of this is illustrated in Figure 3.16. In this study, the maximum strain selected was 0.15%, and the oscillation frequency was set at 1 Hz. This ensured that the parameters chosen for subsequent DMA tests remained within the linear viscoelastic region, yielding reliable results.

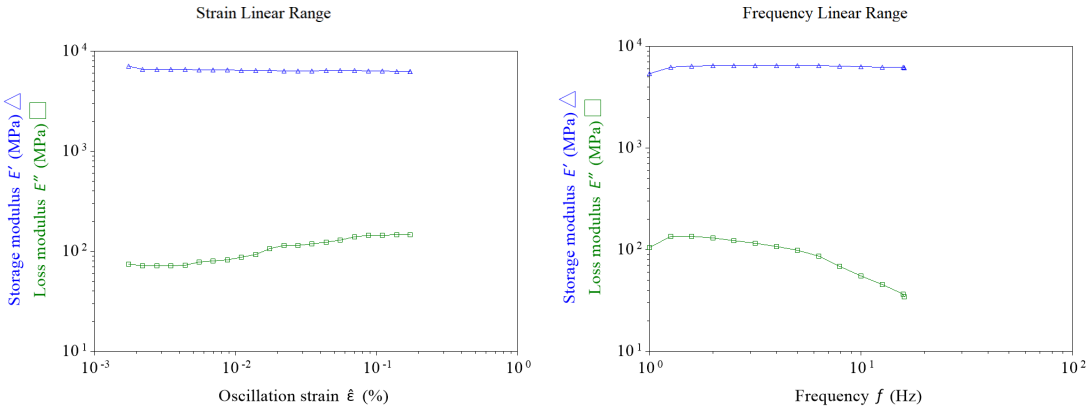


Figure 3.16: Illustration depicting the linear range of viscoelastic properties response as a function of frequency and oscillation strain amplitude fluctuations at room temperature (22.5 °C). The frequency sweep was conducted at a constant strain amplitude of 0.15% from 1 Hz to 16 Hz, while a logarithmic sweep for strain amplitude was performed at a constant frequency of 1 Hz, spanning an amplitude range from 1.76e-3% to 0.175%.

#### 3.4.4.2 Smart Composite's Viscoelastic Properties

Figure 3.17 displays the outcomes from two temperature ramp experiments, where the temperature increased from 23.5 °C to 165 °C at a rate of 5 °C/min. In both experiments we applied an oscillation strain of 0.15% at a frequency of 1 Hz. Initially, the storage modulus is high at lower temperatures (7.2 GPa at 30 °C for the first experiment and 9.1 GPa for the second), suggesting that the smart composite maintains a solid state at these temperatures. The storage modulus decreases linearly as the temperature rises, indicating material softening up to the pre-glass transition temperature zone.

The first significant decline in modulus occurs after 80 °C in the first experiment and around 90 °C in the second, coinciding with increased dissipation factor (Tan $\delta$) and loss modulus, marking the onset of the glass transition (Tg). Following Irfan *et al.*, [127] further temperature increases lead to the mobilization of polymer molecular chain segments, turning the composite rubbery. The peak of the dissipation curve indicates the Tg, recorded at 112 °C in the first and an improved 124 °C in the repeated experiment, based on ASTM D4065. This latter result confirms the expected final curing stages of glass fiber composites, typically near 120 °C, and demonstrates the embedded sensor's minimal impact on the composite's structural integrity.

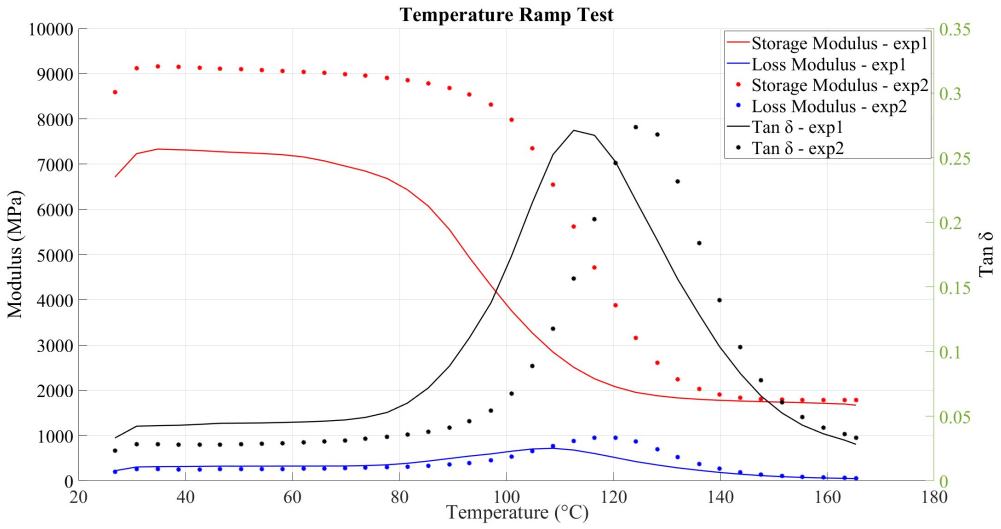


Figure 3.17: Illustration of the results from two ramp experiments showing the changes in storage modulus, loss modulus, and tan $\delta$ as temperature increases from 23.5 °C to 165 °C. Exp 1 and Exp 2 represent the first and the repeated experiment from the same test sample.

#### 3.4.4.3 Electro-thermomechanical Properties

To assess the influence of temperature and dynamic loading fluctuations on the signal response of smart composite materials, the voltage output was tracked and recorded using a PicoScope data acquisition device through PicoLog software. Figure 3.18 presents the temporal responses, including the piezoelectric sensor response, the dissipation factor (Tan $\delta$), and the temperature ramp.

The results indicate that under temperatures up to 105 °C, i.e., the glass plateau region (Region I), the response of the PVDF sensor remains stable, showing no influence from the thermal agitation caused by increasing temperatures. This stability suggests a temperature range within which the smart composite materials can operate without signal interference from thermal effects.

In Region II, the glass transition region, an exponential shift towards the positive side and a significant reduction in amplitude was observed. This behavior is likely due to changes in material properties as it transitions from a glassy to a rubbery state. Notably, the maximum recommended operating temperature for PVDF is 100 °C, which is exceeded in this region. This excessive temperature affects the polarization of the piezoelectric elements. At this stage, energy dissipation peaks, as indicated by the maximum of Tan $\delta$, where the polymer chains gain increased mobility, completing the transition to a rubbery state. This critical point also leads to significant thermal drift due to the mismatched thermal properties, such as expansion and contraction, between PVDF and the composite material, becoming prominent during these phase transitions.

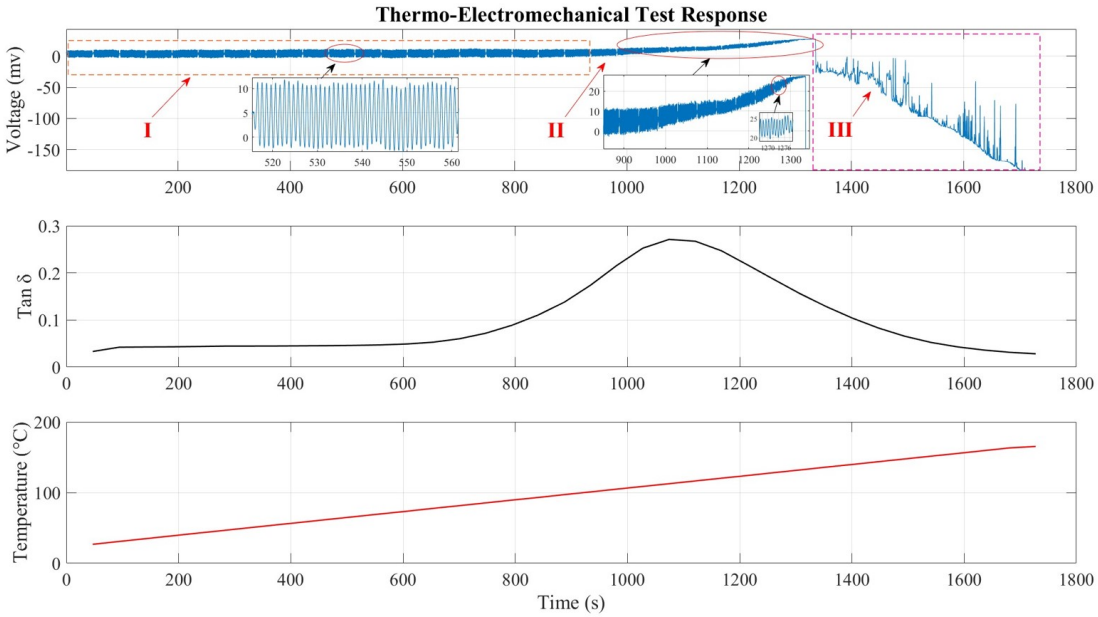


Figure 3.18: Illustration of the thermo-electromechanical properties over time, obtained from a three-point dual-clamped cantilever smart composite DMA test. The test was conducted with an applied strain of 0.15% at a constant frequency of 1 Hz, while the temperature was ramped from 23.5 °C to 165 °C.

As the temperature increases beyond the Tg in Region III, the piezoelectric response degrades significantly at 135 °C. This degradation can be attributed to three main factors. First, the mismatch in the coefficients of thermal expansion between PVDF and glass fiber potentially creates mechanical stresses at their interface. As the composite becomes less rigid, PVDF may slip or deform more easily under mechanical load, thereby reducing the effective transfer of mechanical stress from the glass fiber. Second, at temperatures above the Tg, the adhesive bonding agent used at the interface between PVDF and the adhesive-based copper wires degrades and weakens. This degradation leads to the wires sliding and potentially losing their connection, as the adhesive could be replaced by non-conductive epoxy resin during this rubbery state. Third, the temperature approaches the Curie temperature of the PVDF material, the point at which the material loses its piezoelectric properties, rendering the embedded sensor non-piezoelectric. Above 110 °C, the material experiences a reduction in its piezoelectric properties, known as depolarization onset, with significant polarization loss likely occurring at 135 °C. These factors collectively undermine the performance and reliability of the smart composite material at these elevated temperatures.

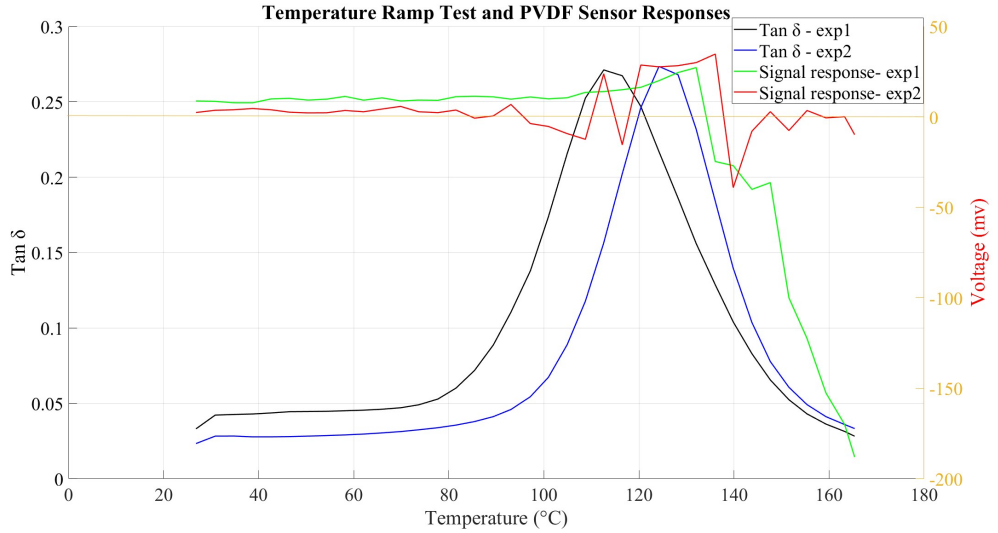


Figure 3.19: Illustration of the thermo-electromechanical properties as a function of temperature.

Figure 3.19 presents the piezoelectric response and the dissipation factor as a function of temperature. The results show a poor sensor response in the repeated experiment, confirming that when the smart composite was subjected to further temperature rise, a significant depolarization occurred. A conclusion can then be drawn from these findings to propose the optimal operating temperature of such smart composite materials.

## 3.5 Summary and Conclusions

In this chapter, a comprehensive fabrication and test process of a smart composite has been demonstrated in detail. In response to the rising ecological challenges and to the evolution of the technical composite materials with respect to the reduction of the environmental impact, materials were selected accordingly and described. Experiments were conducted to evaluate the piezoelectric intrusion impact on the global composite structure and to investigate the effectiveness of the manufacturing process to preserve the piezoelectric properties of the embedded element in the finished product.

The results demonstrated that with the application of PVDF film 52 $\mu$m thick, the effect on the structure is minimal. The tomograph results show minor to no resin pockets in the region where the piezoelectric element is located. This assures the mechanical integrity of the composite structure while introducing beneficial functional properties. Additionally, ILSS test results highlights the minimal impact of PVDF material on mechanical performance, showcasing a mere 0.69% degradation which was comparable to the reported results in the literature (pt-PVDF with degradation of 0.73%) a slight improvement is noted in our work. These findings emphasize PVDF film as a reliable choice for integration into composite materials. Compared to PZT, our utilization of copper-wired PVDF film demonstrated a superior ability to maintain material strength with a 7.11% impact against 15%. Furthermore, our assessment of resin pockets resulting from integration showed only minor resin pockets and no visible voids at the edges of the embedded element, particularly compared to composites with embedded bulk ceramics.

Based on the electromechanical experimental results, the integrated active element response displays high sensitivity to static and dynamic loading. With the growing need for continuous

structural health monitoring in the aeronautics and space industries, these test results indicate promising developments in integrating PVDF film patches as sensors for monitoring the health of composite structures. The recorded voltage response suggests good potential for obtaining energy from vibrations to deploy autonomous structural health monitoring systems. Besides, it has been recommended that the harvested energy could be used to power structural health monitoring systems [128].

The proposed use of natural fibers in developing smart materials was successfully demonstrated. However, as the X-ray micro-computed tomography results demonstrated, the flaws indicate some weakness that precludes their use in primary parts of aerospace structures. In fact, flax fibers have very low intrinsic properties when compared to carbon fibers comparable to glass fibers. Nevertheless, they can be used in secondary and interior parts where sensing is required. Because of its exceptional electrical insulation properties, it can be placed inside carbon fiber composite materials during fabrication after the incorporation of active elements to form a hybrid carbon-flax fiber composite. Natural fibers are also known to be very sensitive to moisture, which catalyzes their degradation; however, by encapsulating between carbon fiber plies, this effect can be avoided.

Additionally, the chapter provides critical insights into the thermo-electromechanical performance of smart composite materials under dynamic loading and temperature variations. The materials exhibit stable electromechanical behavior below their glass transition temperature (Tg), with a consistent response observed up to temperatures of approximately 105 °C. Beyond this point, it undergoes significant degradation in piezoelectric properties due to thermal stresses, mismatched thermal expansion coefficients, and depolarization. These findings emphasize the importance of considering operating temperature ranges to ensure the reliability and longevity of smart composites.

Significantly, this research experimentally determines the optimal operating temperature for these materials, paving the way for their further optimization and deployment in structural health monitoring systems. This is of utmost importance in the aerospace and civil engineering sectors, where the reliability of materials under varying environmental conditions is a key concern. By identifying the temperature threshold at which smart composites maintain their functional integrity, engineers can design more effective monitoring systems that anticipate and

mitigate potential failures due to thermal effects, inspiring a new wave of innovation in the field.

For the first time, this study offers a relevant understanding of the interplay between thermal and electromechanical factors in smart composites, providing a valuable reference for future research and development. The ability to pinpoint the specific temperature range within which these materials operate optimally enhances their applicability and contributes to the development of more durable and efficient smart systems. These advancements are expected to significantly improve critical infrastructure maintenance and safety, ultimately extending structures' lifespan and performance by incorporating these advanced materials.

In light of these findings, the subsequent chapter aims to delve into the potential applications of these materials.

# Chapter 4

# Evaluation of the Prospective Applications of Smart Composite Materials

---

## Contents

## 4.1 Introduction

As highlighted in previous chapters, piezoelectric materials have diverse applications and can be seamlessly integrated with fiber-reinforced composite structures without compromising their desirable properties, as demonstrated in Chapter 3. This chapter explores the potential applications of these smart composite structures, with a particular emphasis on their capabilities in energy harvesting (EH) and structural health monitoring (SHM) for aeronautic structures.

## 4.2 Embedded Piezoelectric Elements Towards Energy Harvesting

### 4.2.1 Related Literature

Energy harvesting (EH), or energy scavenging, refers to the process of capturing ambient energy and converting it into electrical energy. According to Kim *et al.* [129], EH involves gathering small amounts of energy from one or more nearby sources, such as movement (e.g., wind, wave), light, thermal gradients, and radiofrequency signals, and storing it for later use.

In this study, we are particularly interested in kinetic, i.e., vibrational energy harvesting, which can generally be achieved using magnetic or piezoelectric harvesting techniques. This process is enabled by the direct piezoelectric effect, where piezoelectric materials transform surrounding vibrations into usable electrical energy. It is worth noting that while piezoelectric energy harvesting offers a method for capturing vibrational energy, its output power is relatively low [130]. Sodano *et al.* [83], and other numerous researchers point out that the energy obtained is typically insufficient to directly power electronic devices, necessitating its accumulation in a storage device like a rechargeable battery. The efficiency of these devices depends on the advancement of techniques for collecting and storing harvested energy. Due to their high impedance, these devices generate high voltage but low current [38]. The EH strategy has revolutionized wireless sensing technology. These wireless sensors are typically designed to monitor in remote locations and occasionally within structures. Consequently, accessing these sensors to replace their batteries can be challenging. Through energy recuperation, piezoelectric materials capture ambient energy from the environment, which is then used to power these sensors and their batteries, extending their lifespan [129].

In the context of aeronautics, EH can be realized using active composites with embedded strain piezoelectric harvesters that take advantage of the strain of a vibrating aeronautical component. Moro *et al.* [128], for example, in their investigation of vibration energy harvesting for use in aircraft, placed the piezoelectric patches on the wing slats of a plane, noting that the most exploitable vibrations come from turbulence and random engine vibrations. These vibrations are beneficial because they last the entire flight when the slat is deployed and retracted. The energy obtained from this dynamic strain has one of the essential uses in aeronautics: powering the structural health monitoring systems [38, 128, 131]. Interested readers may refer to the thorough review of EH technologies for the structural health monitoring of airplane components presented by Zelenika *et al.*, [131]. Moreover, Pearson *et al.*, [38] investigated the feasibility of vibration EH to supply wireless sensor nodes for continuous health monitoring of aerospace structures. Therefore, this part of the thesis investigates the feasibility of employing smart composites to harness vibrational energy from aeronautic structures.

### 4.2.2 Associated Finite Element Analysis (FEA) Modeling

Modeling was conducted using COMSOL Multiphysics to analyze the potential of a smart composite beam integrated with a piezoelectric element for supplying considerable energy under vibration analysis. Additionally, this modeling aimed to validate our design and experimental test configurations. In this investigation, a 250 mm by 50 mm by 0.952 mm flax fiber-based composite plate was designed in 3D and integrated with a PVDF film measuring 60 mm by 12 mm by 0.052 mm as illustrated in Figure 4.1a. The parameters of flax material were user-defined according to the provided material properties presented in Table 3.1, and the piezoelectric material parameters of PVDF were taken from the COMSOL Materials Library. For the solid mechanics part, a fixed constraint boundary condition was added to the fixed end, and the end of the cantilever was left free. To emulate the shaker, a boundary load was applied to the top surface of the plate. A free tetrahedral mesh with an extra fine size was used for meshing to ensure detailed resolution. The study conducted was time-dependent, with a domain probe utilized to acquire signals from the embedded PVDF element. A time-dependent study was essential for accurately capturing the energy harvesting system's dynamic response and transient behavior, providing realistic insights into its performance under varying loading conditions. Additionally, a Rayleigh damping model was employed to accurately capture the dynamic response of the cantilevered beam with an embedded piezoelectric element during the time-dependent analysis.

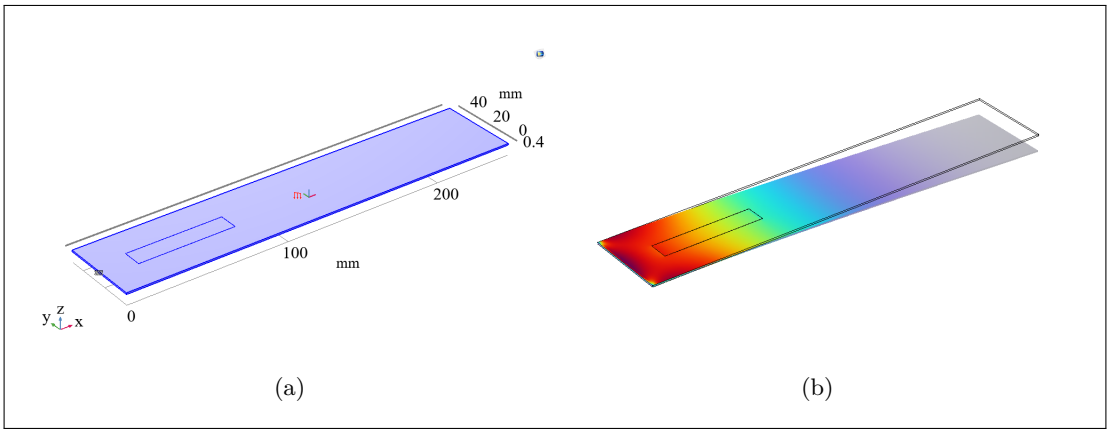


Figure 4.1: Illustration of: a) the designed geometric model of a smart composite beam integrated with a piezoelectric element, and b) a modeling surface plot showing the stress distribution from a time-dependent study under a boundary load.

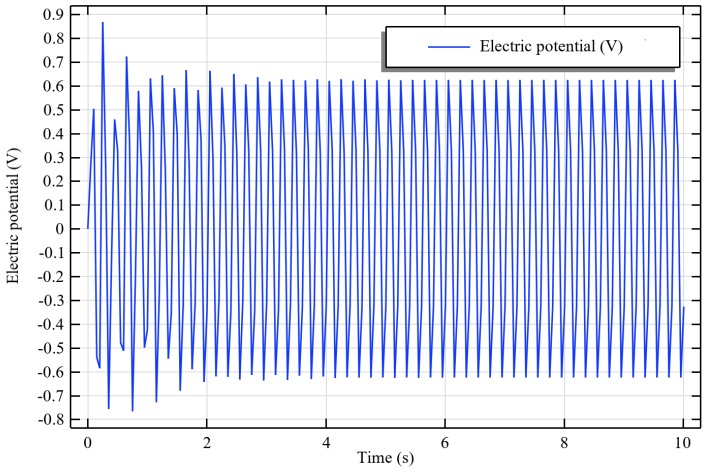


Figure 4.2: The model response, obtained from FEA modeling

The surface plots in Figure 4.1b illustrate the stress distribution at an instant on the cantilever when subjected to vibrational bending, with maximal stress being exhibited at the clamped end as expected. On the other hand, figure 4.2 presents the voltage response of the embedded piezoelectric element, showing an approximate value of 1.2 V peak-to-peak. This value indicates the piezoelectric element's capability to generate a substantial amount of energy, which can be utilized in energy harvesting to enhance autonomous structural health monitoring, where batteries do not need to be a concern. It should be noted that this analysis was performed to provide a qualitative idea of the expected experimental results. Further parameter optimization could be carried out to obtain quantitative results that align with experimental tests.

### 4.2.3 Experimental Investigations

Experiments were conducted to determine the maximum current and power generated from these new composite structures when subjected to vibrations at a given frequency. The new experiment was set up as shown in Figure 4.3, with the output voltage being passed through resistance in series. The equipment used in this experiment comprised a linear power amplifier (LDS LPA 100 by Bruel & Kjaer), a permanent magnet shaker (LDS V201), a function generator

(HM 8030-3), a picoscope (PICOSCOPE 2204A), a power supply (EA-PS 2384-03B), and a honeycomb optical breadboard (M-IG-32-2).

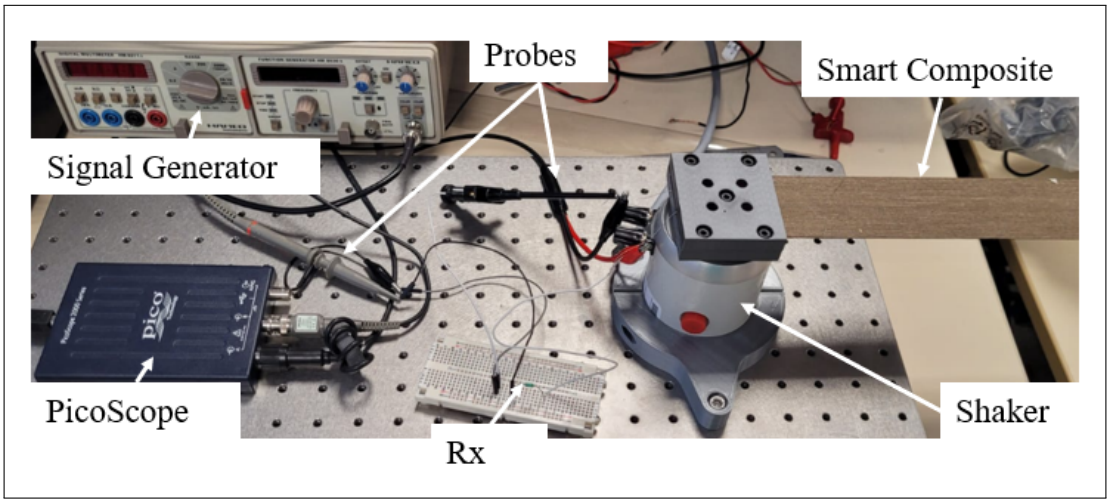


Figure 4.3: The system's current and power extraction experimental set-up.

Two probes were employed: one to directly monitor the signal originating from the oscillating smart composite (CH1) and another to capture the signal after its passage through the resistor Rx (CH2). Different Rx values were systematically evaluated to prevent interference with the system-generated signal, and the resulting outputs were observed using a PicoScope. Figure 4.4 presents the circuit utilized to evaluate current from the system.

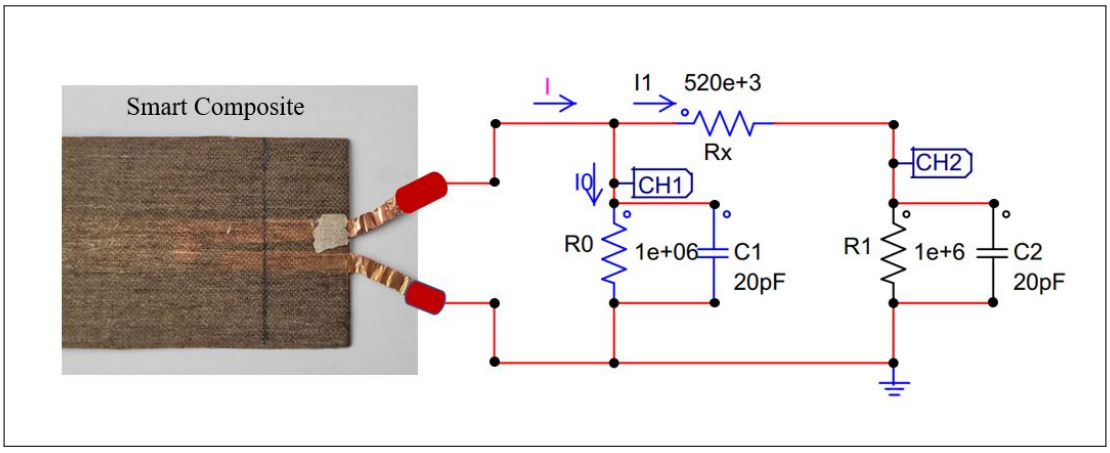


Figure 4.4: The system's current and power extraction circuit.

According to the current divider rule, considering the circuit shown in Figure 4.4, the total current can be computed using the formula:

$$I = I0 + I1 \tag{4.1}$$

where *I1* is given by;

$$I1 = \frac{R0}{R1 + R0} I = \frac{V0 - V1}{Rx} \tag{4.2}$$

Therefore the current generated by the system can be obtained from:

$$I = \left(\frac{R1 + R0}{R0}\right)\left(\frac{V0 - V1}{Rx}\right) \tag{4.3}$$

To compute the root mean square values of the current and the voltage obtained from the systems, the following formulas were considered:

$$I_{\text{RMS}} = \frac{I_{\text{peak}}}{\sqrt{2}} \quad \text{and,} \quad V_{\text{RMS}} = \frac{V0_{\text{pk-pk}}}{2\sqrt{2}} \tag{4.4}$$

Thus the root mean square power can be evaluated as:

$$P_{\text{RMS}} = I_{\text{RMS}} \cdot V_{\text{RMS}} \tag{4.5}$$

### 4.2.4 Discussions

During this investigation, three distinct samples were examined for maximal output power. In the first sample, a PVDF piezo patch was incorporated within the midplane, precisely positioned between layers 3 and 4 of the laminate structure. The second sample encompassed a piezo patch between layers 4 and 5, while the third sample entailed a piezo patch inserted between layers 5 and 6 of the smart composite beam. Samples were clamped and vibrated using an LDS V201 shaker (see Figure 4.3). The obtained results were compiled and presented in Table 4.1.

It is worth noting that the probes' capacitances C1 and C2 were observed to have no impact on the system's response. This was evident from the fact that the signal response for CH1 and CH2 were in phase, this can be visualized in Figure 4.5 and 4.6. We could attribute this to

low operating frequencies (13.18 Hz); thus, the component impedance is very high, leading to minimal to no observable influence. This can be understood from the formula provided below.

Table 4.1: The experimental results of the current and power measurements at 13 Hz using a 520 kΩ resistor in series with the system.

| **Sample (Piezo Position)** | **Frequency [Hz]** | **Peak to Peak Voltage [mV]** | $V_{RMS}$ **[mV]** | $I_{RMS}$ **[$\mu$A]** | **Power [$\mu$W]** |
|---|---|---|---|---|---|
| Layer 5-6 | 13.18 | 1550.7 | 548.3 | 1.5919 | 0.8727 |
| Layer 4-5 | 13.18 | 802.1 | 283.6 | 0.7580 | 0.2150 |
| Layer 3-4 | 13.18 | 169.0 | 59.8 | - | - |

$$Z_c = \frac{1}{\omega C}, \quad \text{where} \quad \omega = 2\pi f \tag{4.6}$$

Figure 4.5 and 4.6 present the test results. The system response for a smart composite structure that contains piezo between lamina 5 and 6 produced more power (see Figure 4.5). This presents potential energy harvesting from the vibrating structures, which could aid in powering the structural health monitoring sensor nodes.

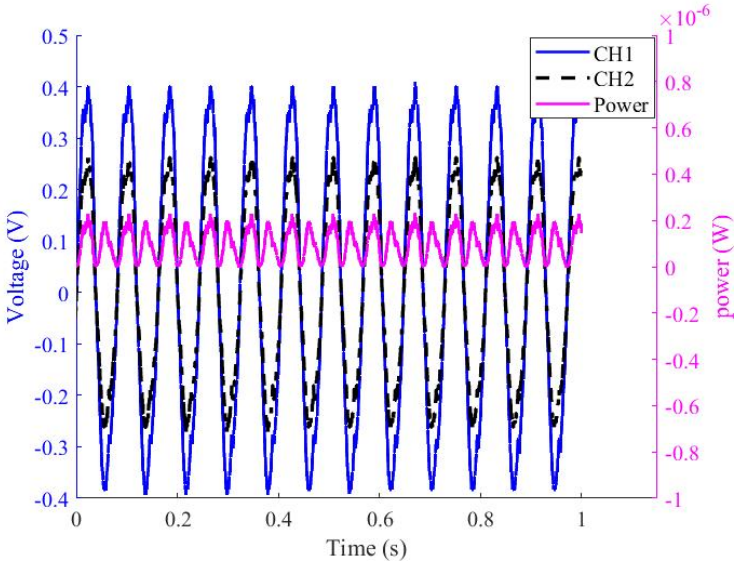


Figure 4.5: The system's response, obtained from the sample with a piezo patch embedded in layers 4-5 of the laminate composite and excited at a frequency of 13.18 Hz, showcases an output power of 0.2150 $\mu$W.

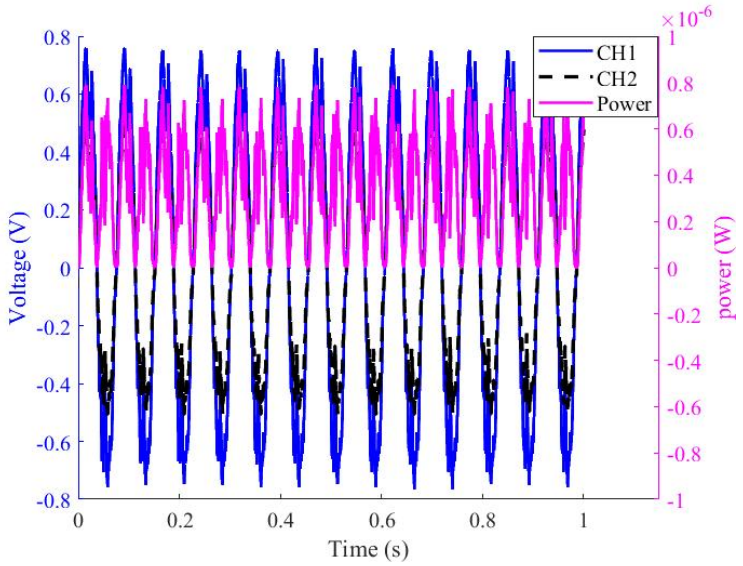


Figure 4.6: The system's response, obtained from the sample with a piezo patch embedded in layers 5-6 of the laminate composite and excited at a frequency of 13.18 Hz, showcases an output power of 0.8727 $\mu$W.

At this point, it becomes essential to determine the effectiveness of a PVDF (Polyvinylidene fluoride) material embedded in FlaxPreg composite to convert mechanical vibrations into electrical energy, which could be applicable in energy harvesting. Therefore, evaluating its Figure of Merit (FOM) could provide insight into the maximum power output of our structure under vibrations. To determine this FOM, we consider the operational mode in which our design functions—specifically, the thickness mode ($d_{33}$)—and this assessment is conducted within the realm of low-frequency vibrations.

Our choice of $d_{33}$ is driven by the fact that the PVDF is poled in this direction, making it the most responsive to mechanical stress along this axis. This mode ensures that we are utilizing the material's highest efficiency for energy conversion. Although the beam is subjected to bending, the PVDF material remains poled in the $d_{33}$ direction, meaning that the most effective piezoelectric response occurs when mechanical strain is applied along this axis. While the strain varies across the thickness of the beam under bending, the $d_{33}$ direction remains the primary axis for energy conversion. Thus, even under bending conditions, the $d_{33}$ mode is the most appropriate choice for capturing the maximum electrical response from the piezoelectric material, as it aligns with the dominant strain direction. To facilitate this evaluation, we employ

the formula provided below:

$$FOM = \frac{{d_{33}}^2}{\varepsilon_{33}} \quad [132] \tag{4.7}$$

where $d_{33}$ is the piezoelectric strain constant in meters per volt (m/V) and $\varepsilon_{33}$ is the permittivity constant in farads per meter (F/m). The value of $d_{33}$ is -33×$10^{-12}$ m/V and $\varepsilon$ is 110×$10^{-12}$ F/m. Upon substituting these values in the formula above the FOM is determined to be $9.9 \times 10^{-12}\ m^2/V^2$. While this FOM value alone gives valuable information on the material's conversion efficiency, it should be considered alongside actual power output. Our experiments have confirmed the generation of microwatts of power, aligning with the expectations set by this FOM. These results demonstrate the practical applicability of our PVDF-enhanced smart composite material for efficiently harvesting energy from mechanical vibrations.

Another very crucial parameter that is very important to determine is the energy storage density (ESD), which can be obtained in a simplified way from the equation below:

$$ESD = \frac{1}{2} \times \varepsilon \times E^2 \quad [133] \tag{4.8}$$

where $\varepsilon$ is the dielectric constant and E is the generated voltage. This equation holds because our operation at relatively low frequencies allows for approximating the embedded piezoelectric element as a parallel plate capacitor. Taking the earlier provided value of the $\varepsilon$, and E to be the $V_{RMS} \approx 0.5483$, and the embedded PVDF patch area as (0.060 m×0.012 m), we obtain a normalized ESD value of $\approx 2.2965 \times 10^{-08}\ J/m^3$. Our material's ability to store energy and generate microwatt power makes it highly valuable for autonomous structural health monitoring in aeronautics, enhancing safety and reliability.

In summary, this section has briefly discussed the potential functionalization of classical composite parts by integrating active materials for energy recovery. The following section delves deeper into utilizing these advanced structures for monitoring and enhancing the safety of aerostructures. Their demonstrated capability for self-powering aims to enable continuous monitoring.

## 4.3 Embedded Piezoelectric Elements Towards Structural Health Monitoring

### 4.3.1 Related Literature

The ongoing evolution of materials and structures, characterized by heightened functionality, reliability, and performance, has facilitated the integration of sensors, processing units, and control mechanisms at various points within structural systems or through co-fabrication processes [134]. Currently, various industrial sectors, such as aerospace, are striving for a greener future to achieve high performance with optimal energy efficiency. As a result, promising solutions such as lightweight fiber-reinforced composite materials for aerospace structures have been adopted [18, 19]. There is, however, no doubt that the widespread use of these composite materials for aircraft parts, including engine fan blades, fuselage, wings, and other critical underlying components as presented in Chapter 1, requires the continuous monitoring of their mechanical integrity during operation, since these components are vulnerable to failure due to overloads and fabrication flaws that occur throughout the manufacturing process, in order to prevent their progression [24].

Indeed, despite the well-established nature of the NDT technologies, autonomous monitoring systems are still in high demand. The solution lies in harnessing the potential of intelligent structures, particularly in industries like aeronautics. Substantial downtime occurs due to routine maintenance, leading to lost revenue when aircraft are grounded for inspection and repairs. This section explores an innovative approach using smart materials to enhance condition-based maintenance, ultimately cutting life-cycle costs. The study emphasizes a paradigm shift toward SHM, utilizing embedded sensors for real-time monitoring. In fact, the current literature reveals a significant increase in research on SHM systems for composite materials, with researchers actively investigating various methodologies, notably those utilizing integrated sensors [28, 29, 40, 41, 78, 81, 85, 89, 109, 112, 135, 136]. For example, Paget et al. [87] conducted an illustrative study on damage detection using the Lamb wave technique by embedding a piezoceramic transducer in composites. Lamb waves, defined as elastic waves propagating in a solid plate with free boundaries [42, 87], were leveraged for their exceptional sensitivity to early-stage structural

deterioration, employing PZT sensors for wave transmission and reception. The study introduces methods of identifying impact damages from Lamb waves, including the amplitude-based method, which compares wave responses before and after damage, and the time-based method, which analyzes changes in Lamb wave modes over time. The study demonstrates the efficacy of these techniques in damage detection systems for composites. However, it provides limited discussion of the specific variations in local amplitude concerning the severity of damage to the structure.

Several other studies have been conducted on SHM methods with embedded piezoelectric sensors. In their comprehensive review, Philibert et al. [42] delve into Lamb-wave-based technologies for the monitoring of the structural health of composite materials in aircraft applications. The study explores diverse methods and techniques employed in damage detection, primarily emphasizing those utilizing piezoelectric transducers. The authors introduce an intriguing damage assessment and monitoring concept, incorporating passive and active sensing approaches. In the realm of passive sensing, measurements rely on the disturbance of the structure caused by an unforeseen event, like an impact or the development of a crack. Such events typically produce elastic waves, continuously detected by sensors monitoring structural health [44]. In contrast, the active sensing approach employs an actuator to generate a controlled signal that travels through the structure. An integrated sensor captures these signals, and any deviations from the established baseline signal indicate potential growth or damage initiation [137]. However, a comprehensive study is still required to thoroughly comprehend and categorize the most effective methodologies for the analysis and detection of various types of damage based on the data collected from these seemingly promising approaches.

Masmoudi et al. [40] employed a passive sensing approach to monitor the structural health of composites, incorporating implanted piezoelectric sensors and utilizing the acoustic emission (AE) technique. This method was proven to be effective for real-time damage monitoring, generating transient ultrasonic waves in response to damage development within the material. In their work, they positioned the sensor in the midplane of a laminated composite structure. They subjected it to three-point bending tests with static and creep loading while continuously employing the AE technique to monitor the response. The analysis of these AE signals revealed three distinct acoustic signatures corresponding to different damage mechanisms in composites:

matrix cracking, fiber–matrix debonding, and fiber breakage. This study is, however, limited to observations based on the amplitude change under static loading, not providing further features of interest in detection other than the amplitude distribution. In contrast, Chen et al. [28] applied active sensing with a fully distributed set of integrated piezoelectric sensors, utilizing the time-of-flight (ToF) technique, a method based on a wave's propagation time measurement. Their investigation introduces the application of Fast Fourier Transforms (FFT) in analyzing signal responses to understand the impact of damage and elucidate the relationship between the response and its magnitude. However, the study confines its examination solely to the amplitude of the FFTs. It is imperative to incorporate diverse parameters to identify and classify specific damage characteristics effectively.

Therefore, in response to the growing demand for innovative solutions in the competitive aeronautic industry, our work aims to fabricate a cutting-edge smart composite structure with embedded sensors for SHM. Indeed, to compete in a highly competitive market environment, the aviation sector is actively exploring ways to reduce maintenance costs for aircraft, and full-scale SHM systems remain a subject of ongoing investigation. Eventually, this could be achieved by harnessing the potential of embedded sensors within the aircraft structure; this study, therefore, seeks to usher in a significant paradigm shift, eliminating the need for external sensors and enhancing the identification and monitoring of barely visible impact damages in composite structures, as well as significant and noticeable damages that may result from impact during operation. This part of the thesis focuses on refining SHM methods, ultimately contributing to a more efficient and cost-effective approach to aircraft maintenance in the future.

This study begins its exploration by examining the passive sensing approach, focusing on evaluating AE signals. The primary objective is identifying the optimal piezoelectric element for integration into SHM systems. The study assesses their suitability for the continuous monitoring of structural deterioration and their impact on the overall composite structure. An active sensing approach centered on Lamb wave propagation and corresponding damage diagnosis methods is introduced. An amplitude-based approach, utilizing correlation functions, is presented to gauge the damage severity. Further analysis is conducted in the frequency domain to extract multiple feature parameters for damage detection. A damage index function is formulated based on these extracted parameters. A finite element modeling approach using the COMSOL Multiphysics

software version 6.2 is also introduced aiding in understanding the damage's impact and the wave propagation behavior within structurally compromised systems. Finally, the experimental data are meticulously compared and validated against the results obtained from numerical analysis.

### 4.3.2 Materials Used and the Fabrication Processes Applied

The materials considered in this study are an Epoxy E-Glass Woven prepreg (HexPly® M34/41%/300H8/G), an adhesive-based conductor in the form of copper foil tape, and FV301940/3 polyvinylidene fluoride (PVDF) polymer-based piezoelectric material. The properties of these materials are presented in Chapter 3.

Additionally, a lead zirconate titanate material (PZT 5H ref. PIC 151), with a 0.2 mm thickness, also referred to as soft PZT, developed and supplied by Physik Instrumente (PI), Karlsruhe, Germany, was explored for integration. The PZT's properties are well described in the study of Ioan et al. [72] and presented in Table 4.2.

Table 4.2: Material properties of lead zirconate titanate (PZT), a ceramic-based piezoelectric material.

| **Material** | **Density** | **Max Operating Temperature** | **Piezo Strain Constant** | **Young's Modulus** | **Thickness** |
|---|---|---|---|---|---|
| PZT | 7870 [kg/m$^3$] | 230 [°C] | $d_{31}$= −300<br>$d_{33}$= 600<br>[($10^{-12}$) C/N] | 62 [GPa] | 0.2 [mm] |

Following the fabrication process and steps highlighted in the previous chapter, similar approach was employed to manufacture smart composite samples of varying sizes as depicted in Figure 4.7, however, in the present case, distinct materials and a unique wiring procedure for the active elements were utilized.

Two square plates of 100 mm×100 mm featuring six Epoxy E-Glass prepreg plies oriented at 0° were prepared for our study. Piezoelectric material patches were embedded on both ends of the plate between the 5th and the 6th lamina. One of the square plates was composed of a 20 mm × 20 mm × 0.2 mm PZT 5H patch on one end, intended to act as a signal generator/transmitter (actuator), and on the other end was a 20 mm × 20 mm × 0.052 mm PVDF piezo film patch, anticipated to act as a sensor/receiver. The other plate featured patches of the same material,

a PVDF film, measuring 20 mm × 10 mm × 0.052 mm. Additionally, two 200 mm × 30 mm smart composite beam plates were fabricated, with one featuring a 20 mm × 20 mm PZT 5H and the same size of PVDF film patch in the other sample integrated into the middle part of the beam at the same layer positions as those embedded in the square plates.

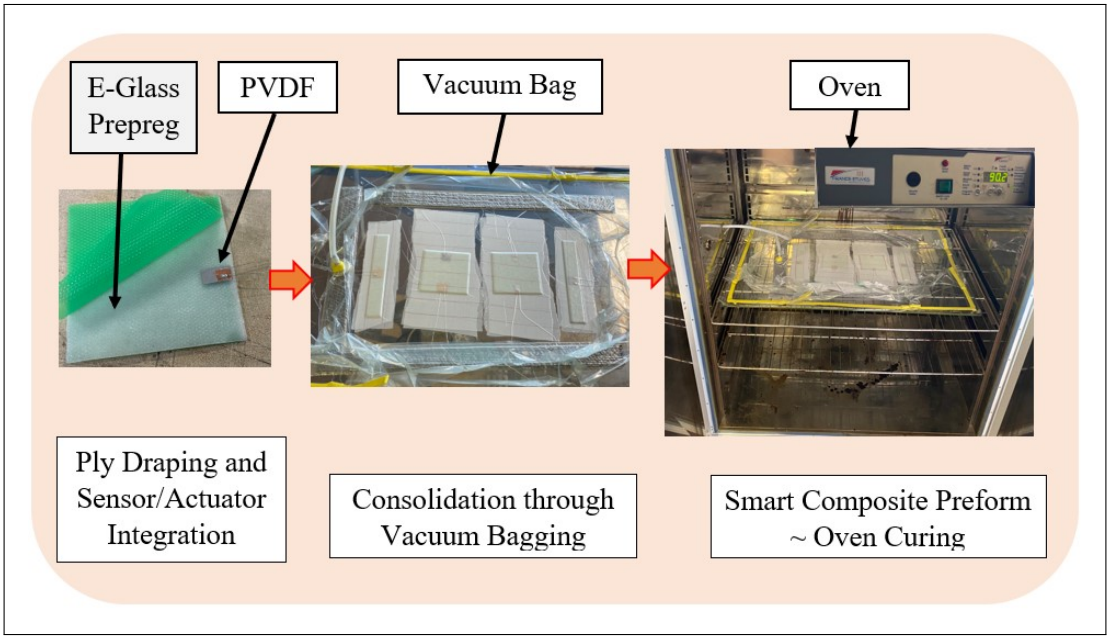


Figure 4.7: Samples fabrication process through consolidation molding with a curing temperature of 90 °C for 90 min.

The embedded piezoelectric patches were wired utilizing adhesive-based copper conductors with tinned copper wires soldered onto them to achieve a desirable length for easy data gathering. The consolidated prefabricated smart composite plates were cured in an oven under 1 bar pressure at 90 °C for 90 min. De-molding was subsequently completed, and the resulting samples were collected for experimental tests.

### 4.3.3 Evaluation of the Viability of Embedded Piezo-Type Sensors for Structural Health Monitoring Using a Passive Sensing Approach and Their Impact on the Structure

The experimental setup for the analysis of the potential of the embedded PZT and PVDF patches to detect faults within fiber-reinforced composites in real time while in passive mode is shown in Figure 4.8. The 200 mm × 30 mm × 1.7 mm smart composite beams presented in the figure below were subjected to a 4-point bending test on the Zwick Roell Z100 material testing equipment, manufactured by ZwickRoell in Ulm, Germany to facilitate this evaluation. The loading span was set to half of the support span, following the ASTM D6272 standard. The test sample was preloaded to 1 N and continually deflected with a 5 mm/min cross-head speed until it failed.

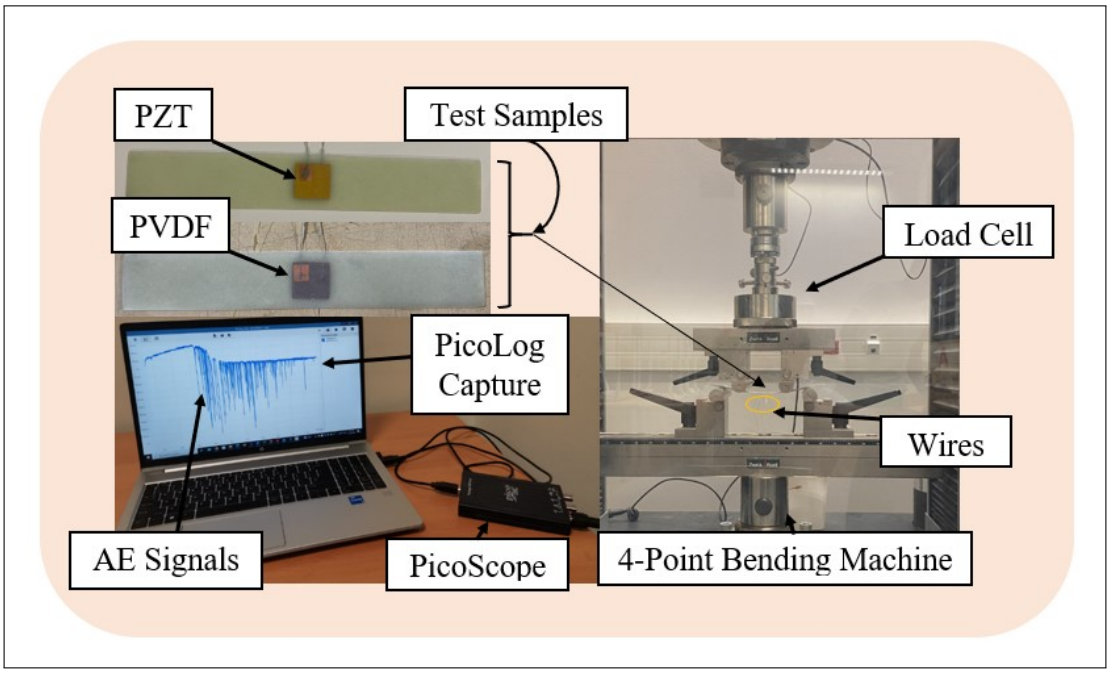


Figure 4.8: Four point bending test of the fabricated smart composite plates featuring embedded PVDF and PZT sensors to investigate passive sensing approach through acoustic emissions (AE).

Concurrently, after reaching the preload value, PicoLog 7, a data logging software in streaming mode, was set to collect real-time data from the embedded sensor and display the response,

which relied on the PicoScope 2000 series (2204A) for data acquisition. This recording provided relevant information for the SHM evaluation, including the time of material failure and the maximum flexural strength that it could withstand shortly before damage propagation. In contrast to other studies within the same framework, such as those conducted by Lampani et al. [112] and Tuloup et al. [138], which solely rely on the evolution of electrical capacitance to evaluate damage, our current work captured acoustic signals. This approach was employed to assess the suitability of both PVDF and PZT materials in detecting damage initiation. Furthermore, it was extended to verify the influence of integrating these materials into fiber-reinforced composite structures.

### 4.3.4 Evaluation of Actuator–Sensor Configuration in Active Sensing Approach

Figure 4.9 illustrates the experimental setup utilized in the active sensing approach. A 100 mm×100 mm×1.7 mm plate with a single pair of actuator-sensor underwent testing using the pitch-catch method described in [137, 139, 140]. Leveraging the sensitivity of Lamb waves to structural damages like cracks, this SHM test employed an embedded PZT to generate Lamb waves. These waves were transmitted across the plate and captured by a passive PVDF sensor. The received signal served as the baseline for an undamaged structure, referred to as "Healthy" in this study. Subsequently, artificial damage in the form of a through-hole was induced, and signal responses from various damage sizes were collected. These data were then compared with the baseline of the undamaged structure, aiming to verify potential variations and assess the feasibility of the active sensing approach for SHM.

The equipment used in this experiment comprised a digital function generator (Topward 8112 developed by SpenceTek, Inc., Cupertino, CA, USA), a digital oscilloscope (Tektronix TBS 2104 manufactured by Tektronix, Inc., Beaverton, OR, USA), a power supply (EA-PS 2384-03B developed by EA Elektro-Automatik group, North Rhine-Westphalia, Germany), a honeycomb optical breadboard (M-IG-32-2 manufactured by Newport Corporation, Irvine, CA, USA), and an in-house voltage amplifier, presented in Figure 4.10, bearing the characteristics illustrated in Figure 4.12.

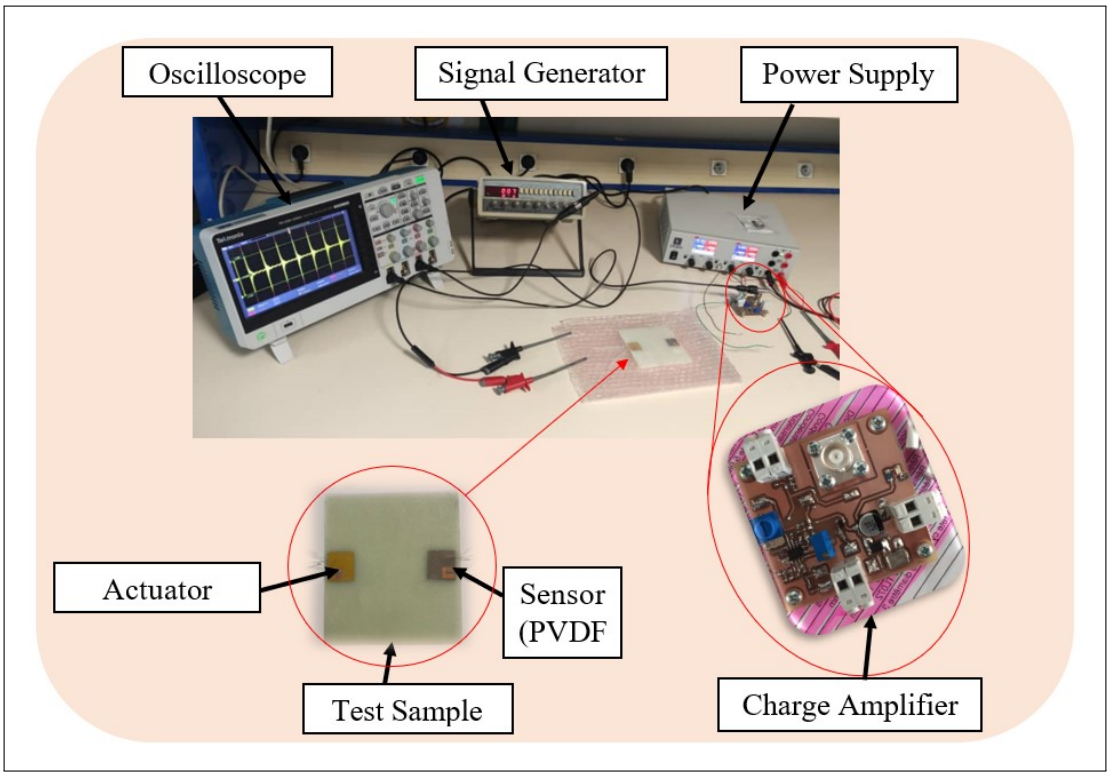


Figure 4.9: Investigation of the active sensing approach through actuator–sensor configuration (pitch-catch) based on Lamb wave propagation. A rectangular waveform with an amplitude of 31.75 V was applied to the PZT at a frequency of 6 Hz.

Figure 4.10 illustrates the circuit of the amplifier specifically designed and manufactured for this study. The configuration consists of two cascaded operational amplifiers operating in closed-loop mode with negative feedback. This design ensures that the operational amplifier (OP-Amp) does not reach saturation and functions in the linear mode. At the input of the sensor signal, a capacitor is incorporated to eliminate any DC signal, allowing only the preservation of the AC signal response generated by the Lamb wave. Following the gain formula of the inverting amplifier (-Rf/Rin) and utilizing the given parameters, the voltage gain was determined to be 25. A simulation was conducted to determine the amplifier's bandwidth following the circuit illustrated presented in Figure 4.11. Figure 4.12 depicts the simulation results, revealing the $-3$ dB frequency point at 374 kHz.

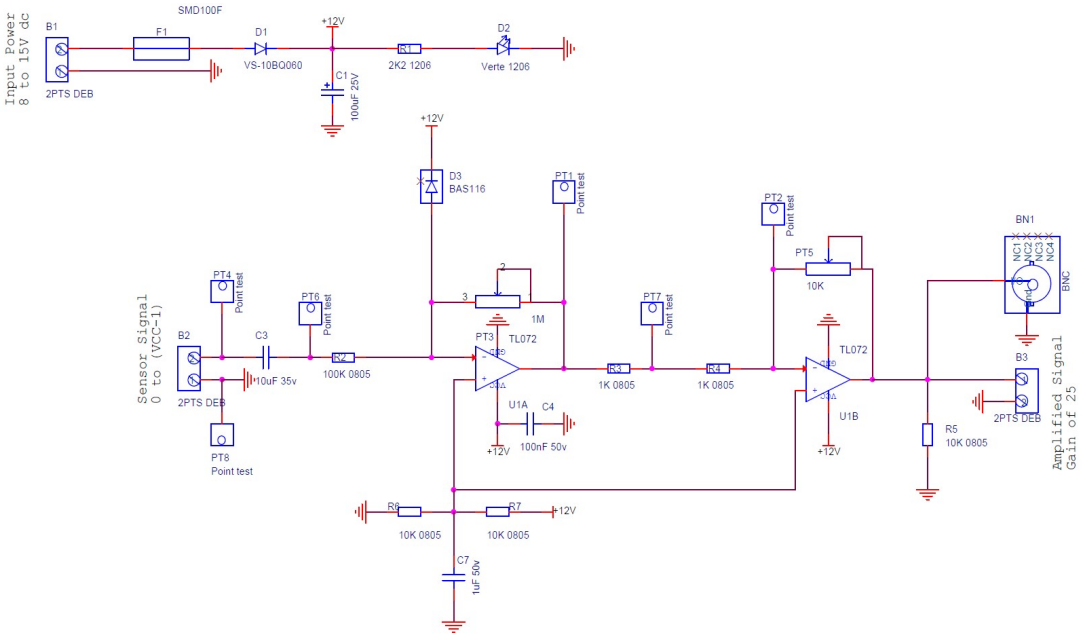


Figure 4.10: A schematic of the charge/voltage amplifier designed and manufactured to amplify the magnitude of the sensor signal.

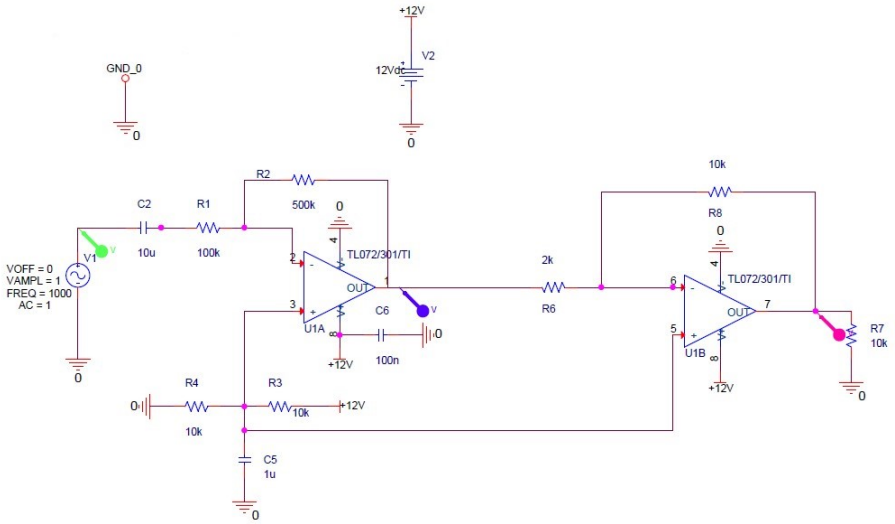


Figure 4.11: Illustration of the amplifier simulation circuit.

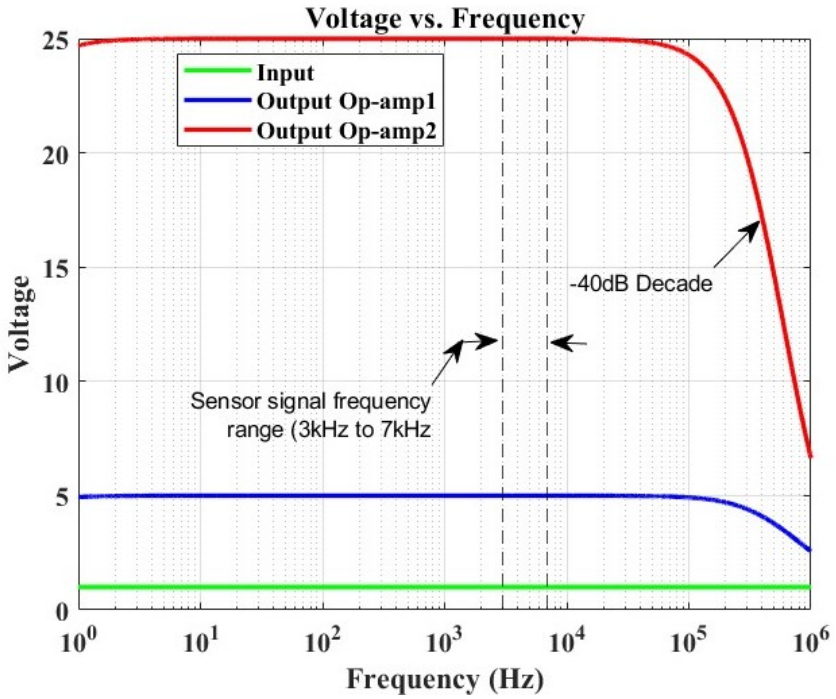


Figure 4.12: Frequency response simulation of an OrCAD-based amplifier, illustrating a voltage gain of 25 and a −3 dB frequency point at approximately 374 kHz. The sensor signal frequency range demonstrates a constant gain without any filter interference.

The primary concern lies in evaluating the impact of the amplifier on the recorded sensor signal. The sensor signal frequencies were analyzed, indicating a frequency range of 3–7 kHz. It was observed that the amplifier did not adversely affect the signal response, as the range remained consistent throughout the frequency response evaluation of the amplifier, with no filter interference. Consequently, the amplified signal was deemed suitable for SHM investigation within the scope of this study.

### 4.3.5 Assessment of Finite Element Modeling (FEM) through Active Sensing

A finite element analysis based on the COMSOL Multiphysics software's solid mechanics module was implemented to complement and validate the experimental data in the study of the active sensing SHM approach. The developed model, illustrated in Figure 4.13 with the associated dimensions, included defined material properties for the glass fiber presented in Chapter 3.

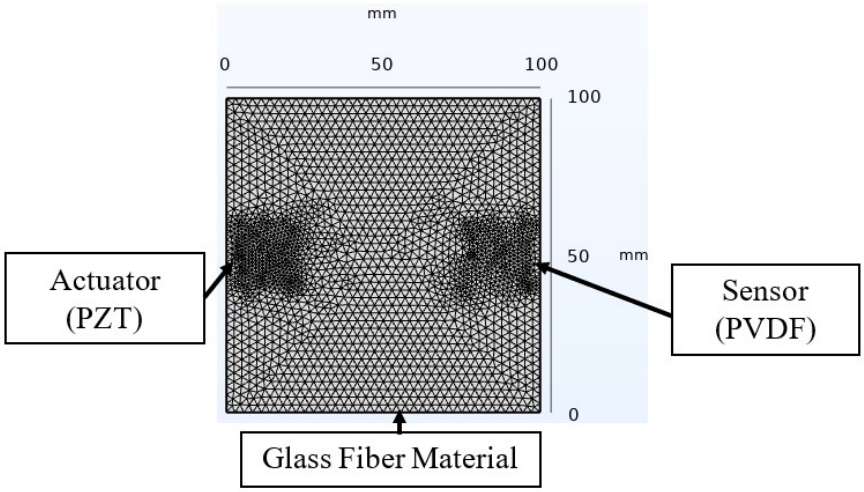


Figure 4.13: Finite element modeling of the Lamb wave propagation technique for SHM based on COMSOL Multiphysics software.

For the piezoelectric elements, materials were selected from COMSOL's material library. The analysis assumed perfect bonding at the material interfaces in the smart composite throughout the test, ensuring that no slippage occurred between different layers [141]. In this approach, a step signal was applied to the PZT, and a domain probe captured the transient response from the PVDF sensor. The model utilized a free tetrahedral mesh with a normal density to optimize the computation time, selected after a mesh refinement approach, which showed a negligible impact on the received signal. The study, executed in the time domain, employed a fixed time step of $3.2 \times 10^{-6}$ s, matching the acquisition period in the experiment. A fixed timestep was chosen to ensure consistency with the experimental data, aligning the simulation and experimental results for accurate comparison. Additionally, using a fixed timestep provided better numerical stability, as it reduced the risk of instability or divergence in the simulation. It simplified the computational process by maintaining a consistent temporal resolution, improving convergence, and ensuring reliable results. Furthermore, a fixed timestep reduced computational overhead and made the post-processing of data more straightforward, as the data was recorded at uniform intervals. Similar damages to those induced in the experiment were investigated to analyze the variability.

## 4.4 Results and Discussion

This section presents the results obtained from the experimental tests conducted for both the passive and active sensing approaches, accompanied by corresponding discussions. Additionally, numerical modeling results are provided and compared with the experimental findings. Each discussion includes deductions relevant to the design and considerations for SHM strategies.

### 4.4.1 Passive Sensing Approach

#### 4.4.1.1 Mechanical Aspect

The load–displacement curve from the four-point bending test of the specimens with PZT and PVDF embedded is shown in Figure 4.14. This test was carried out solely to determine the mechanical behavior of smart composite materials when these two different types of piezoelectric materials are embedded, as well as to conclude their suitability to act as passive sensors while selecting the best that can capture the AE signal for continuous damage monitoring. This study is necessary since the literature has supported the embedding technique with the aim of protecting sensors from their surrounding environment, while creating integrated structure with smooth surfaces that could ensure, for instance, sustained aerodynamics in plane structures.

The loaded samples show two domains in the load–displacement curve: a linear elastic deformation zone followed by a plastic deformation zone with a non-linear displacement. This observation is consistent with the findings of Lampani et al.'s [112] investigation. Indeed, at the start of the test, the specimen bent without slipping on the bottom fixture. Still, as time passed, after the material's yield strength was reached, significant slippage was observed, with the deflection curvature increasing between the two fixtures, resulting in the non-linear zone depicted in the figure. This result could also be related to the fact that, in the case of four-point bending tests of flexible materials, a zone with a rapid rupture is rarely observed since the material may fail by folding without noticeable cracks.

The sample with the PZT-based element demonstrated higher ultimate strength than its counterpart, highlighting the significant impact of the embedded piezoelectric element on the response. This phenomenon can be attributed to the implanted elements' tendency to increase

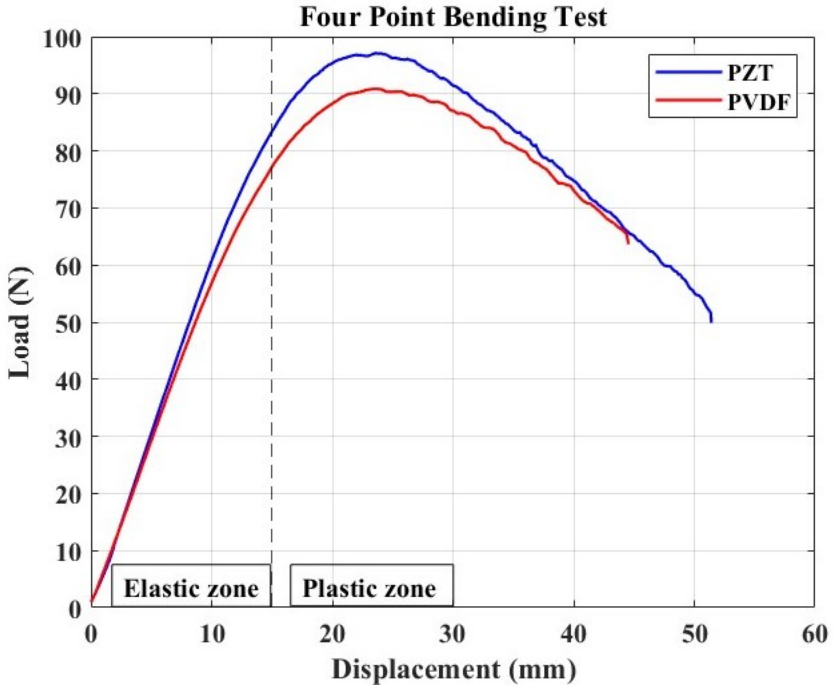


Figure 4.14: Load–displacement curve resulting from the 4-point bending test with noticeable linear (elastic) and non-linear (plastic) zone. Maximum load attained by a sample with PZT is 97.1 N, and it is 90.8 N for that with an embedded PVDF patch.

the host structure's stiffness [29, 112]. Consequently, we applied the flexural stress formula specific to a four-point bending test for our test case, where the loading point is set at half the support span. This formula is presented in Equation 4.9, following the ASTM D6272 - 2 standard test method for the flexural properties of unreinforced and reinforced plastics and electrical insulating materials by four-point bending. The maximum flexural strength determined for the PZT-based sample was 7.6174 MPa, compared to 7.1252 MPa for the PVDF-based sample. These results indicate that the PZT ceramic sample was approximately 6.9% stiffer than the one with a polymer-based piezoelectric element.

$$\sigma_{f_{max}} = \frac{3F_{max}L}{4bd^2} \tag{4.9}$$

where $F_{max}$ is the maximum load attained, $L$ is the support span, $b$ is the width of the beam, and $d$ is the beam thickness.

It is also critical to note the smoothness of the curve shortly after the ultimate strength

point. The response becomes non-smooth at this point in the load–displacement curve, which could indicate the onset of BVID in the form of microcracks. This decision is intended to be made based on the signal acquired continually in this setup, as these damages are expected to generate elastic waves in the form of AE impacts, which may then be captured and transmitted by the passive embedded sensor.

#### 4.4.1.2 Sensor Performance

In the SHM approach, there is a distinct advantage to using piezoelectric materials' electromechanical properties, which allow them to operate as transducing elements. As a result, the evaluation of the embedded piezo elements' capacity to identify the beginning and progression of damage in composite structures was evaluated using the results of the four-point bending test, which involved continuously recording the sensor signal response in real time by the experimental setup.

Figure 4.15 depicts the signals of AE events recorded during the bending test, alongside the load curves plotted against time. This presentation aims to visually capture the evolution of the AE responses with reference to the mechanical behavior of the material subjected to the test.

The first curve in blue corresponds to the responses of the samples bearing PZT as a sensor. It can be seen that within the linear domain, where the beam experiences compression from the loading points with a linear displacement, the PZT experiences tension and yields a slightly linear positive response, as can be observed from the AE events captured. This could be explained by the fact that, at this point, the PZT remains compliant with the bending of the host structure. Immediately, the yield strength of the material is reached at the 90 s point, the interlaminar stresses become significant, and the displacement at this point is close to 10 mm, where the material starts to slip, beginning to create a large curvature and non-uniform displacement, leading to the bending of the PZT material as it nears the yield strength; this explains the sudden change in voltage to negative.

Realizing the nature of ceramics to be brittle, a clicking sound from the cracking PZT could be heard as the bending progressed. Despite this, the sensor remained stable, consistently capturing AE events. The initiation of damage elevated the compression forces on the PZT at the material's maximum yield strength, resulting in peak responses. Indeed, as the bending

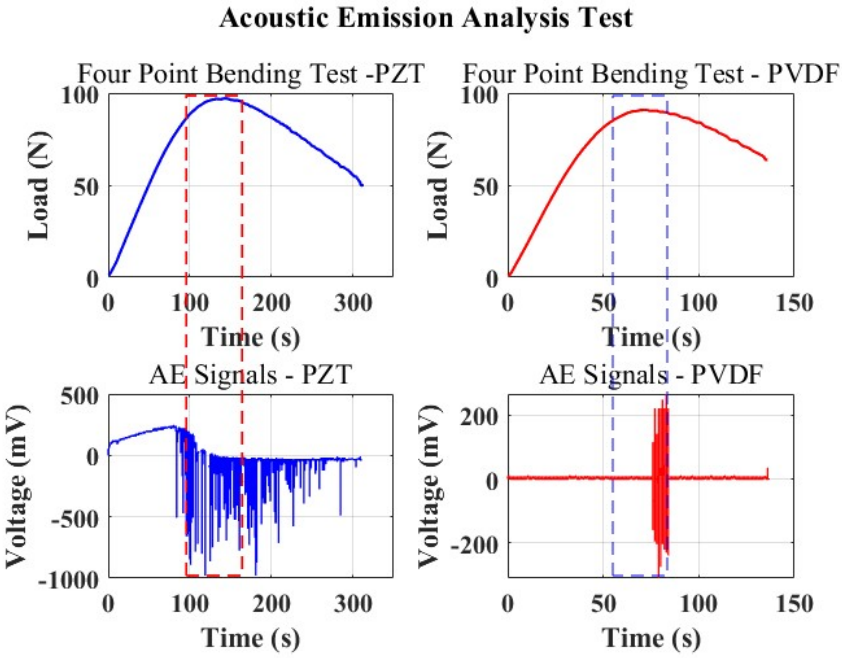


Figure 4.15: Acoustic emissions generated from the micro fractures in the loaded smart composite beam alongside the load–time curves.

strains weakened the beam's mechanical performance, the sensor constantly detected AE hits. The cracking sensors suggest that the origin of microcracks within the material aligns with the embedded sensor region. This event causes localized stress concentration, which may help to explain the unpredictable signal recorded by the PZT.

In contrast, the smart composite beam with a PVDF sensor, unlike the former, remains compliant with the loading due to its flexibility and tracks the bending of the structure while remaining sensitive to any damage. The PVDF sensor records an acoustic signal and continuously registers this signal until the load is no longer increasing as a result of the failed structure and continuous slippage of the beam. In Figure 4.15, it is evident that the responses from the PVDF (depicted by the red plots) exclusively capture the signals as the material surpasses its ultimate strength. This observation signifies the detection of AE signals, indicating the occurrence of actual damage to the structure. Additionally, it was observed that the signal decays back to zero, which could indicate that damping mechanisms (such as internal friction or external damping) are causing the energy from the acoustic emission to dissipate quickly. During the

ongoing four-point bending test, the mechanical strain changes introduced led to damping effects within the material. These effects cause energy dissipation from acoustic emissions, resulting in the signal returning to zero after the initial burst.

From these observations, coupled with the previous study on the PVDF influence on the mechanical properties of the host structure [29], PVDF was concluded to have good sensing capabilities as it proved to be reliable in recording AE events only at the point of failure, and, perhaps as a result of its low electromechanical properties compared to PZT, it remained insensitive to noise. PZT, conversely, proves to be sensitive due to its high electromechanical properties; minor variations, which could be in the form of noise, are not exclusive of the received signal from its measurements.

### 4.4.2 Active Sensing Approach

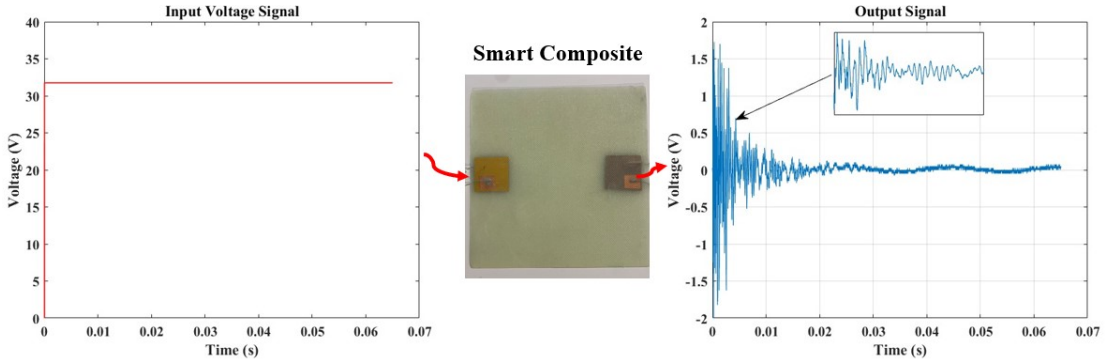


Figure 4.16: A single actuator sensor path illustrating the pitch-catch approach for damage diagnosis and monitoring, with an input signal deployed at a fixed frequency of 6 Hz. At this frequency, sufficient energy was being transferred from the actuator to the composite, allowing for observable vibrations.

In contrast to the passive method discussed earlier, which relies on damage-dependent signal responses for acoustic wave generation in damage monitoring and severity determination, the active sensing approach involves the continuous generation of elastic waves traveling through a material. Figure 4.16 illustrates our testing approach, utilizing a pitch-catch technique with a single actuator sensor configuration. In this setup, PZT generates signals by applying a step input signal, as depicted in the figure, subsequently, a PVDF sensor receives the signals on the opposite end of the plate. The findings given in the preceding section partially influenced the

selection of these components.

Figure 4.17 presents this study's step response output signal, which will be utilized in the measurement to validate the feasibility of conducting SHM within this framework.

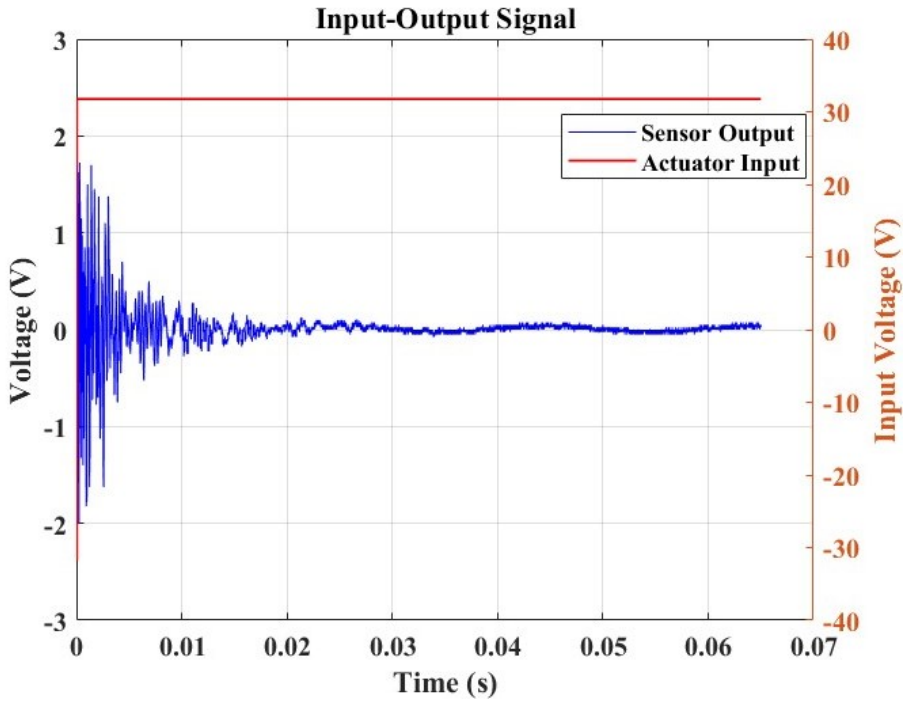


Figure 4.17: A step response from the pristine sample.

In this study, the Lamb wave data received from the sensor were considered for analysis in both the time domain and the frequency domain. The experiments were repeated seven times under identical conditions to ensure the reliability of the results. The goal was to understand how the signals changed and quantify the severity of the damage concerning the hole diameter's influence. This exploration is crucial as signal variations can indicate changes in material properties, signaling the presence of damage in the structure. For the time domain study, the signal responses of varying specimen conditions were compared to the "Healthy" structure posing as the baseline. The variations in the local amplitude concerning the increase in the hole diameter were evaluated.

Figure 4.18 illustrates the amplitude-based damage diagnosis approach. The collected data revealed distinct variations in peak amplitude corresponding to the different hole sizes introduced

into the structure. Notably, the baseline measurement from the undamaged, healthy structure exhibited a peak amplitude of 2 V. Utilizing a relative difference metric calculated concerning this baseline, we observed a clear correlation between increasing hole sizes and higher relative differences. The peak amplitudes rose from 2.05 V for a 5 mm hole to 2.675 V for a 13 mm hole, with corresponding relative differences ranging from 0.025 to 0.3375, as illustrated in Table 4.3. This trend underscores the sensitivity of the monitoring system to structural changes, with larger hole sizes resulting in more pronounced deviations from the healthy baseline. The findings emphasize the efficacy of Lamb wave monitoring in detecting and quantifying structural damages, providing valuable insights for real-time structural health monitoring applications.

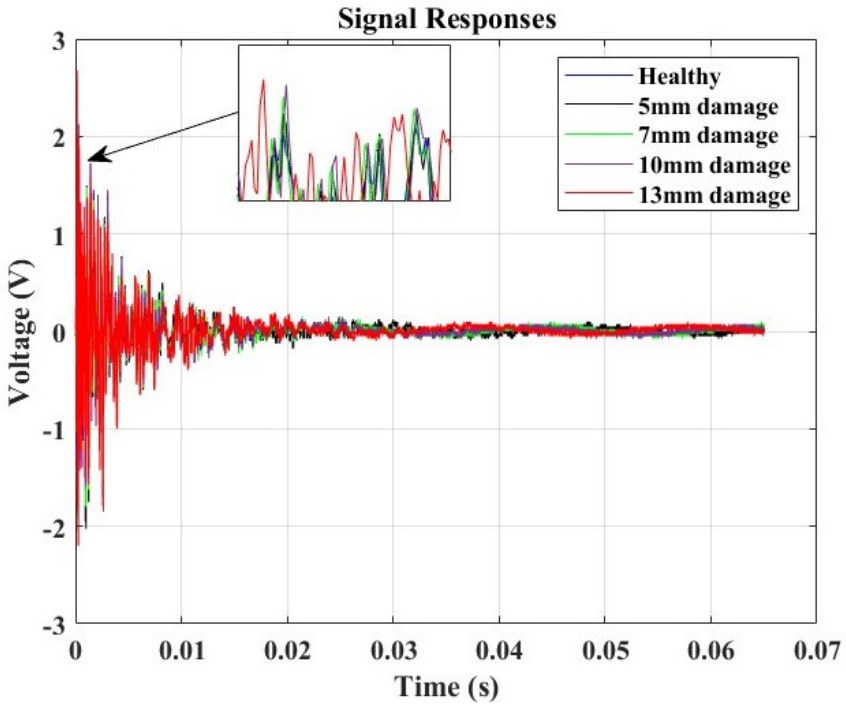


Figure 4.18: Amplitude response analysis for damage detection and correlation analysis.

Table 4.3: Relationship between hole diameter and amplitude change.

| **Hole Diameter [mm]** | **Amplitude Response [V]** | **Relative Difference** |
|---|---|---|
| 5 | 2.050 | 0.025 |
| 7 | 2.350 | 0.175 |
| 10 | 2.575 | 0.2875 |
| 13 | 2.675 | 0.3375 |

Figure 4.19 displays the relationship between the amplitude and damage size (hole size). The plot illustrates a correlation between these variables in the structure. The observation reveals that the response amplitude follows a cubic function when a hole is introduced during the SHM test utilizing Lamb waves. This increase in amplitude can be attributed to the altered structural stiffness resulting from the introduced hole damage, facilitating easier wave propagation. To further understand this correlation, a polynomial interpolation approach was employed to fit the response ($R^2 = 1$). The resulting correlation function is presented in Equation (4.10), highlighting a non-linear relationship between the amplitude and hole size.

$$A = 0.001\lambda^3 - 0.037\lambda^2 + 0.486\lambda + 0.423 \tag{4.10}$$

where $A$ refers to the amplitude and $\lambda$ represents the hole diameter size variable.

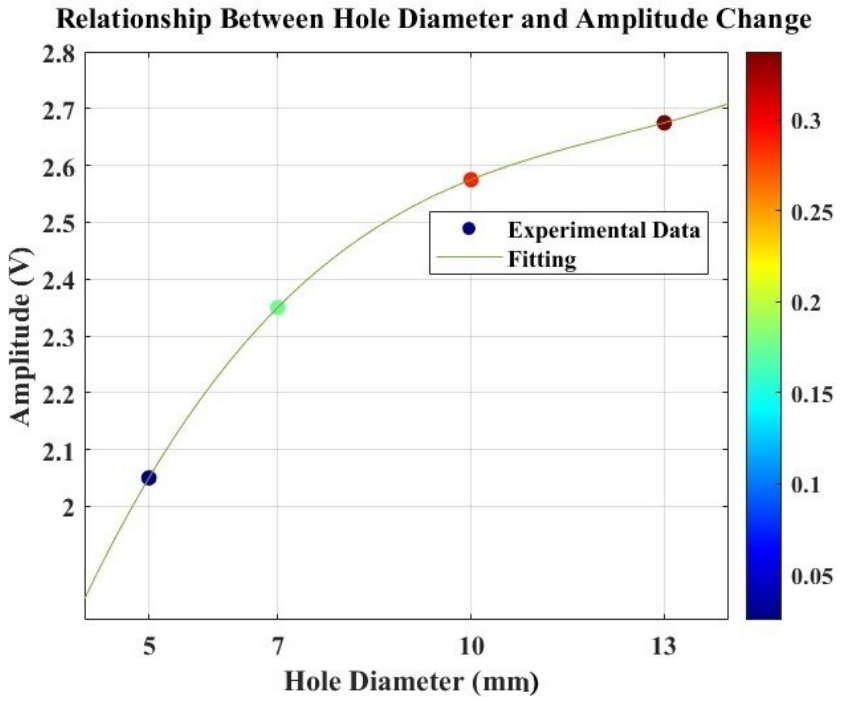


Figure 4.19: Relationship between hole diameter and amplitude responses alongside their relative differences from the baseline signal for damage diagnosis, exhibiting a non-linear relation where the amplitude of the response is influenced by the cubic power of the hole size.

However, this amplitude-based correlation function may not be sufficient to describe the severity of the damage in the composite structure, given the non-linear behavior of fiber-

reinforced composites with alterations in the material properties; therefore, extracting more feature parameters to perform damage diagnosis and description in the composite is imperative while employing the SHM strategy. Following this determination, a further signal processing approach utilizing FFT was implemented to extract more valuable features that could best describe the presence of the damage and the influence of its size.

In the frequency domain, Lamb wave signals were analyzed using Fast Fourier Transforms, as illustrated in Figure 4.20. The time domain signals were transformed, considering a data acquisition frequency of 312 kHz. The objective of this analysis was to identify a combination of parameters that could offer an indicative correlation to the response corresponding to the presence of damage. Based on observations from these plots, a specific frequency range between 8 kHz and 20 kHz was extracted (as depicted in Figure 4.21), where the influence of the introduced damage on the structure appeared to be significant. This extraction was undertaken to streamline the evaluation of pertinent parameters that could offer a reliable damage index for the SHM study.

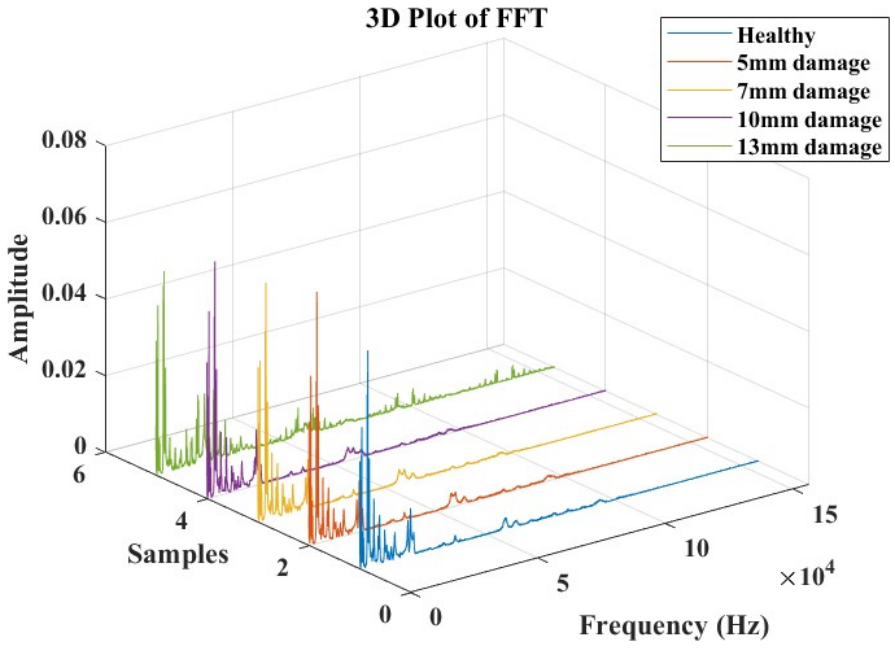


Figure 4.20: Fast Fourier Transform response analysis for damage detection and severity identification.

Table 4.4: Relationship between hole diameter and the extracted features in the frequency domain, showing the evolution of the damage indices.

| **Hole Diameter [mm]** | **Peak Frequency** | **Area under the Curve** | **Centroid Frequency** | **Relative Difference-Peak Freq.** | **Relative Difference-Area** | **Relative Difference-Centroid Freq.** | **Damage Indices** |
|---|---|---|---|---|---|---|---|
| Baseline | 19,861.7670 | 28.0935 | 29,846.5018 | – | – | – | – |
| 5 | 19,723.4111 | 28.7185 | 30,160.4476 | −0.0070 | 0.0222 | 0.0105 | 0.0144 |
| 7 | 19,600.4280 | 29.3909 | 30,211.4998 | −0.0132 | 0.0462 | 0.0122 | 0.0274 |
| 10 | 19,354.4618 | 30.3196 | 30,556.2719 | −0.0255 | 0.0792 | 0.0238 | 0.0480 |
| 13 | 16,418.2409 | 37.3246 | 31,530.3745 | −0.1734 | 0.3286 | 0.0564 | 0.2066 |

Table 4.4 summarizes the extracted parameters, including peak frequency values, the area under the curve, and the centroid frequency. Each of these three parameters displayed a monotonic trend with the magnitude of the damage within the selected frequency range. Subsequently, the relative differences in their evolution were computed. This led to the proposal of a damage index correlation function for the diagnosis of damage in this test approach.

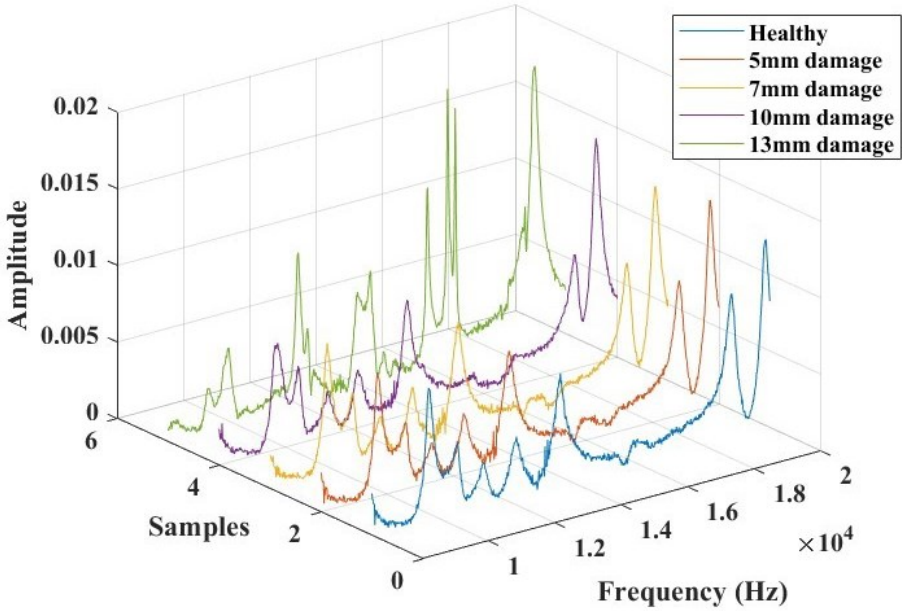


Figure 4.21: The selected frequency range (8,000 Hz to 20,000 Hz) for damage identification feature extractions and analysis.

Equation (4.11) illustrates the computed damage index obtained by weighting the identified relevant parameters regarding their influence on the overall damage assessment in the structure.

The relevance of this established damage index lies in its ability to quantify the extent of damage or deviation from the healthy baseline. The regular computation of this damage index can form part of the proposed SHM strategy, where trends or sudden spikes in the damage indices can signal changes in structural health over time. From the observation of the data from Figure 4.22, it is evident that higher values of the damage index signal more significant damage, as was observed from the previous amplitude-based study correlation, where the larger relative difference values sufficed to indicate more substantial deviation from the healthy state of the composite structure.

$$\text{Damage Index} = \sqrt{w_1\alpha^2 + w_2\beta^2 + w_3\gamma^2} \tag{4.11}$$

where $\alpha, \beta, \gamma$ represent the relative differences in the peak frequency, area under the curve, and centroid frequency, respectively, and $\omega_1, \omega_2, \omega_3$ are the weights for the corresponding squared relative differences.

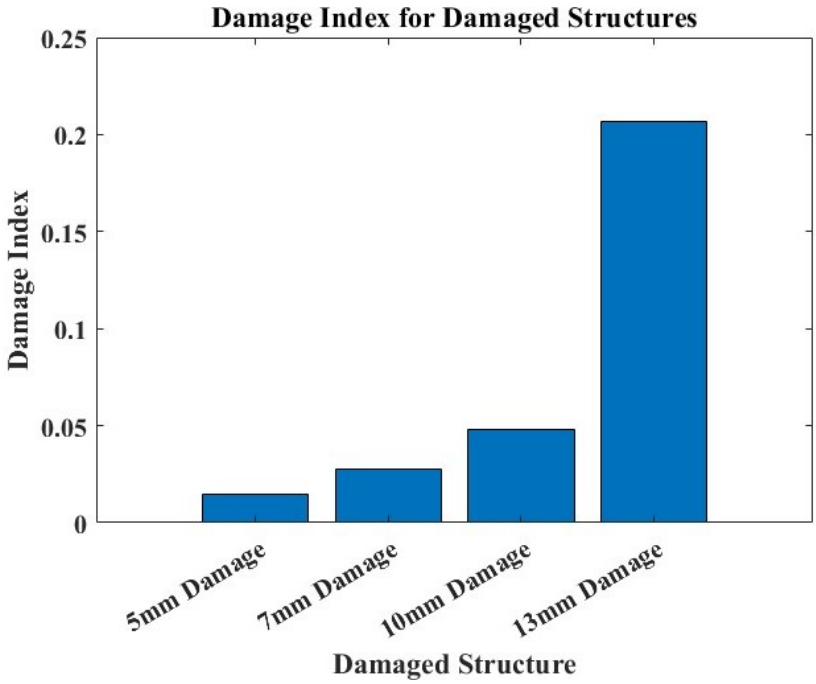


Figure 4.22: A damage index plot of the damaged structure cases.

Figure 4.22 shows a damage index plot against structures with varying hole damage sizes.

The plot illustrates the variations in damage indices across different structures, highlighting the increasing trend as the damage size increases. The damage indices serve as a crucial indicator of structural health, facilitating the identification of deteriorating conditions that require attention. This analysis supports the implementation of condition-based maintenance strategies in aerospace structural systems.

### Numerical Analysis

Figure 4.23 displays the outcomes of the finite element method analysis using the pitch-catch sensing approach implemented in COMSOL. The results exhibit a transient response similar in form to the one obtained from the experimental data presented in Figure 4.16. A similar attenuation trend is seen in the simulation's Lamb wave signal, which converges with the experiment's observed period. These findings complement and validate the experimental study conducted within the framework of active sensing in this work.

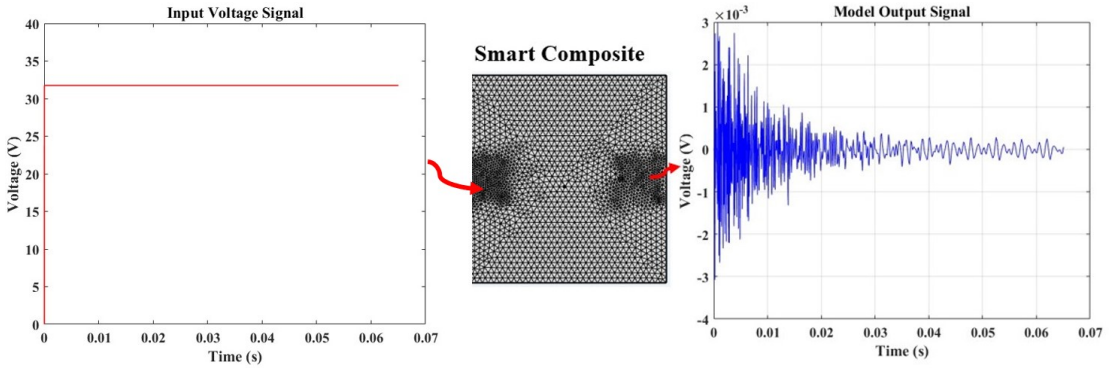


Figure 4.23: The numerical model simulation involving a step voltage input with an amplitude of 31.75 V and a fixed time step of 3.2 $\times 10^{-6}$ s.

The surface plots in Figure 4.24 illustrate displacement magnitudes with varying damage sizes. An observation reveals that, due to changes in material properties induced by damage, the Lamb wave traveling through this region undergoes scattering in multiple directions—notably, the degree of spreading increases with the severity of the impact on the structure. The signals obtained from this damage diagnosis approach are thus deemed reliable for application in implementing SHM.

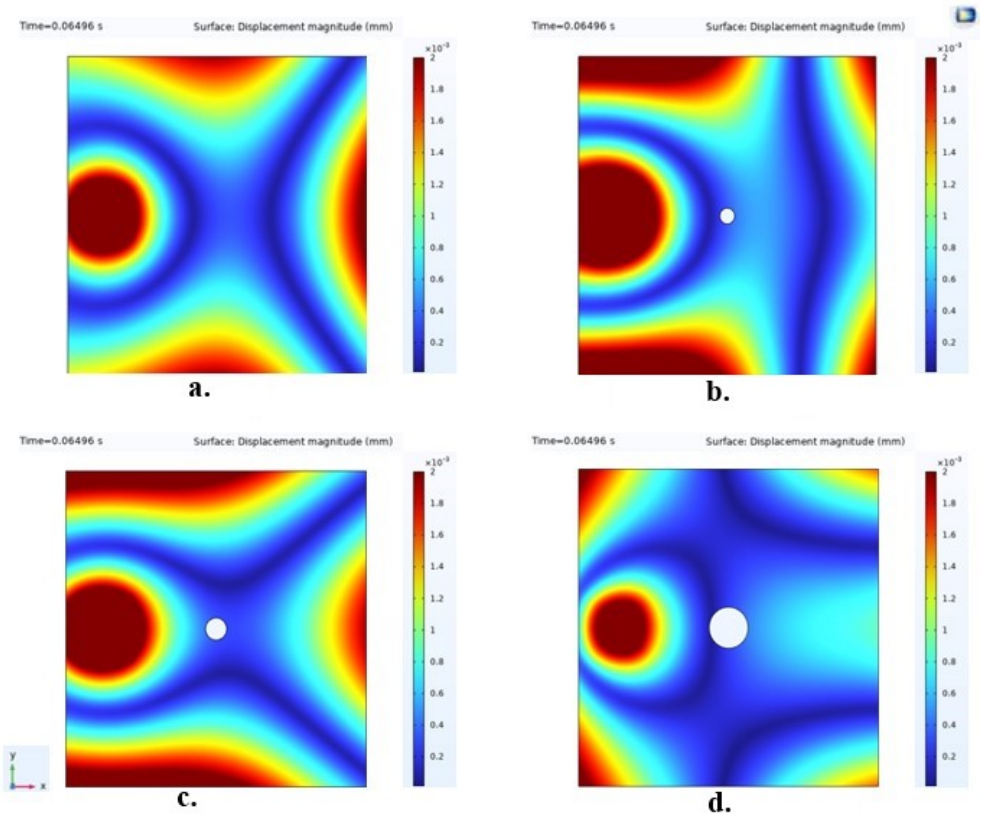


Figure 4.24: The surface plots of the analyzed sample cases displaying the displacement magnitude for visualization of the disturbance created by damage on the Lamb waves. In these representations, (**a**) illustrates the healthy structure in its intact state, (**b**) shows a structure with 5 mm hole damage, (**c**) demonstrates a structure with 7 mm hole damage, and (**d**) displays a structure with 13 mm hole damage.

A Fast Fourier Transform of the transient response signals for the four modeled cases was performed, and a frequency range was analyzed to compute relevant parameters. Figure 4.25 shows the resulting plots for this frequency window. The centroid frequency feature, the center of mass of the frequency distribution, which has found interest in the study of AE signals for damage assessment [142] and structural health monitoring, was extracted as a parameter of interest. The observed discrepancies in centroid frequency between the selected analysis range of 8 kHz to 20 kHz and the resultant centroid around 30 kHz can be attributed to several factors. The presence of significant higher-frequency components beyond the analysis range likely influenced the centroid frequency, pulling it upward due to their contribution to the overall energy distribution. Additionally, the windowing effects and potential signal leakage during

processing might have caused energy to spread outside the intended range, further impacting the centroid calculation. The distribution of signal energy, concentrated at higher frequencies, also plays a crucial role in shifting the centroid frequency. The results revealed an increasing trend in this characteristic parameter, indicating changes in structural properties. Table 4.5 presents a comparison of the feature parameter between the experimental findings and FEM results. The results demonstrate strong agreement with a minimal variation of less than 2%, validating the active sensing approach for SHM.

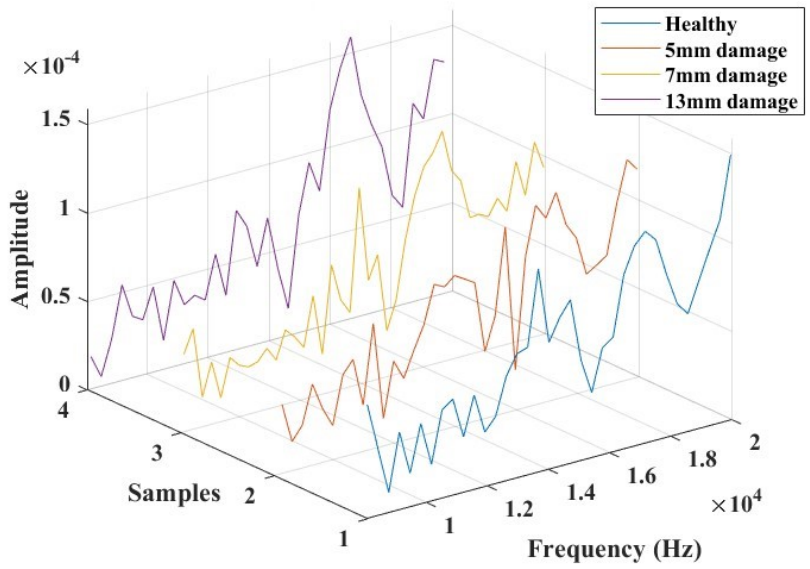


Figure 4.25: The selected frequency range for damage identification feature extractions and analysis for the simulated plate in COMSOL.

Table 4.5: Comparison of experimental and FEM results based on centroid frequency variation (<2% deviation).

| Hole Diameter [mm] | Centroid Frequency— Simulation | Centroid Frequency— Experiment | % Difference |
|---|---|---|---|
| Pristine (Healthy) | 30,224.5970 | 29,846.5018 | 1.3 |
| 5 | 30,607.5207 | 30,160.4476 | 1.5 |
| 7 | 30,750.5275 | 30,211.4998 | 1.8 |
| 13 | 30,947.5353 | 31,530.3745 | 1.9 |

## 4.5 Summary and Conclusions

This chapter has thoroughly investigated the potential applications of smart composites in energy harvesting and structural health monitoring. A comprehensive blend of numerical analysis and empirical experimentation convincingly demonstrated the feasibility of deploying these advanced materials to achieve the outlined objectives. The findings reveal that integrating active and traditional fiber-reinforced materials results in functionalized structures capable of efficiently harvesting substantial energy from ambient vibrations. These insights pave the way for future innovations in deploying smart composites in energy harvesting and structural integrity monitoring domains.

Additionally, this chapter explored various SHM methods, delving into smart composite fabrication, experimental testing, numerical analysis, and signal processing approaches. The primary objectives were to assess the suitability of thin film piezoelectric elements for SHM in fiber-reinforced composite structures and enhance the damage identification and severity classification methods.

The initial focus involved implementing an experimental study based on a passive sensing approach. The findings revealed that PVDF thin film, compared to PZT piezo materials, is well suited to the sensing of impact damages due to its low noise sensitivity and ability to capture AE signals from the onset of damage. Additionally, these sensors proved effective in analyzing the material's load-bearing capacity. Notably, the influence of these sensors on the mechanical behavior of the host composite structure was observed, with PZT showing compromises in the flexibility of the composite structure, as indicated by the computed maximal flexural strengths.

Subsequently, a pitch-catch active sensing approach based on Lamb wave propagation was introduced, accompanied by extensive signal processing methodologies. This led to the development of a damage size correlation function and a damage index, demonstrating the high sensitivity of Lamb wave propagation to structural deterioration caused by alterations in material properties. The non-linear correlation between the damage size and severity was attributed to the complex coupling of parameters influenced by damages in composites. Combining the extracted characteristic parameters with the associated weights was considered for comprehensive damage interrogation from the signal responses. It must be noted that the developed correla-

tion equation and damage index equation presented in this chapter provide a methodology for establishing these frameworks but may not be generalizable.

Finally, a finite element modeling approach was employed to study the Lamb wave propagation behavior in response to damage. The numerical analysis validated the experimental data, showing good agreement with a deviation of less than 2% concerning the centroid frequency. While these investigations contribute valuable insights to ongoing studies in structural health monitoring integration technologies, it is important to note that the work presented in this chapter was limited to specific environmental test conditions.

# Chapter 5

# Enhanced Defect Detection and Recognition in Aeronautic Composite Structures Using Machine Learning and In-Situ Sensing: A Case Study

---

## Contents

## 5.1 Introduction

The previous chapter addressed the implementation of structural health monitoring, detailing how embedded piezoelectric sensors provide real-time data on the structural integrity of aeronautic components, thereby enhancing safety and maintenance efficiency. However, the damage index and correlation equations presented for damage detection and monitoring might not always be sufficient to provide real-time status when large amounts of data are fed to the feature extraction systems, highlighting the need for advanced artificial intelligence algorithms. This chapter presents a novel approach to SHM in aeronautical composite materials, leveraging embedded sensor data and advanced machine learning techniques for enhanced performance and simplified fault detection and identification. As discussed in previous chapters, the study utilizes an in-situ sensing system that integrates polymer-based piezoelectric sensors within the composite structure, enabling direct measurement and high-quality data acquisition. By employing a Gram angle field-based time-frequency transformation, the proposed method effectively captures fault information from the in-situ measurements. The study validates the proposed approach

by completing diagnostic validation and identification of single and compound faults, such as scratches, holes, cuts, and other defects highlighted in Chapter 1, using simple machine learning models. The findings in this chapter underscore the potential of combining in-situ sensing and advanced machine-learning techniques for improved structural health monitoring in aeronautical composite materials.

## 5.2 Related Literature

The evolution of aeronautic engineering is marked by continuous innovation aimed at enhancing the performance, safety, efficiency, and longevity of aircraft structures [143]. Central to this quest is the development of advanced materials and diagnostic technologies that promise to revolutionize how we understand and manage the health of these structures [144].

Introducing fully embedded piezo sensors has opened up new possibilities for real-time, non-invasive monitoring of composite materials via in-situ sensing [103, 126]. These sensors, capable of generating and responding to mechanical waves, offer a unique advantage in detecting and locating damage within the structure through techniques such as acoustic emissions [103, 145] and lamb wave analysis [42]. Indeed, they can monitor the condition of the material in real time, capturing subtle changes that may indicate the onset of damage [126]. However, the sheer volume of data produced and the complexity of interpreting this information present substantial challenges [146]. It is within this context that machine learning (ML) algorithms - a subset of artificial intelligence that empowers computers to learn from data, identify patterns, and make decisions with minimal human intervention [147], emerge as a transformative tool capable of analyzing complex datasets to identify anomalies that are indicative of structural flaws [148]. It is anticipated that advanced machine learning algorithms will be able to automate the detection, classification, and even prediction of damage progression in composite materials, thereby improving real-time monitoring in aerospace engineering [149].

Numerous studies have investigated advanced machine learning-based SHM methods, primarily focusing on data-driven ML algorithms [146, 150, 151, 152] and physics-informed ML approaches [153, 154]. However, while physics-informed ML offers a theoretically robust framework, it often falls short in practical scenarios, particularly detecting damage in fiber-reinforced

polymer composites. These shortcomings include high computational costs and a dependency on accurate physical models, which may not effectively capture the complex behaviors of damage in composites. Additionally, their models may require much more time to adjust in environments where conditions change frequently or unpredictably. Consequently, data-driven ML algorithms are becoming increasingly popular due to their adaptability to diverse data patterns and minimal reliance on extensive physical knowledge, making them better suited for practical SHM applications [153].

However, these data-driven ML methods lack high-quality data, challenging the establishment of fault assessment and quantification in composite structures [155]. This results in the implementation of sophisticated machine learning tools that are slow in damage diagnosis, computationally costly, require a large amount of data and require much more power to execute. This can be attributed to the reliance on the indirect measurements of signals using surface-attached sensors on the structures. In such cases, we observe the interaction between damage information and environmental disturbances within the signals in dynamic situations where loads and environmental conditions vary [156, 157], thus influencing the signals nonlinearly and making them difficult to manage, necessitating extensive pre-processing and complex ML algorithms for training and extracting associated damage-sensitive features.

The research work presented in this chapter aims to leverage integration technology by fully embedding a polymer-based piezoelectric sensor within the composite structure. This in-situ sensor system enables direct data collection, streamlining the preprocessing and application of machine learning models for fault diagnostics, thereby reducing computational costs. The contributions of this chapter include:

- Structurally integrated in-situ sensing system, embedded in composite materials by laminate lay-ups.

  The sensor, embedded within the structure, directly acquires transmitted signals from the failure source and remains sensitive to small changes. This positioning minimizes interference from environmental disturbances and mechanical integrity, enhancing the accuracy of failure detection by eliminating transmission errors and making it robust against noise. This setup allows for explicit tracking as damage evolves without needing to consider the coupling mechanism between the sensor and defect information.

- End-to-end capture of in-situ measurement fault information by applying gram angle field-based time-frequency transformation.

  By employing a "Gram matrix" which is used to measure the inner products of vectors, capturing the geometric relationships among the signal components in the time-frequency domain. This failure feature capturing approach allows for a deeper analysis of the signal, focusing on identifying unique characteristics or patterns by examining the angles and orientations between different time-frequency components.

- Complete diagnostic validation and identification of single and compound types of Scratch, hole, cut and other faults with the simple ML models.

  This contribution highlights the effective use of simple machine learning (ML) models to perform diagnostic validation and identify different types of defects, such as scratches, holes, cuts, and other damages. These models are capable of distinguishing between single defects and combinations of multiple defects, providing a streamlined and efficient approach to fault diagnosis in various applications.

## 5.3 Presentation of Materials and Methods

### 5.3.1 Materials and Smart Composite Manufacturing

In this chapter, the smart composites were developed using the materials and processes described in Chapter 3. Figure 5.1 illustrates the fabrication process of smart composite samples. In Figure 5.1a., the process begins with cutting copper tape wires and piezoelectric film to specified dimensions, followed by the wiring step. Figure 5.1b. details a critical procedure to evaluate short-circuiting of the electrodes during the piezoelectric film cutting and assess the electrical properties, particularly capacitance and resistance. Figure 5.1c. depicts the draping of glass fiber prepreg and the placement of the wired sensor within the preform lamina. This leads to Figure 5.1d., where the preformed samples are positioned on the mold plate, sandwiched between two peel plies crucial for absorbing excess resin during the curing process and ensuring a uniform surface of the fabricated composite.

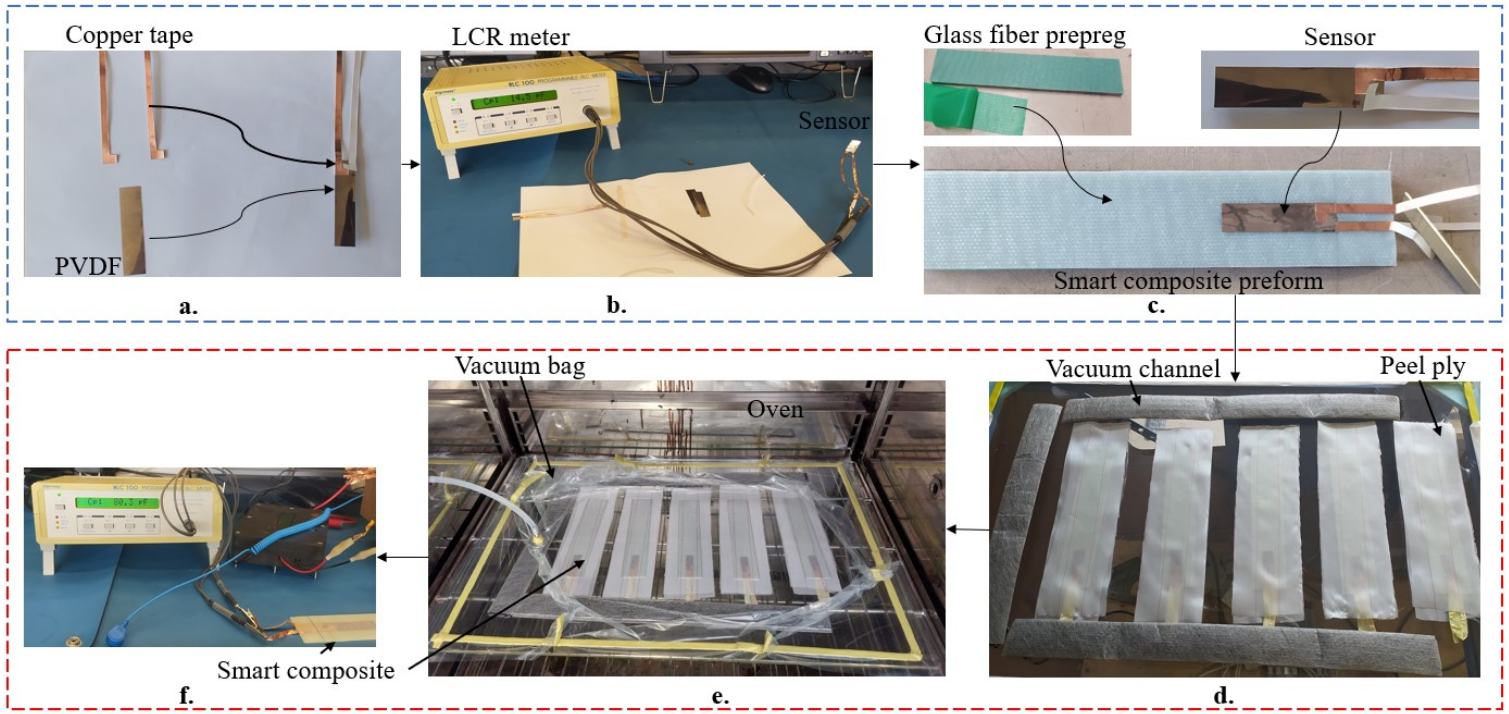


Figure 5.1: Illustration of the smart composite manufacturing process, showcasing both the materials and equipment used during fabrication. The composite plates, measuring 50 mm by 250 mm, were consolidated at a temperature of 90 °C during 90 minutes.

Figure5.1d. also shows the vacuum-assisted consolidation molding, where heat from the oven and pressure from the compressor are applied to the mold to ensure complete resin infiltration. The final step, Figure 5.1e., illustrates the measurement of the electrical properties of the demolded composite plate, which is then prepared for electromechanical testing.

### 5.3.2 Direct and Indirect Sensing Approaches

Figure 5.2 illustrates the measurement techniques evaluated in the current study. Traditionally, surface-attached sensors are employed for non-destructive testing and structural health monitoring of composite structures. However, these sensors present limitations in aerospace structures where continuous and autonomous monitoring is essential. Their vulnerability to damage from impacts, such as bird strikes or degradation of the adhesive bond over time, can compromise their effectiveness. Additionally, environmental dynamics significantly affect the sensor signals, complicating the distinction between actual structural health and noise-induced anomalies. This necessitates the implementation of sophisticated data analysis techniques to isolate noise effects. Moreover, these sensors typically depend on external power sources, requiring periodic battery replacements due to limited battery lifespans.

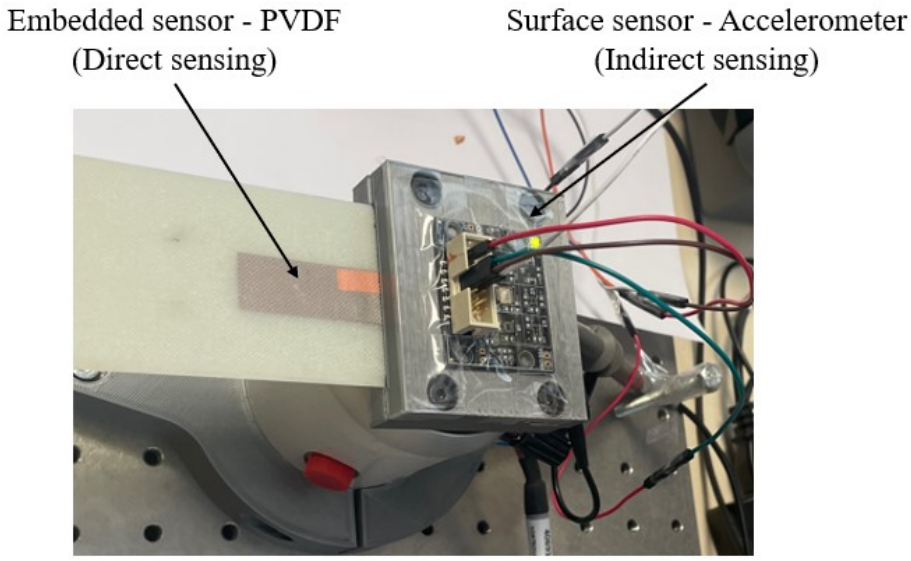


Figure 5.2: Sensing approaches: direct and indirect sensing techniques, featuring an embedded piezoelectric sensor and a surface-attached traditional accelerometer.

Therefore, fundamental research areas were identified following the future direction highlighted in the recent review on advanced sensor technologies for NDT and SHM by Hassani and Dackermann [156]. They recommended developing smart materials with self-powered, noise-resistant, cost-effective, and environmentally friendly sensors. Self-sensing materials capable of instantly detecting damage-induced structural changes remain desirable in ongoing studies. Consequently, this work implements direct measurement, fully embedding a piezo film element within the structures. It compares its damage assessment capabilities to traditional surface-attached sensors that rely on indirect damage detection techniques, similar to those presented in Section 1.2.2, Figure 1.4.

### 5.3.3 The Defect Description

In the aerospace industry, maintaining the structural integrity of composite materials is critical due to the catastrophic nature of potential failures. In this study, various damages were induced to model their physical impacts. The experimental induction of these artificial damages, holes, scratches, cuts, and combinations reflects real-world scenarios that aircraft composite structures can encounter as illustrated in Figure 5.3. Such damages might result from lightning strikes, which can puncture or scorch the composite, or mechanical failures, such as loose nuts or bolts [158]. These components can create hole-like defects or cuts when subjected to continuous stress or vibration, which occurs at scales ranging from nanometers to centimeters and, if undetected, may worsen over time. Creating these specific damages is crucial for obtaining data and training machine learning algorithms for real-time structural SHM. This approach ensures the detection and classification of significant damage types in the aerospace domain. It enhances the reliability and safety of aircraft operations by facilitating immediate corrective actions before minor damages escalate into significant failures. Thus, the justification for selecting these types of damages lies in their relevance and frequency of occurrence in aerospace applications, which calls for their early detection and management.

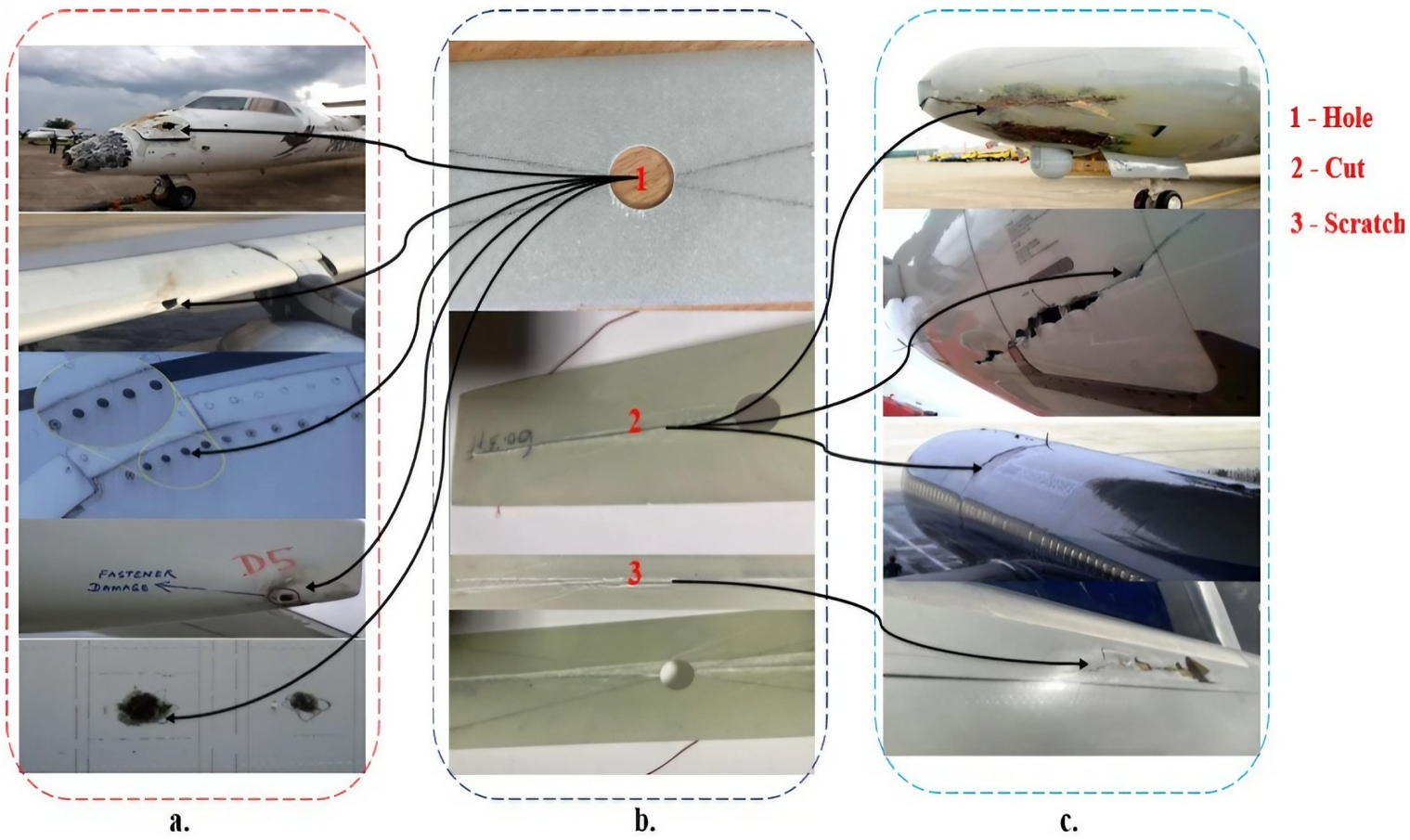


Figure 5.3: Illustration of Common Aircraft Defects: (a) Displays damages from lightning strikes and missing bolts in fastener assemblies. (b) Presents simulated damage examples based on real-world scenarios studied in our research. (c) Depicts damages, including cuts and scratches caused by debris, lightning, bird strikes, and impacts from hailstones.

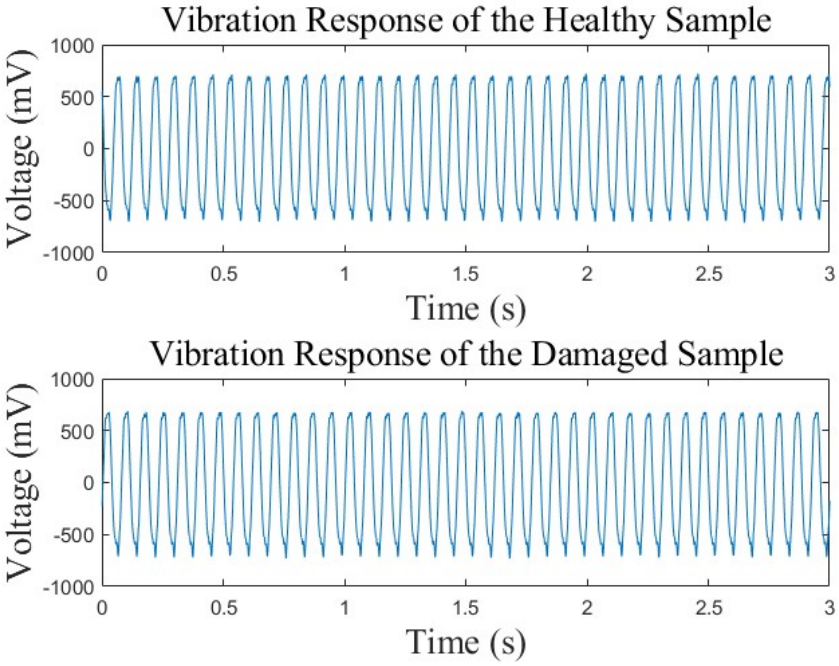


(a) Time domain response.

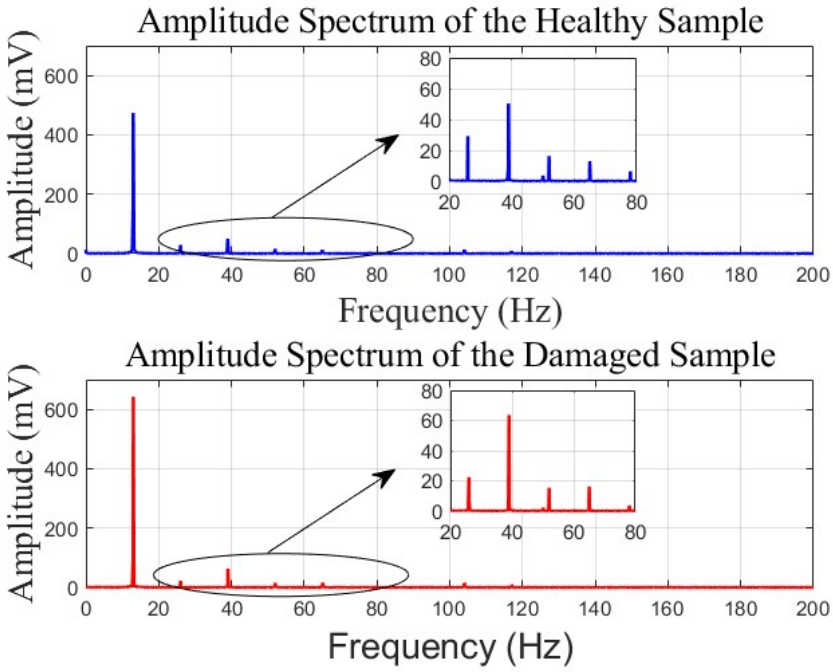


(b) Frequency domain response.

Figure 5.4: Comparative analysis of vibrational responses from intact and defective samples to illustrate the effects of underlying defect mechanisms.

#### Defects Mechanism

The defects alter the vibrational characteristics of the smart composite structure, resulting from changes in the material's local stiffness and mass distribution. To visualize this phenomenon, a plot was generated using the raw data collected from the vibration responses of both the pristine and damaged samples, as presented in Figure 5.4. The goal of this visualization is to extract defect indicators. However, the impact on the time domain response (Figure 5.4a) is not visible, even though the defect may have altered the modal shapes and natural frequencies. This lack of clarity arises because the signal combines many overlapping frequencies and vibration modes. However, when the data is transformed into the frequency domain using a Fast Fourier Transform (FFT), shown in Figure 5.4b, these shifts become apparent. The spectral peaks shift and vary in amplitude, highlighting the presence and impact of the defect on the structure's dynamic behavior. Therefore, to accurately diagnose and characterize such defects, employing a model that operates in the frequency domain is essential. This model would extract features sensitive to the defect mechanism, which is crucial for developing diagnostic models that detect and evaluate structural integrity.

## 5.4 Case Study

### 5.4.1 Experimental Setting and Data collection

Figure 5.5 illustrates the experimental setup and the equipment utilized, which includes a digital function generator (Topward 8112), a digital oscilloscope (Tektronix TBS 2104), a power supply (EA-PS 2384-03B), a permanent magnet shaker (LDS V201), a linear power amplifier (LDS LPA 100 by Bruel & Kjaer), and a honeycomb optical breadboard (M-IG-32-2). Data collection is carried out using a PicoScope 2000 series (2204A) through PicoLog (version 6.2.9) software, which interfaces directly with the embedded sensor, and an Arduino UNO (R3), which facilitates data acquisition from the surface sensor via MATLAB (R2023b) software.

Table 5.1 presents the details of the experiment. In order to test the structure in a more realistic environment and account for variations that might influence the results, data collection was performed at three different periods: morning, afternoon, and evening. The tests spanned

across six frequencies, including the natural frequency and its harmonics, i.e., 6.5 Hz, 13 Hz, 19.5 Hz, 26 Hz, 32.5 Hz, and 39 Hz, with each frequency tested for 1 minute. The experiments were repeated for a specific number of times to ensure reliability. This comprehensive approach captures the effects of environmental changes on the material's dynamic behavior and generates a robust dataset essential for developing reliable machine-learning algorithms. By providing a diverse and representative dataset, this method enhances the ability of machine learning models to predict and generalize well across various real-world conditions, ultimately improving the decision-making process in SHM.

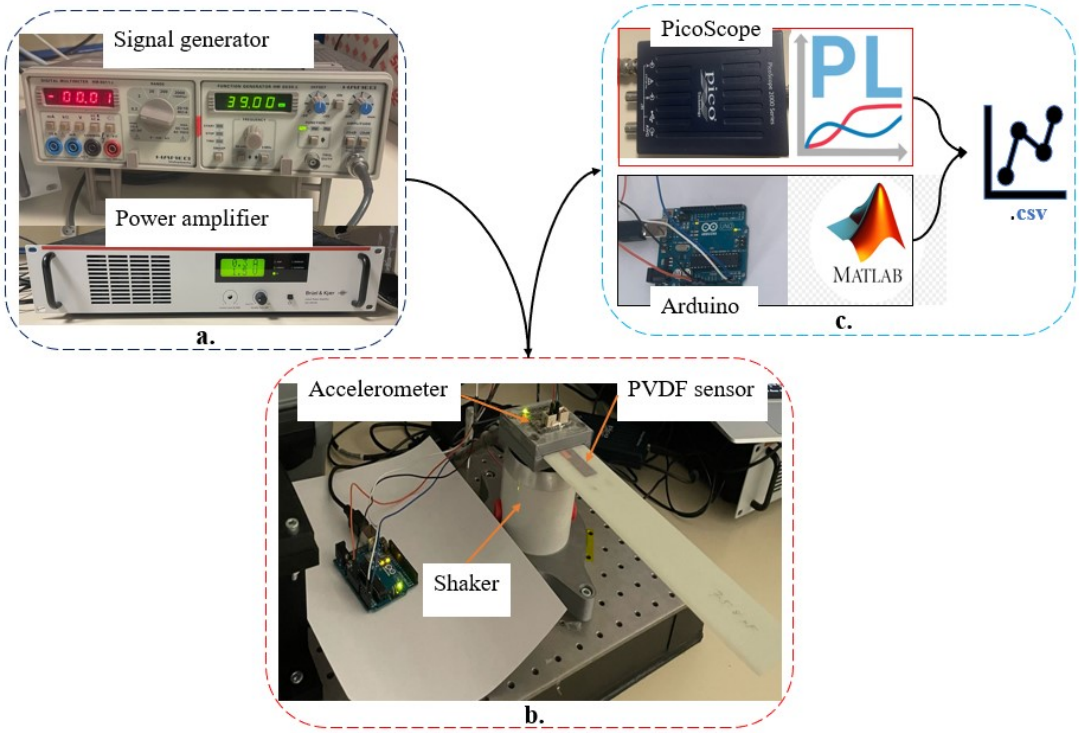


Figure 5.5: Experimental setup: **a)** Illustration of signal generation and amplification; the signal generator supplies a sine wave signal spanning 6 harmonics, determined from the natural frequency of the test sample, to the amplifier. **b)** Setup of the smart composite plate on the test platform, which is clamped onto a shaker for vibration tests. **c)** Data acquisition setup specific to the two different sensors used in the study.

Table 5.1: Experimental vibrational test details for healthy and damaged composite samples, measured across five harmonics and the natural frequency of 13 Hz and conducted in the morning, afternoon, and evening, with multiple repetitions for reliability.

| **Sample Type** | **No. of samples** | **Total No. of Experiments** | **Repetition of Experiments per Frequency** |
|---|---|---|---|
| Healthy | 3 | 270 | 5 Times |
| Damaged(Hole) | 1 | 90 | 5 Times |
| Damaged(Scratch) | 1 | 90 | 5 Times |
| Combined(Scratch + Hole) | 1 | 18 | 1 |
| Complex(Scratch + Hole + Cut) | 1 | 18 | 1 |
| Combined(Cut + Hole) | 1 | 36 | 2 Times |

### 5.4.2 Data Preprocessing and Labeling

Following the acquisition of raw data for machine learning, preprocessing, and labeling become the next crucial steps that must be undertaken to obtain a quality dataset. Such a dataset should accurately reflect the underlying patterns without noise-related biases. This preprocessing involves a data cleansing process, which addresses errors in the raw data, such as missing values, outliers, and duplicate entries, and involves correcting them manually or automatically [159, 160]. The process also includes data scaling and standardization for suitable analysis. On the other hand, data labeling, which involves assigning a label or category to each data entry based on predefined criteria, is one of the most crucial steps, especially for supervised machine learning models. In these models, the system learns to predict outcomes based on the already identified and contextualized datasets [161]. Accurate labeling ensures that the model will make correct associations between structural state patterns and predictions. For example, in the SHM application set for study in the current research, this process is necessary to indicate the structure's presence and type of defect.

One-hot encoding was employed to label the conditions represented in our dataset. This method involves transforming each category into a binary vector with all zeros, except for a single "one" at the position of the category. Using one-hot encoding ensures ML models give each label the same weight, an essential consideration for classification tasks such as the ones in this study with several state categories. For the SHM dataset utilized, six labels corresponding

to various structural states "Healthy", "Hole", "Scratch", "Scratch+Hole", "Scratch+Hole+Cut", and "Hole+Cut" were defined. The label space encompasses at least four independent failure labels based on a priori expert knowledge. Each sample is typically assigned a single label corresponding to a binary classification scheme. Considering the combination of different failures, the resulting one-hot encoding incorporates compound failure property columns, as depicted in Table 5.2. This approach ensures that each state is treated as distinct and independent without implying any ordinal relationship. Consequently, ML models can recognize and classify the different structural states based solely on their unique signatures.

Table 5.2: Mapping of binary feature tuples to condition labels for data processing. Each tuple represents the presence (1) or absence (0) of certain features corresponding to specific conditions in the dataset.

| One-hot Encoding | Compound Fault Label | Real Status |
|---|---|---|
| 0, 0, 0, 0 | 1 | Healthy |
| 1, 0, 0, 0 | 1 | Healthy |
| 0, 1, 0, 0 | 2 | Scratch |
| 1, 1, 0, 0 | 2 | Scratch |
| 0, 0, 1, 0 | 3 | Hole |
| 1, 0, 1, 0 | 3 | Hole |
| 0, 1, 1, 0 | 4 | Scratch-Hole |
| 1, 1, 1, 0 | 4 | Scratch-Hole |
| 0, 0, 0, 1 | 5 | Cut |
| 1, 0, 0, 1 | 5 | Cut |
| 0, 0, 1, 1 | 7 | Hole-Cut |
| 1, 0, 1, 1 | 7 | Hole-Cut |
| 0, 1, 0, 1 | 6 | Scratch-Cut |
| 1, 1, 0, 1 | 6 | Scratch-Cut |
| 0, 1, 1, 1 | 8 | Scratch-Hole-Cut |
| 1, 1, 1, 1 | 8 | Scratch-Hole-Cut |

The data was prepared through 5-fold cross-validation, randomly splitting the dataset into five equal parts. The model is built using four parts and validated on the fifth. This cycle is executed five times to ensure each part serves once as the validation set, with no overlap between training and testing data [162].

### 5.4.3 Feature Extraction

Figure 5.6 illustrates the data and feature extraction process. The process involves acquiring sensitive parameters indicative of the structural integrity state from pre-processed datasets [163].

These features can be manually or automatically extracted from the sensor data, thus relying on proper sensing technology. Relevant features, which are exploited in either the time or frequency domain through the consideration of statistical features, become the input for the ML model. With the knowledge that the collected data exhibit slight variation in the time domain, a frequency domain method was implemented, specifically the Short-Time Fourier Transform (STFT). In essence, the STFT approach splits the data into a specified segment that is achieved by applying a sliding window function to the signal. Each segment is then analyzed separately by subjecting it to a Fourier Transform, resulting in a 2D representation of the data, capturing how the frequency components vary over time. The mathematical description of STFT can be found in the work of Sairamya *et al.* [164].

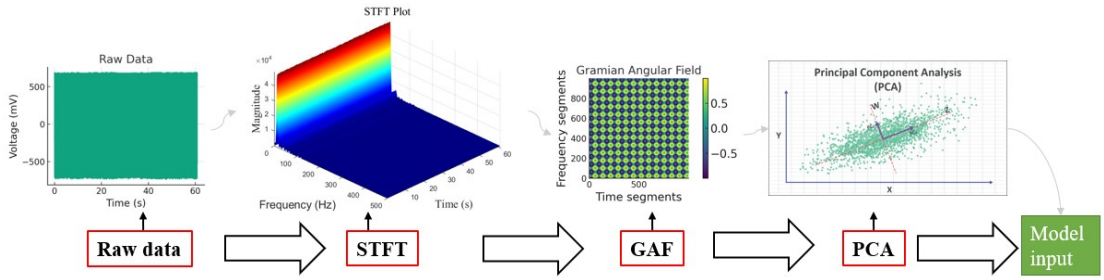


Figure 5.6: Illustration of the data processing and feature extraction.

Following this analysis, wherein the magnitudes of frequency components were extracted, these results were converted to a Gramian Angular Field (GAF). This method uses trigonometric transformations to capture temporal relationships in the data. The GAF transformation converts time-frequency data by encoding its magnitude and phase information. This makes it easier to analyze and interpret the data visually and provides clearer insight into the feature patterns [165, 166]. After obtaining these results, scaling and standardization were performed to render the data suitable for input into Principal Component Analysis (PCA). PCA is a statistical technique employing vector space transformations to reduce feature dimensionality, condensing a larger dataset into manageable data while preserving significant patterns and trends critical for anomaly detection in ML models. A mathematical description of PCA is provided in [167, 168].

Consequently, within the context of this study, PCA was utilized to decrease the dimensionality of the frequency-time matrix by extracting a specific number of principal components, particularly 20. These components denote the directions of maximal variance in the data, effectively isolating the most consequential features from the STFT results and diminishing noise and less informative data segments. The output from PCA underwent further normalization using a standard scaler, which adjusted the data to a scale with zero mean and unit variance. This normalization step was paramount for the ML algorithm to ensure the equitable contribution of all features to the analysis, averting the predominance of features with larger scales in the model's learning mechanism. Figure 5.7 represent the first eight principal components obtained from a dataset after applying PCA.


Figure 5.7: Principal Component Analysis visualization: This series of line graphs illustrates the first eight principal components extracted from a dataset, highlighting the temporal variation in features of healthy structures compared to those with scratch or hole defects. The x-axis represents time progression, and the y-axis shows the values of the principal components. Each graph reveals distinct patterns across the three conditions, emphasizing their differences.

### 5.4.4 Model Comparison

Table 5.3 summarises this study's ML models and their associated tasks. The models used are Support Vector Machine (SVM) for anomaly detection, Random Forest (RF) for classification of single and combined failure states. The table describes whether the models require labeled data, the type of sensor used to collect the data, the necessity for retraining, and the dataset variations for each model.

Table 5.3: Overview of machine learning models employed in the study.

| Model | Labeling | Task | Sensor Type | Data Discription |
|---|---|---|---|---|
| SVM | unlabeled | anomaly detection | embedded sensor | 54 Healthy and 36 Unhealthy dataset |
| RF | labeled | classification | embedded sensor | Single failure state |
| RF | labeled | classification | embedded sensor | combined failure state |
| RF | labeled | classification | embedded sensor/surface sensor | Multi-class with new features |
| Retrained - RF | labeled | classification | embedded/surface sensor | Multi-class with new features |

This study primarily utilizes a One-Class SVM [169, 170] to detect anomalies in structural datasets. Initially, the objective is to identify any anomalies before pinpointing the specific types of defects. The effectiveness of embedded sensors versus surface sensors in detecting these anomalies is then assessed to determine which sensor type more accurately captures the features of structural defects. After confirming the presence of damage, the focus shifts to identifying the specific type of structural damage present in the combined dataset. For this purpose, an RF classifier [171] was implemented for damage recognition. Multi-class labeling was employed, and the model was trained and tested on its ability to classify the types of defects accurately.

#### Best Model Configuration Search Strategy

In this study, the search for the optimal configuration of the SVM and RF classifiers is undertaken using GridSearchCV, an effective tool from the sci-kit-learn library used as a search method. This specific methodology is divided into the conjunctive query, which evaluates predetermined grid parameters for each model to find the best combination of parameters that might result in higher accuracy [172]. Its application stems from the complexity and sensitivity of the ML algorithms towards hyperparameter settings. The notable parameters for SVM are presented in Table 5.4, and those of the RF classifier are illustrated in Table 5.5.

Table 5.4: Optimal hyperparameters for Random Forest model.

| Parameter | Value | Description |
|---|---|---|
| max_depth | 10 | Determines the maximum depth of every tree in the forest, allowing the model to adequately capture the complexity of the data while assisting in the prevention of overfitting. |
| max_features | 0.1 | Splits nodes automatically using all available features, maximizing the model's capacity to consider diverse information during learning. |
| min_samples_leaf | 5 | Guarantees that every leaf has a minimum of one sample, offering the highest level of decision-making granularity. |
| min_samples_split | 5 | This parameter controls the minimum number of samples that are needed to split an internal node. |
| n_estimators | 16 | Specifies the number of trees in the forest, ensuring robust predictions and stability in the model's performance. |

With GridSearchCV, we can determine what combination of the regularization parameters plays a significant role in the best-fit model. It is a two-step process that entails the model estimation following parameter search around the training dataset and parameter validation by applying a cross-validation method. Thus, cross-validation leads to the selection of hyperparameters, which will contribute to achieving a consistent model within a specific data sample and for different sets [173]. Therefore, the best parameters found are utilized in the final model configuration, which ensures that the models are effective at making correct predictions on unseen data [174]. This is crucial for our case study in composite health monitoring.

Table 5.5: Optimized SVM parameters.

| Parameter | Value | Description |
|---|---|---|
| C | 100 | C corresponds to the regularization parameter; it manages the trade-off between a smooth decision boundary and a low-error classifier. |
| Gamma | 0.001 | The kernel coefficient for the 'sigmoid' kernel, influencing the shape of the decision function [175]. |
| Kernel | sigmoid | Specifies the type of kernel used, which in this case is 'sigmoid', suitable for non-linear data classification. |

## 5.5 Results and Discussion

### 5.5.1 Feature Visualization

Indeed, GAF images make specific patterns more discernible to human and computer algorithms than traditional STFT plots, particularly for composite materials where defect features are highly non-linearly correlated. In the context of SHM, the GAF visualizations presented in Figure 5.8 illustrate the various defect states ranging from a pristine, undamaged material (Figure 5.8a) to composites with single defects (Figure 5.8b, hole defect; Figure 5.8c, scratch defect) and complex compound defects (Figure5.8d - 5.8g). These images serve as a matrix where the color intensity and distribution patterns correspond to the angular spectrum of time series data generated from the composite material under vibrational test. Notably, the homogeneity in the healthy sample's matrix sets a baseline against which the defect-induced anomalies can be contrasted, with the perturbations in the angular spectrum vividly capturing the manifestation of defects within the material's structure.

The variations observed across these visualizations indicate changes in the material's dynamic properties, namely stiffness, and damping, which are directly affected by the presence and type of defects induced on the structure. For example, a healthy material sample (Figure 5.8a) typically exhibits uniform angular spectral patterns reflective of consistent stiffness and damping across the material. This consistency is disrupted in the presence of defects; hole defects (Figure 5.8b), for instance, may result in the reduction of the local stiffness and alteration of the damping characteristics due to the material removal and the resulting stress concentration, which is translated into the GAF as more pronounced color variations or intensity shifts. Similarly, scratch defects (Figure 5.8a) and compound defects (Figure 5.8d - 5.8f) introduce localized changes in the material properties; scratches creates surface discontinuities affecting the load transfer and thus modify the angular spectrum (this might not be well visualized in our case since the induced scratch was not deep enough and might necessitate computer algorithm such as image processing algorithms, machine learning models, and signal processing techniques, to extract associated features).

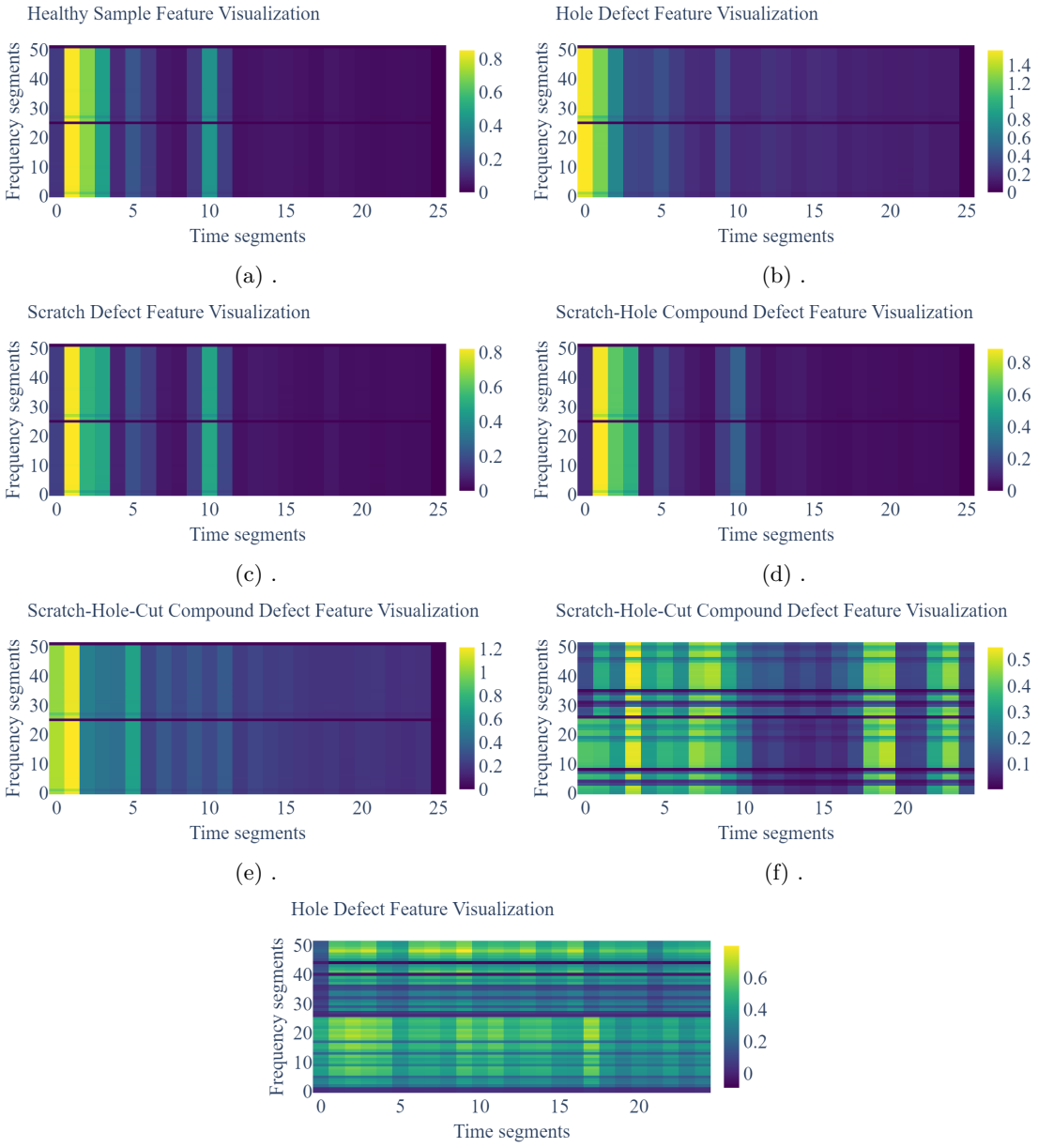


Figure 5.8: Comparative Gramian angular field (GAF) visualizations of composite material defects, using embedded (Figure 5.8a - 5.8e) and surface (accelerometer) (Figure 5.8f - 5.8g) sensor responses to assess integrity and health at various damage levels.

In contrast, compound defects present overlapping features of different damages, as seen in the scratch-hole-cut defect (Figure 5.8e), where the composite effect significantly reduces material stiffness and produces more pronounced low frequencies in the GAF matrix.

It is worth noting that the images presented in Figure 5.8a - 5.8f illustrate the transformation of the time series data obtained from the embedded sensor, and we can see that we have a clear dynamic following concerning the advancement of the damage severity and type, reflecting the high quality of the data captured.

In the last two figures, Figure 5.8e and 5.8f, the patterns captured by the sensors attached to the surface are noticeably different from the patterns observed in the preceding images, which is likely attributable to environmental noise, inconsistencies from the excitation sources in real-life applications, and data acquisition system noise. The frequency is still evident. However, it is not trivial to identify the frequency region that could precisely describe the defect type. Based on the apriori knowledge, the environmental signals can introduce false signals unrelated to the material's intrinsic properties or structural flaws, which can be seen in the GAF as irregular, stochastic color variations that obscure the underlying defect signatures, making interpretation of the material's health status more complicated. The fact that the surface attached sensor is prone to noise sources leads to the observed less coherent angular spectral representation. The lack of a straightforward dynamic response pattern in these visualizations also implies the absence of direct coupling between the sensors and the material's internal structure. Unlike embedded sensors, which are more effective in capturing the propagation of waves and resonances within the material. Consequently, data obtained from surface sensors requires sophisticated signal processing techniques to filter out noise and extract meaningful information. Due these challenges, in-situ sensing proves to be vital for the practical deployment in future SHM systems.

### 5.5.2 Anomaly Detection

Figure 5.9 displays the confusion matrix for defect detection. Rows represent the original categories of the targets, and columns indicate the assigned classifications. Figure 5.9a demonstrates the SVM model's ability to identify anomalies using data from the fully embedded sensor, achieving an accuracy of 76% for both healthy and defective samples, with at least a 24% misclassification rate in each category. This suggests that the boundary between healthy and defective states in composite structures is not distinctly defined, likely due to similar feature overlaps in certain conditions. This inference is supported by feature visualization in the previous section, which shows a nearly identical response distribution between healthy states and scratch defects

in time-frequency angular spectra. Consequently, such outcomes are expected when the SVM algorithm considers these similarities.

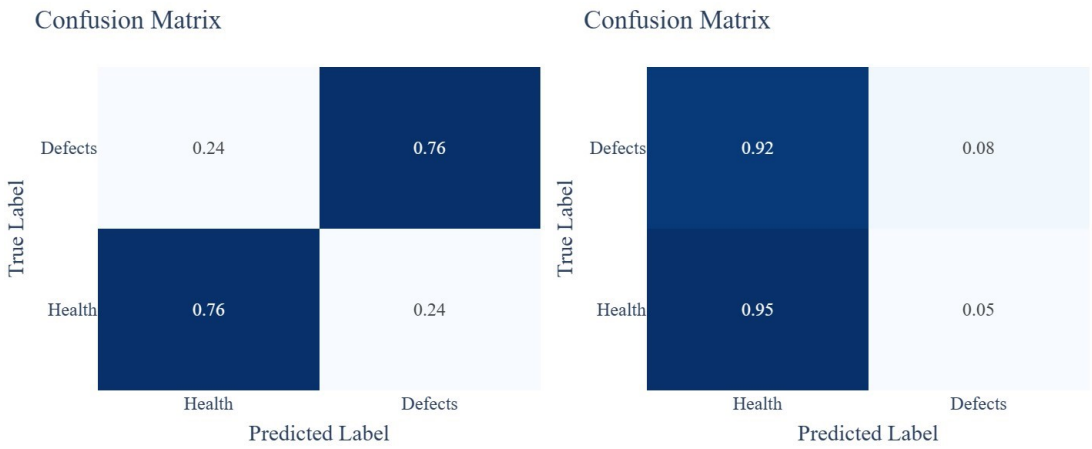


(a) Confusion matrix from fully embedded sensor data.

(b) Confusion matrix from surface attached sensor data.

Figure 5.9: Normalized confusion matrices of anomaly detection based on SVM. The evaluated dataset comprises those obtained from direct and indirect sensing approaches.

Figure 5.9b presents the confusion matrix of anomaly detection using data from the surface-attached sensor with an older model (trained model). The model predominantly identifies all samples as healthy, demonstrating an accuracy of 95% for healthy samples and detecting only 0.08% as defective. This indicates the model's ineffectiveness in distinguishing between the two states, possibly due to the noisier data from surface sensors obscuring defect-related information. Moreover, some channels might not clearly differentiate due to overlapping information, inadvertently enhancing the appearance of healthy features. Consequently, it becomes apparent that detecting anomalies is more straightforward with fully embedded sensors, even when simpler algorithms are employed.

### 5.5.3 Defect Type Recognition and Classification

Figure 5.10 displays the confusion matrix of the Random Forest (RF) model, assessed using a test dataset encompassing five classes: healthy, scratch, hole, scratch-hole combination, and scratch-hole-cut combination defect. This matrix categorizes the target classes (actual class) against the predicted outputs derived from the test data. The model accurately identified four

classes with 100% precision, underscoring its potential for practical, real-world application. However, the scratch defect class showed a notable classification error, with 11.11% of samples erroneously identified as hole defects. This misclassification, possibly stemming from challenges in discerning clear patterns in scratch defects as indicated by GAF visualizations, poses significant risks in practical scenarios. Misidentifying a minor scratch as a more severe hole defect could lead to unwarranted operational repair shutdowns, resulting in unnecessary expenses. Similarly, underestimating severe defects could precipitate grave failures from overlooked damages. Overall, the RF model demonstrates robust performance with an overall accuracy exceeding 98%, yet the specific issue with scratch defect misclassification needs addressing to enhance its reliability in practical applications.

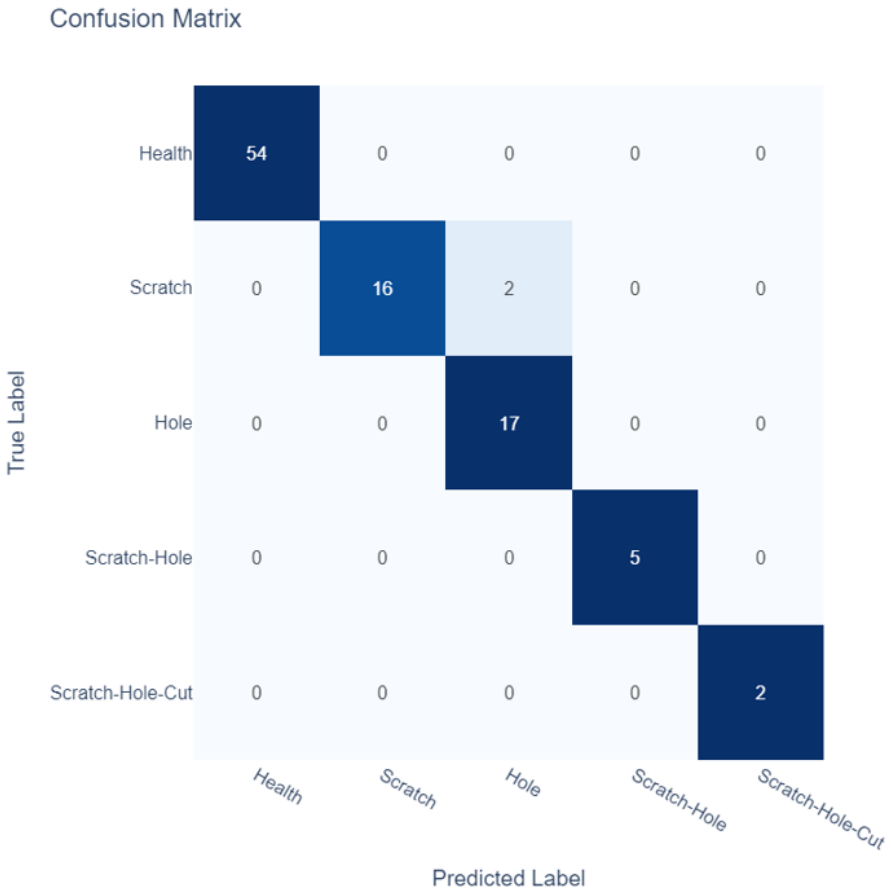


Figure 5.10: Confusion matrix of the RF model based on five classes derived from in-situ sensing approach.

Figure 5.11 shows the testing results of the previously trained RF model on two defect classes using data from a surface sensor across 24 experiments. The model's performance was weak; in the hole defect category, only 3 out of 12 samples were correctly classified, with the others mislabeled as healthy, scratch, or scratch-hole. For the scratch-hole-cut category, all samples were incorrectly classified as healthy, hole, or scratch-hole. This misclassification correlates with the overlap of patterns and noise observed in the GAF feature maps, likely due to indirect sensing methods where proper information shares channels, complicating the distinction of specific defect classes. Consequently, this poor classification performance necessitates retraining the model to capture better and integrate these data patterns.

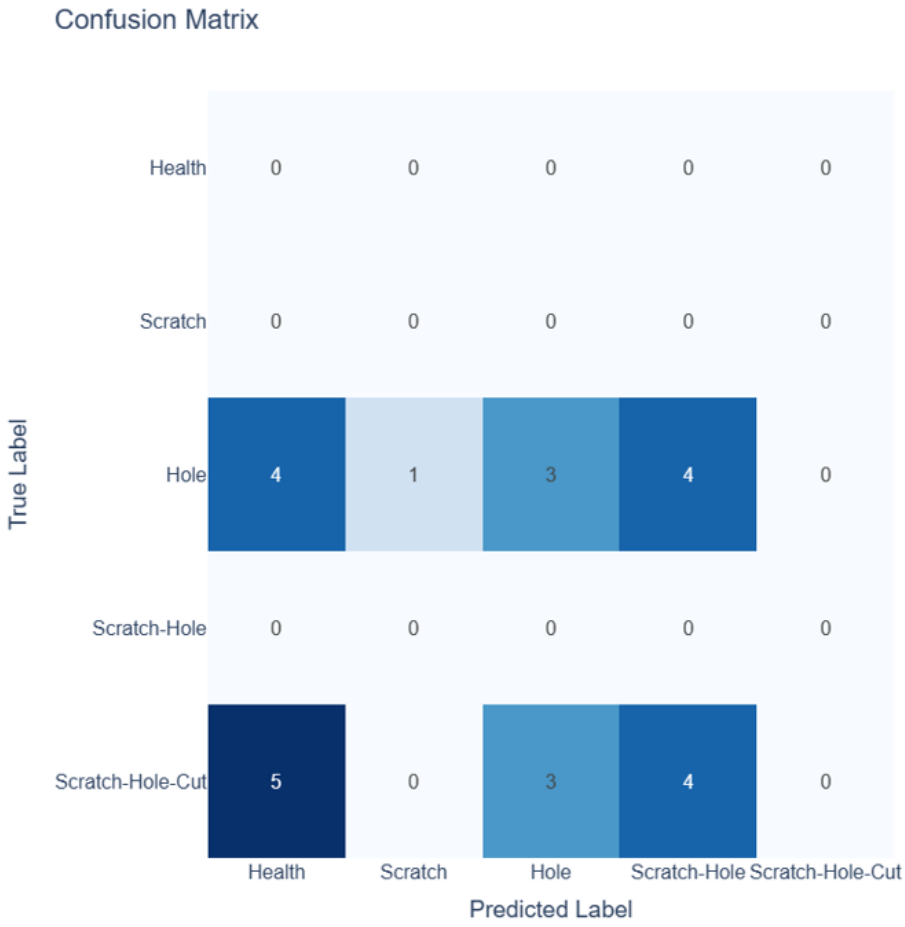


Figure 5.11: Confusion matrix of the RF model tested on surface sensor data without retraining.

Figure 5.12 shows the resulting model performance after retraining with the surface data. The model is evaluated with four test experiments: hole defect data and scratch-hole-cut defect data. The model performs well in single defect identification but poorly in combinations. The incorporation of new data influences its diagnostic capabilities. For instance, the scratch-hole defect combination has its prediction accuracy lowered, identifying actual scratch-hole defects as scratch-hole-cut.

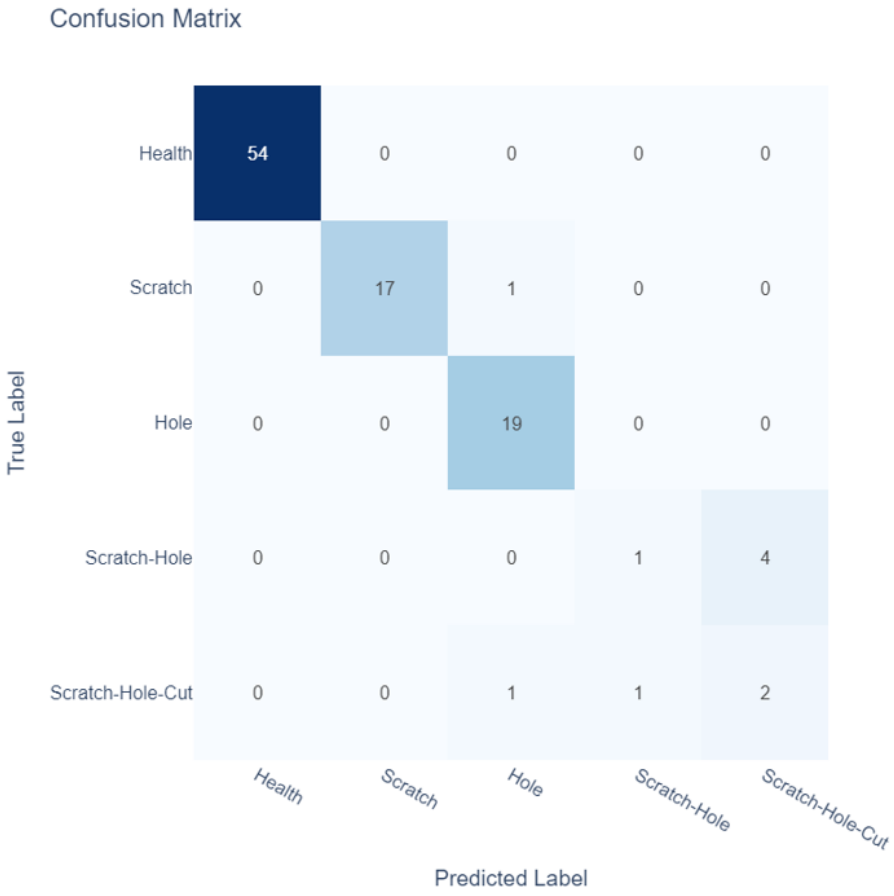


Figure 5.12: Confusion Matrix of the retrained RF model incorporating the surface sensor data.

This observation can be attributed to the unclear and overlapping feature pattern boundaries introduced by the surface-attached sensor data. The issue can be explained by the fact that the sensor is placed far from the failure sources and, after the structure transmission, fails to capture defect-indicative signals correctly. There is still difficulty in the scratch-hole-cut

combination due to feature overlaps, as the two samples are misclassified as hole and scratch-hole. However, in the case of the hole defect, the defect was correctly recognized as a hole in both sensing approaches. This means that when this type of fault occurs in the structure, it changes significant parameters that are very clear for the model to capture, unlike in the scratch-hole-cut combination. Therefore, it is evident that the in-situ sensor can capture weak patterns, which are impossible with indirect measurement.

### 5.5.4 Improving Random Forest by Applying Attention Mechanism

In this model, raw in-situ data are interpreted through high-quality features, creating representations that serve as a vital link between the ML model and the attributes of physical reality. These representations are crucial for achieving robust generalization and interpretability. The Gram's angle transformation applied to the time-frequency spectra from the original fault measurement signals, as discussed in this study, is highly representative. Its generalization capabilities are essential for the reliability and practical application of the low-cost, easily deployable Random Forest model derived from the training data. Typically, after learning individual faults in the training samples, the ability of the Random Forest model to accurately identify unseen composite faults in practice becomes a significant concern. To validate this, the "Hole-cut" experiments were conducted to gather data concerning this composite fault, enhancing the diagnostic generalization capabilities of the Random Forest model. The results are illustrated in Table. 5.6, and the model performance is presented in Figure 5.13. The provided figure and table reveals the RF model's generalization performance as tested with the new data obtained from the "Hole-cut" combination damage scenario. It highlights limited ability in distinguishing this new defect type, although it has learned the simple "Hole" and "Scratch-Hole-Cut" defects in advance. The one-hot encoding on "Hole-cut" recognition results is incomplete, suggesting potential issues like model bias and insufficient training data for these categories. This indicates a need for model reassessment, possibly focusing on better feature representation and interpretation for RF model in working on less frequent categories to enhance overall predictive accuracy and robustness.

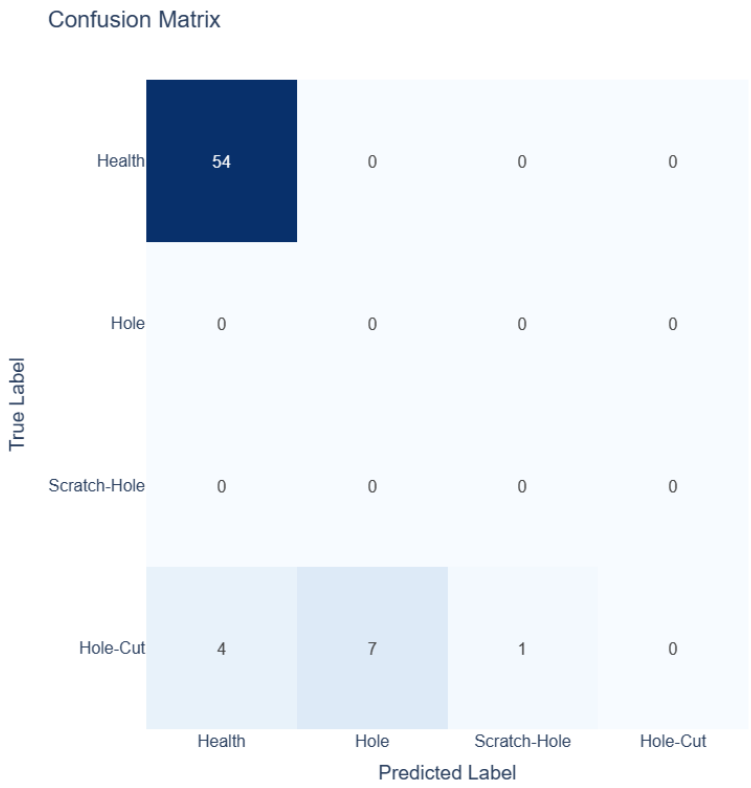


Figure 5.13: Confusion Matrix of the trained RF model on the unseen data bearing a hole-cut damage combination.

Table 5.6: Hole-cut samples prediction results. All twelve hole-cut samples are misclassified. Seven samples are labeled as having a simple hole defect, four as healthy, and one as having scratch-hole defect features.

| **Sample No.** | **Predicted Results** | **Predicted Faults** | **Real Faults** |
|---|---|---|---|
| 1 | [0, 0, 1, 0] | Hole | Hole-Cut |
| 2 | [0, 1, 1, 0] | Scratch-Hole | Hole-Cut |
| 3 | [0, 0, 1, 0] | Hole | Hole-Cut |
| 4 | [0, 0, 0, 0] | Healthy | Hole-Cut |
| 5 | [0, 0, 1, 0] | Hole | Hole-Cut |
| 6 | [0, 0, 1, 0] | Hole | Hole-Cut |
| 7 | [0, 0, 0, 0] | Healthy | Hole-Cut |
| 8 | [0, 0, 1, 0] | Hole | Hole-Cut |
| 9 | [0, 0, 1, 0] | Hole | Hole-Cut |
| 10 | [0, 0, 1, 0] | Hole | Hole-Cut |
| 11 | [0, 0, 0, 0] | Healthy | Hole-Cut |
| 12 | [0, 0, 0, 0] | Healthy | Hole-Cut |

Generally, a robust ML tool with strong generalization ability must excel in three critical aspects: high-quality feature extraction, comprehensive feature interpretation, and effective utilization of these insights in decision-making processes. In many studies, the latter two aspects are often integrated into a black-box model, such as a deep neural network. However, the lack of interpretability, high computational costs, and deployment rigidity have long deterred composite SHM researchers.

For this reason, we explore the possibility of a bridging technique, i.e., constructing an end-to-end diagnostic model using a simple attention layer as a parser of features, replacing PCA in the original approach, as illustrated in Figure 5.14. The complete bridging mechanism comprises three sequential steps:

- Constructing a basic neural network layer incorporating the attention mechanism, the linearly projected features are used to generate an attention map. Specifically, the attention mechanism calculates the importance weights, or attention scores, for each position in the feature map. This is typically done through dot product, producing an attention map that matches the dimensions of the GAF feature map. This attention map represents the importance of each position. The generated attention map is then normalized (e.g., using a softmax function) to ensure the weights sum to 1. Next, this attention map is element-wise multiplied with the original feature map. This operation adjusts the feature values based on their corresponding weights in the attention map, amplifying important features while suppressing less important ones. The result of this multiplication is the feature map weighted by the attention mechanism, referred to as the modified features.

- Employing the pre-trained Random Forest model as a secondary level model, trained and forecasted using the features derived from the neural network.

- Implementing model distillation: utilizing the Random Forest's output to train an additional output layer connected to the original neural network. This process facilitates the neural network's acquisition of the capability to emulate the predictions of the Random Forest.

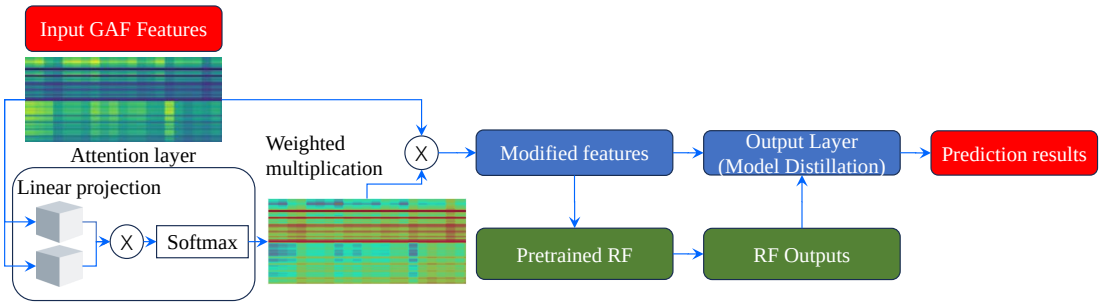


Figure 5.14: Improving Random Forest by applying attention mechanism in GAF features automatic selections.

The proposed model is still trained on a dataset that does not contain "Hole-Cut" fault types, and the original Random forest is used as a parameter-frozen classifier during the training process, and then the attention layer embedded in the input space is trained using only the training set and early stop and check are used during the training process. The weights and parameters of the best-performing attention layer are saved using early stop and checkpoints to prevent overfitting. The improved model's performance is presented in Figure 5.15 and the results based on one-hot encoding are summarized in Table 5.7.

Comparing the results in Table. 5.6 and Table. 5.7, the following findings can be drawn:

- The proposed bridging technique, which combines a simple attention layer as a feature parser with the pre-trained Random Forest model and model distillation, shows promising results in improving the model's generalization ability for composite fault diagnosis.
- After applying the proposed bridging technique, the model demonstrates improved performance in identifying the "Hole-Cut" fault category, correctly classifying 9 out of 12 samples. This suggests that the attention mechanism and model distillation helps the model to better capture and learn the characteristics of the "Hole-Cut" fault, enhancing its diagnostic capabilities.

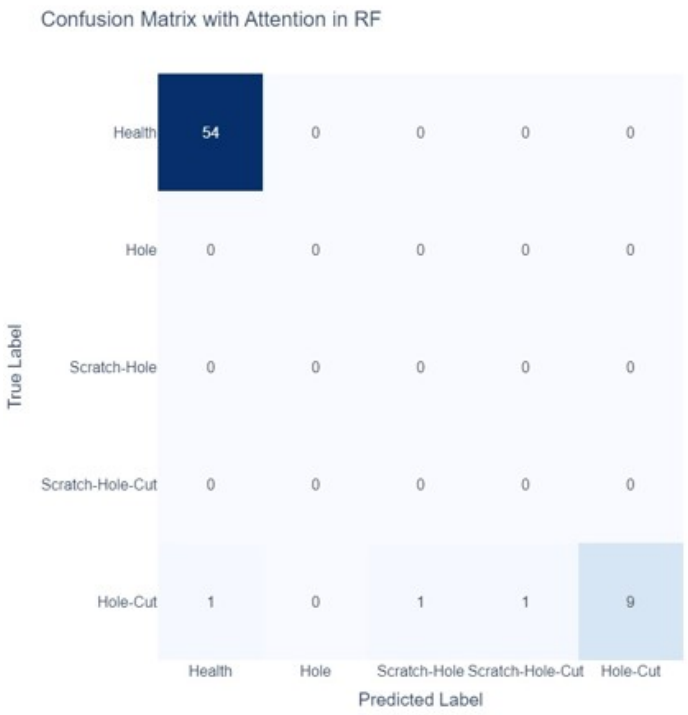


Figure 5.15: Confusion matrix of the trained RF model on unseen data with a hole-cut damage combination, incorporating the attention mechanism.

Table 5.7: Sample Predictions and Faults. Out of twelve samples, nine were identified correctly. One sample was misclassified as healthy, one as a scratch-hole combination defect, and one as scratch-hole-cut damage. These results demonstrate the model's robustness in capturing defect type features with the attention mechanism.

| **Sample No.** | **Predicted Results** | **Predicted Faults** | **Real Faults** |
|---|---|---|---|
| 1 | [0,0, 1, 1] | Scratch-Hole | Hole-Cut |
| 2 | [0,0, 1, 1] | Scratch-Hole-Cut | Hole-Cut |
| 3 | [0,0, 1, 1] | Hole-Cut | Hole-Cut |
| 4 | [0,0, 1, 1] | Hole-Cut | Hole-Cut |
| 5 | [0,0, 1, 1] | Hole-Cut | Hole-Cut |
| 6 | [0,0, 1, 1] | Hole-Cut | Hole-Cut |
| 7 | [0,0, 1, 1] | Hole-Cut | Hole-Cut |
| 8 | [0,0, 1, 1] | Hole-Cut | Hole-Cut |
| 9 | [0,0, 1, 1] | Hole-Cut | Hole-Cut |
| 10 | [0,0, 1, 1] | Hole-Cut | Hole-Cut |
| 11 | [0,0, 1, 1] | Hole-Cut | Hole-Cut |
| 12 | [1,0, 0, 0] | Healthy | Hole-Cut |

## 5.6 Summary and Conclusions

In this chapter, a novel approach to structural health monitoring (SHM) of aerospace composite structures is introduced, leveraging embedded sensor data and machine learning (ML) techniques for enhanced fault detection and identification. Initially, an in-situ sensing system was developed, integrating polymer piezoelectric sensors within composite materials for direct measurement and high-quality near-fault data acquisition. Utilizing a time-frequency transform combined with Gram's angle field, this method effectively extracts fault features from these measurements, showing clearer and more distinct fault patterns than traditional surface-attached sensors. Feature interpretation through principal component analysis precedes anomaly detection and classification using a random forest model. The results demonstrate diagnostic accuracies of 100% for combinations of faults such as holes and scratches, and 88.90% for purely scratches, even in small sample sizes.

To assess robustness, the study further tests a new combinatory fault type, "Hole-cut", not present in the training set. By enhancing feature interpretation and using a simple neural network layer with an attention mechanism to preprocess inputs for the pre-trained random forest, a robust model capable of identifying new fault combinations is achieved. These findings suggest that in-situ sensing substantially reduces the complexity of applying ML techniques and holds significant potential for advancing SHM in aerospace applications, ensuring improved performance, reliability, and simplified fault management.

# Chapter 6

# Conclusions and Perspectives

## Contents



## 6.1 General Conclusions

To gain a competitive advantage in the twenty-first century, aircraft manufacturers must emphasize the development of highly functional and energy-efficient materials and structures. The field of aeronautical engineering has undergone significant advancements to improve the performance, safety, efficiency, profitability, and durability of aircraft structures. Progress in materials and diagnostic technologies is fundamental to this endeavor, as it can revolutionize the comprehension and management of the structural health of aircraft. To this aim, this thesis has explored the innovative integration of fiber-reinforced composites with piezoelectric materials to create smart composites with advanced functionality, particularly for applications in struc-

tural health monitoring and energy harvesting. Significant advancements have been made in understanding these multifunctional materials through comprehensive research, encompassing material selection, fabrication processes, and experimental testing.

Chapter 2 presents a comprehensive background of these constituent materials, emphasizing the various types of fiber-reinforced composites and piezoelectric materials, alongside their advantages and potential applications. In this instance, the selection of materials played a critical role in integration. Polyvinylidene fluoride (PVDF) was chosen due to its minimal impact on the structural integrity of the composites and its advantageous piezoelectric properties. The findings of this research demonstrated that PVDF could be integrated into the composites without significant variations in thickness or damage to the fibers, which is essential for maintaining the mechanical performance of the composites.

In Chapter 3, after the selection of the base materials, a meticulous fabrication process was undertaken to produce smart composites. This process was designed to preserve the piezoelectric properties of the embedded elements. The experimental results, obtained through X-ray Tomography analysis, revealed that the integration of a 52 µm thick PVDF film had minimal adverse effects on the overall structure of the composites. The mechanical integrity of the composites remained intact, with only slight degradation in interlaminar shear strength (ILSS). This underscores the reliability and efficiency of PVDF for such applications. The potential utilization of natural fibers in secondary aerospace structures was also explored; despite their lower mechanical properties compared to carbon fibers, they offer promising functional benefits. The thermo-electromechanical performance of the developed smart composites was also a key focus of our research. Our findings highlighted that these materials exhibit stable behavior under dynamic loading and temperature variations up to their glass transition temperature (Tg). Beyond this threshold, degradation in piezoelectric properties due to thermal stresses was observed, emphasizing the need for careful consideration of operating temperature ranges in practical applications. Furthermore, dynamic vibration test responses confirmed their functional properties, which led to exploring their potential applications.

Additionally, they set their operational limits after establishing their mechanical, electromechanical, and thermo-electromechanical properties. We then delved into their prospective practical applications, as presented in Chapter 4, mainly providing a brief overview of energy harvest-

ing capabilities and an extensive investigation of SHM applications. Empirical and numerical analyses demonstrated that these materials could efficiently harvest energy from ambient vibrations, offering a sustainable solution for powering SHM systems. Our findings show that embedded PVDF sensors effectively detect structural anomalies under static and dynamic loading scenarios. It also provides a promising solution for self-powered real-time sensing within structures, enhancing safety through condition-based maintenance.

Chapter 5 presents a case study where an advanced SHM approach was developed using embedded sensors and machine learning techniques. This method significantly improved fault detection and identification by leveraging high-quality data acquisition and sophisticated data analysis, even for complex fault types. Our results highlight the potential of integrating smart composites with machine learning to enhance the reliability and performance of SHM systems in aerospace and other critical applications. A comparison of surface-attached sensors and embedded sensor performance concerning damage detection and recognition was evaluated. It was evident from the results that embedded sensors, which offer in-situ sensing, are highly suitable for monitoring structural health states and can provide high-quality data where damage features and clear patterns can be easily extracted for diagnosis.

In conclusion, this research has laid a robust groundwork for the development of smart composites with embedded piezoelectric sensors. The findings underscore the transformative potential of these materials in enhancing the safety, efficiency, and sustainability of modern aerostructures. The advancements presented in this thesis are poised to ignite a wave of innovation in materials science and engineering, leading to the creation of more resilient and intelligent structural systems. The integration of multidisciplinary techniques, such as advanced artificial intelligence (AI) algorithms, material science, and sensing technologies, for real-time monitoring and structural health diagnosis, heralds a potential revolution in the materials of the future. This innovation holds the promise of reducing accidents caused by operational damages, a challenge that has traditionally been difficult to address at the point of occurrence.

## 6.2 Perspectives

Major industrial players in the aeronautics industry are focusing on research to reduce aircraft maintenance costs through structural health monitoring (SHM) technology to remain competitive in their highly challenging market. Commercial full-scale in-situ SHM systems are still under development. A significant paradigm shift in the aircraft sector will result from a sustainable SHM strategy utilizing self-powered embedded sensors within the structure. The prospect of eliminating the need for disassembling airplanes for routine maintenance checks makes this approach particularly appealing, underscoring the necessity to explore potential fabrication techniques, constituent materials, and optimal SHM methods. Although this thesis has presented promising advancements through comprehensive exploratory research into the piezoelectric functionalization potential for aeronautic composite structures, further research is needed in the following areas:

- **Optimal size and positioning of active Embeds:** future research aims to investigate the optimal dimensions and positioning of active embeds to maximize energy generation at ambient frequencies. Numerical simulations and experimental validations must be carried out to ascertain the optimal configuration for energy harvesting. This entails determining the most suitable shape and arrangement of piezoelectric inserts within the structure. Optimization techniques will be employed to ensure both high sensitivity and efficient energy production.

- **Durability testing:** when subjected to extended periods of dynamic loading, evaluating the anticipated durability of these smart composite materials through multiple testing cycles is crucial to ascertain their long-term efficacy in aeronautical structures.

- **Advanced SHM systems development:** according to the findings and results of this research, future work can contribute to developing more advanced, reliable, and efficient SHM systems. The integration of distributed sensors will be explored, as it may be interesting to investigate the scalability and deployment of embedded sensor networks for monitoring larger composite structures. This study will also consider leveraging self-powered and in-situ monitoring, possibly extending the research to wireless data streaming capa-

bilities. Regarding the ML-based in-situ SHM proposed in my thesis, further work could aim to justify their trustworthiness. Additional research will delve into the relationship between attention mechanism weights in machine learning models and the physical characteristics of composite structures and fault types. Understanding this relationship will provide valuable insights into the decision-making processes of these models, ultimately improving the accuracy and reliability of SHM systems.

- **Consolidation process monitoring:** To continuously monitor the consolidation process in real-time, future work will concentrate on improving the integration of these piezo sensors. In order to detect even the smallest variations in temperature, and pressure, all of which are essential to the curing process.

- **Cross domain applications**: Beyond sensing and energy harvesting for structural health monitoring (SHM) in aerospace, they could play a role in bio-sensing and wearable health monitoring devices as well as infrastructural monitoring.

- **Natural fibers**: Further analysis regarding the uncertainties brought about by the nature of natural fibers should be considered in future studies.

- **Acoustic emissions**: Structural health monitoring based on the acoustic emissions results in our findings requires in-depth analysis to extract failure signatures and to describe their evolution to enhance reliability and generalization.

# Bibliography


[1] Ramakrishnan Thirumalaisamy et al. “Recent Developments in Stimuli Responsive Smart Materials and Applications: An Overview”. In: *Journal of Nanomaterials* 2022 (Sept. 2022), pp. 1–7. DOI: 10.1155/2022/4031059.

[2] W B Spillman, J S Sirkis, and P T Gardiner. “Smart materials and structures: what are they?” In: *Smart Materials and Structures* 5.3 (June 1996), pp. 247–254. DOI: 10.1088/0964-1726/5/3/002. URL: https://doi.org/10.1088/0964-1726/5/3/002.

[3] Yumna Qureshi. “Development of a new generation of fiber sensors for structural health monitoring in composites in real-time”. Theses. ENSTA Bretagne - École nationale supérieure de techniques avancées Bretagne, July 2020. URL: https://theses.hal.science/tel-03405241.

[4] Ioan Alexandru Ivan et al. “Quasi-static displacement self-sensing measurement for a 2-DOF piezoelectric cantilevered actuator”. In: *IEEE Trans on Industrial Electronics* (2017). DOI: 0.1109/TIE.2017.2677304.

[5] Micky Rakotondrabe. “Combining self-sensing with an Unkown-Input-Observer to estimate the displacement, the force and the state in piezoelectric cantilevered actuator”. In: *American Control Conference Washington DC USA* (2013), pp. 4523–4530.

[6] Qinghua Qin. *Advanced Mechanics of Piezoelectricity*. Springer Science & Business Media, Sept. 2013. ISBN: 978-3-642-29766-3.

[7] Sofiane Khadraoui, Micky Rakotondrabe, and Philippe Lutz. “Optimal design of piezoelectric cantilevered actuators with guaranteed performances by using interval techniques”. In: *IEEE/ASME Trans on Mechatronics* 19 (2014), pp. 1660–1668.

[8] Kanty Rabenorosoa and Micky Rakotondrabe. “Performances analysis of piezoelectric cantilever based energy harvester devoted to mesoscale intra-body robot”. In: *SPIE Sensing Technology Applications Baltimore USA*. 2015, pp. 9494–28.

[9] Suvrajyoti Mishra et al. “Advances in Piezoelectric Polymer Composites for Energy Harvesting Applications: A Systematic Review”. In: *Macromolecular Materials and Engineering* 304 (Nov. 2018). DOI: 10.1002/mame.201800463.

[10] Subhransu Kumar Panda and J. Srinivas. “Electro-structural analysis and optimization studies of laminated composite beam energy harvester”. In: *Mechanics of Advanced Materials and Structures* 29.25 (2022), pp. 4193–4205. DOI: 10.1080/15376494.2021.1922787. eprint: https://doi.org/10.1080/15376494.2021.1922787. URL: https://doi.org/10.1080/15376494.2021.1922787.

[11] Dinesh Yadav et al. “Modeling and simulation of an open channel PEHF system for efficient PVDF energy harvesting”. In: *Mechanics of Advanced Materials and Structures* 28.8 (2021), pp. 812–826. DOI: 10.1080/15376494.2019.1601307. eprint: https://doi.org/10.1080/15376494.2019.1601307. URL: https://doi.org/10.1080/15376494.2019.1601307.

[12] Eugenio Brusa Mahmoud Askari and Cristiana Delprete. “Design and modeling of a novel multi-beam piezoelectric smart structure for vibration energy harvesting”. In: *Mechanics of Advanced Materials and Structures* 29.28 (2022), pp. 7519–7541. DOI: 10.1080/15376494.2021.2001122. eprint: https://doi.org/10.1080/15376494.2021.2001122. URL: https://doi.org/10.1080/15376494.2021.2001122.

[13] Yasser Al Hamidi. “Multivariable feedforward control of vibrations in multi-axes flexible structures : applications to multi-axes piezoelectric actuators”. Theses. Université Bourgogne Franche-Comté, Dec. 2017. URL: https://theses.hal.science/tel-02382026.

[14] Susmita Kamila. “Introduction, Classification and Applications of Smart Materials: An Overview”. In: *American Journal of Applied Sciences* 10 (July 2013), pp. 876–880. DOI: 10.3844/ajassp.2013.876.880. URL: https://thescipub.com/abstract/ajassp.2013.876.880.

[15] Bisma Parveez et al. “Scientific advancements in composite materials for aircraft applications: a review”. In: *Polymers* 14.22 (2022), p. 5007.

[16] Alin Diniță et al. “Advancements in Fiber-Reinforced Polymer Composites: A Comprehensive Analysis”. In: *Polymers* 16.1 (2024). ISSN: 2073-4360. DOI: 10.3390/polym16010002. URL: https://www.mdpi.com/2073-4360/16/1/2.

[17] Jens Bachmann, Carme Hidalgo, and Stéphanie Bricout. “Environmental analysis of innovative sustainable composites with potential use in aviation sector—A life cycle assessment review”. In: *Science China Technological Sciences* 60 (Aug. 2017). DOI: 10.1007/s11431-016-9094-y.

[18] K Rogers Langat et al. “Robotic-Assisted Measurement of Fabrics for the Characterization of the Shear Tension Coupling”. In: *Key Engineering Materials* 926 (2022), pp. 1303–1316. DOI: 10.4028/p-f0d0u9.

[19] Yonglin Chen et al. “Manufacturing Technology of Lightweight Fiber-Reinforced Composite Structures in Aerospace: Current Situation and toward Intellectualization”. In: *Aerospace* 10.3 (2023), p. 206. ISSN: 2226-4310. DOI: 10.3390/aerospace10030206. URL: https://www.mdpi.com/2226-4310/10/3/206.

[20] Alexander Grootel et al. “Manufacturing variability drives significant environmental and economic impact: The case of carbon fiber reinforced polymer composites in the aerospace industry”. In: *Journal of Cleaner Production* 261 (Mar. 2020), p. 121087. DOI: 10.1016/j.jclepro.2020.121087.

[21] Dhanasingh Sivalinga Vijayan et al. “Carbon Fibre-Reinforced Polymer (CFRP) Composites in Civil Engineering Application—A Comprehensive Review”. In: *Buildings* 13.6 (2023). ISSN: 2075-5309. DOI: 10.3390/buildings13061509. URL: https://www.mdpi.com/2075-5309/13/6/1509.

[22] Pierre Duchene et al. “A review of non-destructive techniques used for mechanical damage assessment in polymer composites”. In: *Journal of materials science* 53.11 (2018), pp. 7915–7938.

[23] Yutong Fu and Xuefeng Yao. "A review on manufacturing defects and their detection of fiber reinforced resin matrix composites". In: *Composites Part C: Open Access* 8 (2022), p. 100276. ISSN: 2666-6820. DOI: https://doi.org/10.1016/j.jcomc.2022.100276. URL: https://www.sciencedirect.com/science/article/pii/S266668202200041X.

[24] K Dragan et al. "Structural health monitoring of composite structures with use of embedded PZT piezoelectric sensors". In: *Proceedings of the ECCM-16th European Conference on Composite Materials, Seville, Spain*. 2014, pp. 22–26.

[25] Ramamurthy Prabhakaran. "Lightning Strikes on Metal and Composite Aircraft And Their Mitigation". In: *Journal of Aerospace Sciences and Technologies* Paper code V63 N3/729-2011 (Aug. 2011), pp. 208–222. DOI: 10.61653/joast.v63i3.2011.545.

[26] B. Arachchige, H. Ghasemnejad, and M. Yasaee. "Effect of bird-strike on sandwich composite aircraft wing leading edge". In: *Advances in Engineering Software* 148 (2020), p. 102839. ISSN: 0965-9978. DOI: https://doi.org/10.1016/j.advengsoft.2020.102839. URL: https://www.sciencedirect.com/science/article/pii/S0965997820302337.

[27] UT Jagadale, CB Nayak, and G Narute. "Structural health monitoring using piezoceramics smart material". In: *9th international conference on sustainable built environment*. 2018.

[28] Xianlong Chen et al. "Structural health monitoring of a smart composite structure with a Time-of-Flight method". In: *MEDYNA 2017: 2nd Euro-Mediterranean conference on structural dynamics and vibroacoustics*. 2017, pp. 25–28.

[29] Rogers K Langat et al. "Toward the development of a new smart composite structure based on piezoelectric polymer and flax fiber materials: Manufacturing and experimental characterization". In: *Mechanics of Advanced Materials and Structures* 0.0 (2023), pp. 1–15. DOI: 10.1080/15376494.2023.2271746. URL: https://doi.org/10.1080/15376494.2023.2271746.

[30] Joel Bafumba Liseli et al. "An overview of Piezoelectric Self-Sensing Actuation for Nanopositioning Applications: Electrical circuits, Displacement and Force estimation". In: *IEEE Transactions on Instrumentation & Measurement* 69.1 (2020), pp. 2–14. DOI: 10.1109/TIM.2019.2950760.

[31] Ioan Alexandru Ivan et al. “Quasi-static displacement self-sensing measurement for a 2-DOF piezoelectric cantilevered actuator”. In: *IEEE Transactions on Industrial Electronics* 64.8 (2017), pp. 6330–6337. DOI: 10.1109/TIE.2017.2677304.

[32] Rolf Paradies and Martin Ruge. “In situ fabrication of active fibre reinforced structures with integrated piezoelectric actuators”. In: *Smart Materials and Structures* 9 (Apr. 2000), p. 220. DOI: 10.1088/0964-1726/9/2/402.

[33] J. C. Henrandez et al. “Getting Started with PEAs-Based Flapping-Wing Mechanisms for Micro Aerial Systems”. In: *Actuators* 5.2 (2016), p. 14. DOI: 10.3390/act5020014. URL: https://www.mdpi.com/2076-0825/5/2/14.

[34] Xianlong Chen. “Development of a low-cost in-situ material characterization method and experimental studies of smart composite structures”. PhD thesis. Université Bourgogne Franche-Comté, Mar. 2019.

[35] Hari Prasad Konka. “Embedded piezoelectric fiber composite sensors for applications in composite structures”. PhD thesis. Louisiana State University and Agricultural & Mechanical College, 2011.

[36] R. Schulze et al. “Fiber-reinforced composite structures with embedded piezoelectric sensors”. In: *SENSORS, 2014 IEEE*. 2014, pp. 1563–1566. DOI: 10.1109/ICSENS.2014.6985315.

[37] Patrick Rougeot et al. “Design, modeling and simulation of a three-layers piezoelectric cantilevered actuator with collocated sensor”. In: *SPIE Sensing Technology+Applications* 9859 (2016), pp. 139–150. DOI: 10.1117/12.2229515.

[38] Matthew Pearson et al. “Energy Harvesting for Aerospace Structural Health Monitoring Systems”. In: *Journal of Physics: Conference Series* 382 (Aug. 2012). DOI: 10.1088/1742-6596/382/1/012025.

[39] Min Ju et al. “Piezoelectric Materials and Sensors for Structural Health Monitoring: Fundamental Aspects, Current Status, and Future Perspectives”. In: *Sensors* 23 (Jan. 2023), p. 543. DOI: 10.3390/s23010543.

[40] Sahir Masmoudi et al. “Structural Health Monitoring by Acoustic Emission of Smart Composite Laminates Embedded with Piezoelectric Sensor”. In: *Design and Modeling of Mechanical Systems*. Ed. by Mohamed Haddar et al. Berlin, Heidelberg: Springer Berlin Heidelberg, 2013, pp. 307–314. ISBN: 978-3-642-37143-1.

[41] Alfredo Güemes et al. “Structural Health Monitoring in Composite Structures by Fiber-Optic Sensors”. In: *Sensors* 18.4 (2018), p. 1094. ISSN: 1424-8220. DOI: 10.3390/s18041094. URL: https://www.mdpi.com/1424-8220/18/4/1094.

[42] Matthieu Gresil Marilyne Philibert Kui Yao and Constantinos Soutis. “Lamb waves-based technologies for structural health monitoring of composite structures for aircraft applications”. In: *European Journal of Materials* 2.1 (2022), pp. 436–474. DOI: 10.1080/26889277.2022.2094839. URL: https://doi.org/10.1080/26889277.2022.2094839.

[43] Alfredo Güemes. “SHM technologies and applications in aircraft structures”. In: *Proceedings of the 5th International Symposium on NDT in Aerospace, Singapore*. Vol. 1315. 2013.

[44] Victor Giurgiutiu. “17 - Structural health monitoring (SHM) of aerospace composites”. In: *Polymer Composites in the Aerospace Industry (Second Edition)*. Ed. by Philip Irving and Constantinos Soutis. Second Edition. Woodhead Publishing Series in Composites Science and Engineering. Woodhead Publishing, 2020, pp. 491–558. ISBN: 978-0-08-102679-3. DOI: 10.1016/B978-0-08-102679-3.00017-4. URL: https://www.sciencedirect.com/science/article/pii/B9780081026793000174.

[45] Daniel B Miracle, Steven L Donaldson, et al. “Introduction to composites”. In: *ASM handbook* 21 (2001), pp. 3–17.

[46] J.N. Reddy. “Mechanics of Laminated Composite Plates: Theory and Analysis”. In: *CRC-Press* (1996).

[47] Yann Meyer, Rémy Lachat, and George Akhras. “A review of manufacturing techniques of smart composite structures with embedded bulk piezoelectric transducers”. In: *Smart Materials and Structures* 28 (Mar. 2019). DOI: 10.1088/1361-665X/ab0fab.

[48] D Gay. “Composite Materials: Design and Applications”. In: *CRC-Press* (2014).

[49] Véronique Michaud. "A Review of Non-saturated Resin Flow in Liquid Composite Moulding processes". In: *Transport in Porous Media* 115 (Dec. 2016). DOI: 10.1007/s11242-016-0629-7.

[50] Youssef Hamidi and M. Altan. "Process Induced Defects in Liquid Molding Processes of Composites". In: *International Polymer Processing* 32 (Nov. 2017). DOI: 10.3139/217.3444.

[51] F.C. Campbell. *Structural Composite Materials*. ASM International, 2010. ISBN: 978-1-61503-140-5. URL: https://books.google.fr/books?id=D3Wta8e07t0C.

[52] Ivan V. Terekhov and Evgeniy M. Chistyakov. "Binders Used for the Manufacturing of Composite Materials by Liquid Composite Molding". In: *Polymers* 14.1 (2022). ISSN: 2073-4360. URL: https://www.mdpi.com/2073-4360/14/1/87.

[53] V. Michaud and A. Mortensen. "Infiltration processing of fibre reinforced composites: governing phenomena". In: *Composites Part A: Applied Science and Manufacturing* 32.8 (2001), pp. 981–996. ISSN: 1359-835X. DOI: https://doi.org/10.1016/S1359-835X(01)00015-X.

[54] Frank C. Robertson. "Resin transfer moulding of aerospace resins—a review". In: *British Polymer Journal* 20 (1988), pp. 417–429. ISSN: 1934-256X. DOI: 10.1002/pi.4980200506.

[55] M.K. Kang, W.I. Lee, and H.T. Hahn. "Analysis of vacuum bag resin transfer molding process". In: *Composites Part A: Applied Science and Manufacturing* 32 (Nov. 2001), pp. 1553–1560. DOI: 10.1016/S1359-835X(01)00012-4.

[56] S.Van Oosterom et al. "An objective comparison of common vacuum assisted resin infusion processes". In: *Composites Part A: Applied Science and Manufacturing* (2019).

[57] Vigneshkumar Ramdas Tamakuwala. "Manufacturing of fiber reinforced polymer by using VARTM process: A review". In: *Materials Today: Proceedings* 44 (Dec. 2020). DOI: 10.1016/j.matpr.2020.11.102.

[58] Sicong Yu et al. "A Conceptional Approach of Resin-Transfer-Molding to Rosin-Sourced Epoxy Matrix Green Composites". In: *Aerospace* 8.1 (2021). ISSN: 2226-4310. DOI: 10.3390/aerospace8010005. URL: https://www.mdpi.com/2226-4310/8/1/5.

[59] Xinlin Qing et al. “In-situ monitoring of liquid composite molding process using piezoelectric sensor network”. In: *Structural Health Monitoring* (Nov. 2020). DOI: 10.1177/1475921720958082.

[60] Jin Huang et al. “Simulation of Wrinkling during Bending of Composite Reinforcement Laminates”. In: *Materials* 13.10 (2020). ISSN: 1996-1944. DOI: 10.3390/ma13102374. URL: https://www.mdpi.com/1996-1944/13/10/2374.

[61] P. Boisse et al. “Bending and wrinkling of composite fiber preforms and prepregs. A review and new developments in the draping simulations”. In: *Composites Part B: Engineering* 141 (2018), pp. 234–249. ISSN: 1359-8368. DOI: https://doi.org/10.1016/j.compositesb.2017.12.061. URL: https://www.sciencedirect.com/science/article/pii/S1359836817340106.

[62] Pierre Curie. *Notice sur les travaux scientifique*. français. Paris, France: Gauthier-Villars, 1902.

[63] Jan Holterman and Wilhelm Albert Groen. *An introduction to piezoelectric materials and components*. Stichting Apllied Piezo, 2012.

[64] Kenji Uchino. *Advanced piezoelectric materials: Science and technology*. Sept. 2010, pp. 1–678.

[65] Chandra Beera et al. “Piezoelectricity and Its Applications”. In: (Sept. 2021).

[66] Navneet Soin, S.C. Anand, and Tahir Shah. “12. Energy harvesting and storage textiles”. In: Dec. 2016. DOI: 10.1016/B978-1-78242-465-9.00012-4.

[67] Rüdiger G. Ballas. “The Piezoelectric Effect – an Indispensable Solid State Effect for Contemporary Actuator and Sensor Technologies”. In: *Journal of Physics: Conference Series* 1775.1 (Jan. 2021), p. 012012. DOI: 10.1088/1742-6596/1775/1/012012. URL: https://dx.doi.org/10.1088/1742-6596/1775/1/012012.

[68] Ouassim Hamdi, Frej Mighri, and Denis Rodrigue. “Piezoelectric polymer films: synthesis, applications, and modeling”. In: Jan. 2020, pp. 79–101. DOI: 10.1016/b978-0-08-103013-4.00005-4.

[69] Khaled S Ramadan, D Sameoto, and S Evoy. "A review of piezoelectric polymers as functional materials for electromechanical transducers". In: *Smart Materials and Structures* 23.3 (Jan. 2014), p. 033001. DOI: 10.1088/0964-1726/23/3/033001. URL: https://doi.org/10.1088/0964-1726/23/3/033001.

[70] A. Mayeen and N. Kalarikkal. "2 - Development of ceramic-controlled piezoelectric devices for biomedical applications". In: *Fundamental Biomaterials: Ceramics*. Woodhead Publishing Series in Biomaterials. Woodhead Publishing, 2018, pp. 47–62. ISBN: 978-0-08-102203-0. DOI: https://doi.org/10.1016/B978-0-08-102203-0.00002-0. URL: https://www.sciencedirect.com/science/article/pii/B9780081022030000020.

[71] Abdul Aabid et al. "A Systematic Review of Piezoelectric Materials and Energy Harvesters for Industrial Applications". In: *Sensors (Basel, Switzerland)* 21 (2021), p. 4145. ISSN: 1424-8220. DOI: 10.3390/s21124145. URL: https://www.ncbi.nlm.nih.gov/pmc/articles/PMC8234936/ (visited on 07/08/2022).

[72] Ioan Ivan et al. "Comparative material study between PZT ceramic and newer crystalline PMN-PT and PZN-PT materials for composite bimorph actuators". In: *Reviews on Advanced Materials Science* 24.15-16 (Dec. 2010), pp. 1–9.

[73] Nurettin Sezer and Muammer Koç. "A comprehensive review on the state-of-the-art of piezoelectric energy harvesting". In: *Nano Energy* 80 (Feb. 2021), p. 105567. ISSN: 2211-2855. DOI: 10.1016/j.nanoen.2020.105567. URL: https://www.sciencedirect.com/science/article/pii/S2211285520311411 (visited on 07/08/2022).

[74] IEEE. "Standard on Piezoelectricity". In: *ANSI/IEEE Std 176-1987* (1988). DOI: 10.1109/IEEESTD.1988.79638.

[75] S. O. Reza Moheimani and Andrew J. Fleming. *Piezoelectric Transducers for Vibration Control and Damping*. Google-Books-ID: ZR9KAAAAQBAJ. Springer Science & Business Media, June 2006. ISBN: 978-1-84628-332-1.

[76] Gustavo Martins, Paulo Nunes, and Julio Cordioli. "On the optimization of a piezoelectric speaker for hearing aid application through multi-physical FE models". In: Sept. 2014. ISBN: 978-1-138-02725-1. DOI: 10.1201/b17488-57.

[77] Chris Howells. "Piezoelectric energy harvesting". In: *Energy Conversion and Management - ENERG CONV MANAGE* 50 (July 2009), pp. 1847–1850. DOI: 10.1016/j.enconman.2009.02.020.

[78] Xinlin Qing et al. "Piezoelectric Transducer-Based Structural Health Monitoring for Aircraft Applications". In: *Sensors* 19.3 (2019). ISSN: 1424-8220. DOI: 10.3390/s19030545. URL: https://www.mdpi.com/1424-8220/19/3/545.

[79] Raymond M. Measures. "Smart composite structures with embedded sensors". In: *Composites Engineering* 2.5 (1992), pp. 597–618. ISSN: 0961-9526. DOI: https://doi.org/10.1016/0961-9526(92)90045-8. URL: https://www.sciencedirect.com/science/article/pii/0961952692900458.

[80] S. M. Yang and J. W. Chiu. "Smart structures — vibration of composites with piezoelectric materials". In: *Composite Structures* 25.1 (1993), pp. 381–386. ISSN: 0263-8223. DOI: https://doi.org/10.1016/0263-8223(93)90185-S. URL: https://www.sciencedirect.com/science/article/pii/026382239390185S.

[81] R. Janeliukstis and D. Mironovs. "Smart Composite Structures with Embedded Sensors for Load and Damage Monitoring – A Review". en. In: *Mechanics of Composite Materials* 57.2 (May 2021), pp. 131–152. ISSN: 1573-8922. DOI: 10.1007/s11029-021-09941-6. URL: https://doi.org/10.1007/s11029-021-09941-6 (visited on 07/12/2022).

[82] Luke Nelson. "Smart piezoelectric Fibre composites". In: *Materials Science and Technology* 18 (Nov. 2002), pp. 1245–1256. DOI: 10.1179/026708302225007448.

[83] Henry Sodano, Gyuhae Park, and Daniel Inman. "An investigation into the performance of macro-fiber composites for sensing and structural vibration applications". In: *Mechanical Systems and Signal Processing* 18 (May 2004), pp. 683–697. DOI: 10.1016/S0888-3270(03)00081-5.

[84] Krzysztof Dragan. "STRUCTURAL HEALTH MONITORING OF COMPOSITE STRUCTURES WITH USE OF EMBEDDED PZT PIEZOELECTRIC SENSORS". In: (June 2014).

[85] Tianyi Feng, Dimitrios Bekas, and M. H. Ferri Aliabadi. "Active Health Monitoring of Thick Composite Structures by Embedded and Surface-Mounted Piezo Diagnostic Layer". In: *Sensors* 20.12 (2020). ISSN: 1424-8220. DOI: 10.3390/s20123410. URL: https://www.mdpi.com/1424-8220/20/12/3410.

[86] Nina Kergosien et al. "Lead Zirconate Titanate Transducers Embedded in Composite Laminates: The Influence of the Integration Method on Ultrasound Transduction". In: *Materials* 16.8 (2023). ISSN: 1996-1944. DOI: 10.3390/ma16083057. URL: https://www.mdpi.com/1996-1944/16/8/3057.

[87] CA Paget, Klas Levin, and Christophe Delebarre. "Actuation performance of embedded piezoceramic transducer in mechanically loaded composites". In: *Smart Materials and Structures* 11 (Oct. 2002), p. 886. DOI: 10.1088/0964-1726/11/6/309.

[88] H. A. Mobaraki, P. S. Valvo R.-A. Jafari-Talookolaei, and R. Haghani. "Dynamic analysis of a laminated composite plate coupled with a piezoelectric energy harvester and traversed by a moving vehicle". In: *Mechanics of Advanced Materials and Structures* 29.27 (2022), pp. 6835–6853. DOI: 10.1080/15376494.2021.1986182. eprint: https://doi.org/10.1080/15376494.2021.1986182. URL: https://doi.org/10.1080/15376494.2021.1986182.

[89] Luca Lampani and Paolo Gaudenzi. "Innovative composite material component with embedded self-powered wireless sensor device for structural monitoring". In: *Composite Structures* 202 (2018). Special issue dedicated to Ian Marshall, pp. 136–141. ISSN: 0263-8223. DOI: https://doi.org/10.1016/j.compstruct.2018.01.011. URL: https://www.sciencedirect.com/science/article/pii/S0263822317343799.

[90] Russell T. Fairles and Robert A. Glowasky. "Analytical and experimental studies of smart materials and structures incorporating embedded piezoelectric actuators and fiber optic sensors". In: *Smart Structures and Materials 1994: Smart Structures and Intelligent Systems*. Ed. by Nesbitt W. Hagood. Vol. 2190. Society of Photo-Optical Instrumentation Engineers (SPIE) Conference Series. May 1994, pp. 165–170. DOI: 10.1117/12.175179.

[91] Mahoor Mehdikhani et al. "Voids in fiber-reinforced polymer composites: A review on their formation, characteristics, and effects on mechanical performance". In: *Journal of*

*Composite Materials* 53.12 (2019), pp. 1579–1669. DOI: 10.1177/0021998318772152. eprint: https://doi.org/10.1177/0021998318772152. URL: https://doi.org/10.1177/0021998318772152.

[92] Alain Bourmaud et al. "Towards the design of high-performance plant fibre composites". In: *Progress in Materials Science* 97 (2018), pp. 347–408.

[93] Thomas R Shrout and Shujun J Zhang. "Lead-free piezoelectric ceramics: Alternatives for PZT?" In: *Journal of Electroceramics* 19 (2007), pp. 113–126.

[94] MSH Al-Furjan et al. "A review on fabrication techniques and tensile properties of glass, carbon, and Kevlar fiber reinforced rolymer composites". In: *Journal of Materials Research and Technology* 19 (2022), pp. 2930–2959.

[95] SM Sapuan et al. "Materials selection for natural fiber reinforced polymer composites using analytical hierarchy process". In: (2011).

[96] Jyoti Agarwal et al. "Progress of novel techniques for lightweight automobile applications through innovative eco-friendly composite materials: a review". In: *Journal of thermoplastic composite materials* 33.7 (2020), pp. 978–1013.

[97] Muhammad Rizal Muhammad Asyraf et al. "Product development of natural fibre-composites for various applications: Design for sustainability". In: *Polymers* 14.5 (2022), p. 920.

[98] Canan Dagdeviren et al. "Recent progress in flexible and stretchable piezoelectric devices for mechanical energy harvesting, sensing and actuation". In: *Extreme mechanics letters* 9 (2016), pp. 269–281.

[99] LoriAnne Groo, Daniel J Inman, and Henry A Sodano. "Dehydrofluorinated PVDF for structural health monitoring in fiber reinforced composites". In: *Composites science and technology* 214 (2021), p. 108982.

[100] Anjana Jain et al. "Impact and acoustic emission performance of polyvinylidene fluoride sensor embedded in glass fiber-reinforced polymer composite structure". In: *Polymers and Polymer Composites* 29.5 (2021), pp. 354–361.

[101] J Andersons and Roberts Joffe. "Estimation of the tensile strength of an oriented flax fiber-reinforced polymer composite". In: *Composites Part A: Applied Science and Manufacturing* 42.9 (2011), pp. 1229–1235.

[102] Md Zillur Rahman. "Mechanical and damping performances of flax fibre composites–A review". In: *Composites Part C: Open Access* 4 (2021), p. 100081.

[103] Guillem Seychal et al. "Towards in-situ acoustic emission-based health monitoring in bio-based composites structures: Does embedment of sensors affect the mechanical behaviour of flax/epoxy laminates?" In: *Composites Part B: Engineering* 236 (2022), p. 109787. ISSN: 1359-8368. DOI: https://doi.org/10.1016/j.compositesb.2022.109787. URL: https://www.sciencedirect.com/science/article/pii/S1359836822001718.

[104] Jyoti K. Sinha Israr Ullah and Andrew Pinkerton. "Vibration-Based Delamination Detection in a Composite Plate". In: *Mechanics of Advanced Materials and Structures* 20.7 (2013), pp. 536–551. DOI: 10.1080/15376494.2011.643275. eprint: https://doi.org/10.1080/15376494.2011.643275. URL: https://doi.org/10.1080/15376494.2011.643275.

[105] Sami Allagui et al. "In-situ health monitoring of thermoplastic bio-composites using acoustic emission". In: *Journal of Thermoplastic Composite Materials* 0.0 (0), p. 08927057231154548. DOI: 10.1177/08927057231154548. eprint: https://doi.org/10.1177/08927057231154548. URL: https://doi.org/10.1177/08927057231154548.

[106] Fengjia Zhang et al. "Embedded Pt-PVDF sensor without compromising mechanical properties of GFRP for on-line sensing". In: *Thin-Walled Structures* 187 (2023), p. 110702. ISSN: 0263-8231. DOI: https://doi.org/10.1016/j.tws.2023.110702. URL: https://www.sciencedirect.com/science/article/pii/S0263823123001805.

[107] I Kim, HT Hahn, and D Weems. "Impact monitoring in smart composite structures using piezoelectric sensors". In: *Proceedigs of the Sixth Japan-US Conference on Composite Materials*. CRC Press. 2022, pp. 201–209.

[108] Natalie Rauter and Rolf Lammering. "Impact Damage Detection in Composite Structures Considering Nonlinear Lamb Wave Propagation". In: *Mechanics of Advanced Materials and Structures* 22.1-2 (2015), pp. 44–51. DOI: 10.1080/15376494.2014.907950. eprint:

https://doi.org/10.1080/15376494.2014.907950. URL: https://doi.org/10.1080/15376494.2014.907950.

[109] Andreas Hornig et al. "Embedded sensing and actuating in CFRP composite structures - Concept and technology demonstration for tailored embeddable sensor-actuator layers (TEmSAL)". In: *Smart Materials and Structures* (June 2022). DOI: 10.1088/1361-665X/ac7d23.

[110] Asan Muthalif and Azni Nabela Wahid. "Optimal piezoelectric shunt dampers for non-deterministic substructure vibration control: estimation and parametric investigation". In: *Scientific Reports* 11 (Feb. 2021), p. 4642. DOI: 10.1038/s41598-021-84097-w.

[111] Alaa Morad et al. "Application of Piezoelectric Materials for Aircraft Propeller Blades Vibration Damping". In: *International Journal of Scientific and Engineering Research* 6 (Aug. 2015), pp. 513–520.

[112] L. Lampani et al. "Analysis of damage in composite laminates with embedded piezoelectric patches subjected to bending action". In: *Composite Structures* 202 (2018). Special issue dedicated to Ian Marshall, pp. 935–942. ISSN: 0263-8223. DOI: https://doi.org/10.1016/j.compstruct.2018.04.073. URL: https://www.sciencedirect.com/science/article/pii/S0263822317343805.

[113] Federica Daghia. "Active fibre-reinforced composites with embedded shape memory alloys". PhD thesis. Alma Mater Studiorum Università di Bologna, 2008. DOI: 10.6092/unibo/amsdottorato/962.

[114] Andrea Benedetti et al. "Influence of temperature on the curing of an epoxy adhesive and its influence on bond behaviour of NSM-CFRP systems". In: *Composites Part B: Engineering* 89 (Dec. 2015). DOI: 10.1016/j.compositesb.2015.11.034.

[115] Russell T. Fairles and Robert A. Glowasky. "Analytical and experimental studies of smart materials and structures incorporating embedded piezoelectric actuators and fiber optic sensors". In: *Smart Structures and Materials 1994: Smart Structures and Intelligent Systems*. Ed. by Nesbitt W. Hagood. Vol. 2190. Society of Photo-Optical Instrumentation Engineers (SPIE) Conference Series. May 1994, pp. 165–170. DOI: 10.1117/12.175179.

[116] Aarief Syed Khaja et al. “Optimized thin-film diffusion soldering for power-electronics production”. In: *Proceedings of the International Spring Seminar on Electronics Technology* (May 2013), pp. 11–16. DOI: 10.1109/ISSE.2013.6648206.

[117] Tommaso Delpero. “Design of adaptive structures with piezoelectric materials”. PhD thesis. ETH Zurich, 2014.

[118] Mehrdad Ghasemi Nejhad, Richard Russ, and Saeid Pourjalali. “Manufacturing and Testing of Active Composite Panels with Embedded Piezoelectric Sensors and Actuators”. In: *Journal of Intelligent Material Systems and Structures - J INTEL MAT SYST STRUCT* 16 (Apr. 2005), pp. 319–333. DOI: 10.1177/1045389X05050103.

[119] Gary Jones et al. “Characterization, performance and optimization of PVDF as a piezoelectric film for advanced space mirror concepts”. In: (Jan. 2005). DOI: 10.2172/876343.

[120] Measurement Specialties. *Piezo Film Sensors Technical Manual*. English. 950 Forge Avenue Norristown, PA 19403: Measurement Specialties, Inc, 1999.

[121] D Swift. “Elastic moduli of fibrous composite containing misaligned fibers”. In: *Journal of Physics D: Applied Physics* 8 (Jan. 2001), p. 223. DOI: 10.1088/0022-3727/8/3/006.

[122] Fabrizia Ghezzo, Anthony Starr, and D. Smith. “Integration of Networks of Sensors and Electronics for Structural Health Monitoring of Composite Materials”. In: *Advances in Civil Engineering* 2010 (Jan. 2010). DOI: 10.1155/2010/598458.

[123] Ji-Hun Bae, Sung-Woo Lee, and Seung-Hwan Chang. “Characterization of low-velocity impact-induced damages in carbon/epoxy composite laminates using a poly(vinylidene fluoride–trifluoroethylene) film sensor”. In: *Composites Part B: Engineering* 135 (2018), pp. 189–200. ISSN: 1359-8368. DOI: https://doi.org/10.1016/j.compositesb.2017.10.008. URL: https://www.sciencedirect.com/science/article/pii/S1359836817326732.

[124] Hari P Konka, M A Wahab, and K Lian. “The effects of embedded piezoelectric fiber composite sensors on the structural integrity of glass-fiber–epoxy composite laminate”. In: *Smart Materials and Structures* 21.1 (Dec. 2011), p. 015016. DOI: 10.1088/0964-1726/21/1/015016. URL: https://dx.doi.org/10.1088/0964-1726/21/1/015016.

[125] Xiaoming Chen et al. “In-situ damage self-monitoring of fiber-reinforced composite by integrating self-powered ZnO nanowires decorated carbon fabric”. In: *Composites Part B: Engineering* 248 (2023), p. 110368. ISSN: 1359-8368. DOI: https://doi.org/10.1016/j.compositesb.2022.110368. URL: https://www.sciencedirect.com/science/article/pii/S1359836822007417.

[126] Rogers K. Langat et al. “Integration Technology with Thin Films Co-Fabricated in Laminated Composite Structures for Defect Detection and Damage Monitoring”. In: *Micromachines* 15.2 (2024). ISSN: 2072-666X. DOI: 10.3390/mi15020274. URL: https://www.mdpi.com/2072-666X/15/2/274.

[127] MS Irfan et al. “Monitoring the thermomechanical response of aerospace composites under dynamic loading via embedded rGO coated fabric sensors”. In: *Sensors and Actuators A: Physical* 361 (2023), p. 114595.

[128] Domenico Tommasino et al. “Vibration Energy Harvesting by Means of Piezoelectric Patches: Application to Aircrafts”. In: *Sensors* 22.1 (2022). ISSN: 1424-8220. DOI: 10.3390/s22010363. URL: https://www.mdpi.com/1424-8220/22/1/363.

[129] Heung Soo Kim, Joo-Hyong Kim, and Jaehwan Kim. “A Review of Piezoelectric Energy Harvesting Based on Vibration”. In: *International Journal of Precision Engineering and Manufacturing* 12 (Dec. 2011). DOI: 10.1007/s12541-011-0151-3.

[130] “Introduction to Piezoelectric Energy Harvesting”. In: *Piezoelectric Energy Harvesting*. John Wiley & Sons, Ltd, 2011. Chap. 1, pp. 1–18. ISBN: 9781119991151. DOI: https://doi.org/10.1002/9781119991151.ch1. eprint: https://onlinelibrary.wiley.com/doi/pdf/10.1002/9781119991151.ch1. URL: https://onlinelibrary.wiley.com/doi/abs/10.1002/9781119991151.ch1.

[131] Saša Zelenika et al. “Energy Harvesting Technologies for Structural Health Monitoring of Airplane Components—A Review”. In: *Sensors* 20.22 (2020). ISSN: 1424-8220. DOI: 10.3390/s20226685. URL: https://www.mdpi.com/1424-8220/20/22/6685.

[132] Miroslav Mrlík et al. “Figure of merit comparison of PP-based electret and PVDF-based piezoelectric polymer energy harvesters”. In: *Active and Passive Smart Structures and Integrated Systems 2016*. Vol. 9799. SPIE. 2016, pp. 580–587.

[133] Huidong Li, Chuan Tian, and Z. Daniel Deng. "Energy harvesting from low frequency applications using piezoelectric materials". In: *Applied Physics Reviews* 1.4 (Nov. 2014), p. 041301. ISSN: 1931-9401. DOI: 10.1063/1.4900845. eprint: https://pubs.aip.org/aip/apr/article-pdf/doi/10.1063/1.4900845/14572896/041301_1_online.pdf. URL: https://doi.org/10.1063/1.4900845.

[134] Rrahim Maksuti. "Applications of smart materials in mechatronics technology". In: *JAS-SUT Journal of Applied Sciences-SUT* 5.9-10 (2019), pp. 9–13.

[135] Khalil Abdelrahman et al. "Output Estimation and Failure Detection in Piezoelectric Actuators using Transmissibility Operators". In: *Letters in Dynamic Systems and Control* 3.1 (2023), p. 011007.

[136] Pengcheng Jiao et al. "Piezoelectric Sensing Techniques in Structural Health Monitoring: A State-of-the-Art Review". In: *Sensors* 20.13 (2020). ISSN: 1424-8220. DOI: 10.3390/s20133730. URL: https://www.mdpi.com/1424-8220/20/13/3730.

[137] Jeong-Beom Ihn and Fu-Kuo Chang. "Pitch-catch Active Sensing Methods in Structural Health Monitoring for Aircraft Structures". In: *Structural Health Monitoring* 7.1 (2008), pp. 5–19. DOI: 10.1177/1475921707081979.

[138] Corentin Tuloup et al. "Structural health monitoring of polymer-matrix composite using embedded piezoelectric ceramic transducers during several four-points bending tests". In: *Smart Materials and Structures* 29.12 (2020), p. 125011. DOI: 10.1088/1361-665X/abbc59.

[139] Ehsan Ghafari and Na Lu. "Self-polarized electrospun polyvinylidene fluoride (PVDF) nanofiber for sensing applications". In: *Composites Part B: Engineering* 160 (2019), pp. 1–9. ISSN: 1359-8368. DOI: 10.1016/j.compositesb.2018.10.011. URL: https://www.sciencedirect.com/science/article/pii/S1359836818330555.

[140] Connor Griffin and Victor Giurgiutiu. "Piezoelectric Wafer Active Sensor Transducers for Acoustic Emission Applications". In: *Sensors* 23.16 (2023). ISSN: 1424-8220. DOI: 10.3390/s23167103. URL: https://www.mdpi.com/1424-8220/23/16/7103.

[141] Action Nechibvute, Albert Chawanda, and Pearson Luhanga. “Finite element modeling of a piezoelectric composite beam and comparative performance study of piezoelectric materials for voltage generation”. In: *International Scholarly Research Notices* 2012 (2012), pp. 1–11. DOI: 10.5402/2012/921361.

[142] Malik Yahiaoui et al. “Acoustic emission characterization of transgranular cracks in WC–Co cemented carbides During a one-way scratch”. In: *Tribology Letters* 69 (2021), pp. 1–8. DOI: 10.1007/s11249-021-01509-8.

[143] Rahul Soni et al. “A critical review of recent advances in the aerospace materials”. In: *Materials Today: Proceedings* (2023). ISSN: 2214-7853. DOI: https://doi.org/10.1016/j.matpr.2023.08.108. URL: https://www.sciencedirect.com/science/article/pii/S2214785323043663.

[144] Monalisa Das, Sasmita Sahu, and D.R. Parhi. “Composite materials and their damage detection using AI techniques for aerospace application: A brief review”. In: *Materials Today: Proceedings* 44 (2021). International Conference on Materials, Processing & Characterization, pp. 955–960. ISSN: 2214-7853. DOI: https://doi.org/10.1016/j.matpr.2020.11.005. URL: https://www.sciencedirect.com/science/article/pii/S2214785320385771.

[145] M. Kharrat et al. “A signal processing approach for enhanced Acoustic Emission data analysis in high activity systems: Application to organic matrix composites”. In: *Mechanical Systems and Signal Processing* 70-71 (2016), pp. 1038–1055. ISSN: 0888-3270. DOI: https://doi.org/10.1016/j.ymssp.2015.08.028. URL: https://www.sciencedirect.com/science/article/pii/S0888327015003908.

[146] Arman Malekloo et al. “Machine learning and structural health monitoring overview with emerging technology and high-dimensional data source highlights”. In: *Structural Health Monitoring* 21.4 (2022), pp. 1906–1955.

[147] J Matthew Helm et al. “Machine learning and artificial intelligence: definitions, applications, and future directions”. In: *Current reviews in musculoskeletal medicine* 13 (2020), pp. 69–76.

[148] Cheng Qiu and Jinglei Yang. "Machine learning applications in composites: Manufacturing, design, and characterization". In: *Machine Learning in Materials Informatics: Methods and Applications*. ACS Publications, 2022, pp. 65–85.

[149] Igor Kabashkin, Boriss Misnevs, and Olga Zervina. "Artificial Intelligence in Aviation: New Professionals for New Technologies". In: *Applied Sciences* 13.21 (2023). ISSN: 2076-3417. DOI: 10.3390/app132111660. URL: https://www.mdpi.com/2076-3417/13/21/11660.

[150] Muhammad Muzammil Azad, Prashant Kumar, and Heung Soo Kim. "Delamination detection in CFRP laminates using deep transfer learning with limited experimental data". In: *Journal of Materials Research and Technology* 29 (2024), pp. 3024–3035. ISSN: 2238-7854. DOI: https://doi.org/10.1016/j.jmrt.2024.02.067. URL: https://www.sciencedirect.com/science/article/pii/S2238785424003600.

[151] Muhammad Muzammil Azad and Heung Soo Kim. "Hybrid deep convolutional networks for the autonomous damage diagnosis of laminated composite structures". In: *Composite Structures* 329 (2024), p. 117792. ISSN: 0263-8223. DOI: https://doi.org/10.1016/j.compstruct.2023.117792. URL: https://www.sciencedirect.com/science/article/pii/S0263822323011388.

[152] Sungjun Kim et al. "Delamination Detection Framework for the Imbalanced Dataset in Laminated Composite Using Wasserstein Generative Adversarial Network-Based Data Augmentation". In: *Applied Sciences* 13.21 (2023). ISSN: 2076-3417. DOI: 10.3390/app132111837. URL: https://www.mdpi.com/2076-3417/13/21/11837.

[153] Elizabeth Cross et al. "Physics-Informed Machine Learning for Structural Health Monitoring". In: Oct. 2021, pp. 347–367. ISBN: 978-3-030-81715-2. DOI: 10.1007/978-3-030-81716-9_17.

[154] D. Di Lorenzo et al. "Physics informed and data-based augmented learning in structural health diagnosis". In: *Computer Methods in Applied Mechanics and Engineering* 414 (2023), p. 116186. ISSN: 0045-7825. DOI: https://doi.org/10.1016/j.cma.2023.116186. URL: https://www.sciencedirect.com/science/article/pii/S0045782523003109.

[155] Intisar Omar, Muhammad Khan, and Andrew Starr. "Compatibility and challenges in machine learning approach for structural crack assessment". In: *Structural Health Monitoring* 21.5 (2022), pp. 2481–2502.

[156] Sahar Hassani and Ulrike Dackermann. "A Systematic Review of Advanced Sensor Technologies for Non-Destructive Testing and Structural Health Monitoring". In: *Sensors* 23.4 (2023). ISSN: 1424-8220. DOI: 10.3390/s23042204. URL: https://www.mdpi.com/1424-8220/23/4/2204.

[157] Ayoub Keshmiry et al. "Effects of Environmental and Operational Conditions on Structural Health Monitoring and Non-Destructive Testing: A Systematic Review". In: *Buildings* 13.4 (2023). ISSN: 2075-5309. DOI: 10.3390/buildings13040918. URL: https://www.mdpi.com/2075-5309/13/4/918.

[158] Xiangyu Tian et al. "Damage mechanism analysis for carbon fiber reinforced polymer composites with a fastener under lightning strike". In: *Composite Structures* 289 (2022), p. 115465. ISSN: 0263-8223. DOI: https://doi.org/10.1016/j.compstruct.2022.115465. URL: https://www.sciencedirect.com/science/article/pii/S0263822322002586.

[159] Fakhitah Ridzuan and Wan Mohd Nazmee Wan Zainon. "A Review on Data Cleansing Methods for Big Data". In: *Procedia Computer Science* 161 (2019). The Fifth Information Systems International Conference, 23-24 July 2019, Surabaya, Indonesia, pp. 731–738. ISSN: 1877-0509. DOI: https://doi.org/10.1016/j.procs.2019.11.177. URL: https://www.sciencedirect.com/science/article/pii/S1877050919318885.

[160] Qamar Shahbaz Ul Haq. "Chapter 11 - Data Quality". In: *Data Mapping for Data Warehouse Design*. Ed. by Qamar Shahbaz Ul Haq. Boston: Morgan Kaufmann, 2016, pp. 67–82. ISBN: 978-0-12-805185-6. DOI: https://doi.org/10.1016/B978-0-12-805185-6.00011-3. URL: https://www.sciencedirect.com/science/article/pii/B9780128051856000113.

[161] Mélanie Bernhardt et al. "Active label cleaning for improved dataset quality under resource constraints". In: *Nature communications* 13.1 (2022), p. 1161.

[162] Susie Boyce et al. “Evaluation of prediction models for the staging of prostate cancer”. In: *BMC medical informatics and decision making* 13 (Nov. 2013), p. 126. DOI: 10.1186/1472-6947-13-126.

[163] Muhammad Muzammil Azad et al. “Intelligent structural health monitoring of composite structures using machine learning, deep learning, and transfer learning: a review”. In: *Advanced Composite Materials* 33.2 (2024), pp. 162–188.

[164] N.J. Sairamya et al. “Chapter 12 - Hybrid Approach for Classification of Electroencephalographic Signals Using Time–Frequency Images With Wavelets and Texture Features”. In: *Intelligent Data Analysis for Biomedical Applications*. Ed. by D. Jude Hemanth, Deepak Gupta, and Valentina Emilia Balas. Intelligent Data-Centric Systems. Academic Press, 2019, pp. 253–273. ISBN: 978-0-12-815553-0. DOI: https://doi.org/10.1016/B978-0-12-815553-0.00013-6. URL: https://www.sciencedirect.com/science/article/pii/B9780128155530000136.

[165] Yunlai Liao et al. “Damage localization for composite structure using guided wave signals with Gramian angular field image coding and convolutional neural networks”. In: *Composite Structures* 312 (2023), p. 116871. ISSN: 0263-8223. DOI: https://doi.org/10.1016/j.compstruct.2023.116871. URL: https://www.sciencedirect.com/science/article/pii/S0263822323002155.

[166] Jianjian Zhu et al. “Impact energy assessment of sandwich composites using an ensemble approach boosted by deep learning and electromechanical impedance”. In: *Smart Materials and Structures* 32.9 (Aug. 2023), p. 095019. DOI: 10.1088/1361-665X/ace868. URL: https://dx.doi.org/10.1088/1361-665X/ace868.

[167] Carlos Eduardo Teixeira et al. “An ultrasound-based water-cut meter for heavy fuel oil”. In: *Measurement* 148 (2019), p. 106907. ISSN: 0263-2241. DOI: https://doi.org/10.1016/j.measurement.2019.106907. URL: https://www.sciencedirect.com/science/article/pii/S026322411930764X.

[168] Ronny Francis Ribeiro Junior and Guilherme Ferreira Gomes. “On the Use of Machine Learning for Damage Assessment in Composite Structures: A Review”. In: *Applied Composite Materials* 31.1 (2024), pp. 1–37.

[169] Corinna Cortes and Vladimir Vapnik. "Support-vector networks". In: *Machine learning* 20 (1995), pp. 273–297. DOI: 10.1007/BF00994018. URL: https://doi.org/10.1007/BF00994018.

[170] Rogério Rodrigues dos Santos, Tulio Gomes de Paula Machado, and Saullo Giovani Pereira Castro. "Support Vector Machine Applied to the Optimal Design of Composite Wing Panels". In: *Aerospace* 8.11 (2021). ISSN: 2226-4310. DOI: 10.3390/aerospace8110328. URL: https://www.mdpi.com/2226-4310/8/11/328.

[171] Tin Kam Ho. "Random decision forests". In: *Proceedings of 3rd international conference on document analysis and recognition*. Vol. 1. IEEE. 1995, pp. 278–282.

[172] James Bergstra and Yoshua Bengio. "Random search for hyper-parameter optimization." In: *Journal of machine learning research* 13.2 (2012).

[173] Ron Kohavi et al. "A study of cross-validation and bootstrap for accuracy estimation and model selection". In: *Ijcai*. Vol. 14. Montreal, Canada. 1995, pp. 1137–1145.

[174] Trevor Hastie et al. *The elements of statistical learning: data mining, inference, and prediction*. Vol. 2. Springer, 2009.

[175] Intisar Shadeed, Jwan Alwan, and Dhafar Abd. "The effect of gamma value on support vector machine performance with different kernels". In: *International Journal of Electrical and Computer Engineering (IJECE)* 10 (Oct. 2020), p. 5497. DOI: 10.11591/ijece.v10i5.pp5497-5506.

RÉPUBLIQUE FRANÇAISE
*Liberté*
*Égalité*
*Fraternité*

Université de Toulouse

**Titre :** Investigation du potentiel de Fonctionnalisation Piézoélectrique de pièces Aéronautiques Composites

**Mots clés :** Piézoélectrique, Composites, Fonctionnalisation, Structures, Capteurs, actionneurs

**Résumé :** Cette thèse porte sur l'intégration de matériaux piézoélectriques dans des structures composites renforcées de fibres longues afin de développer des composites intelligents dotés de fonctionnalités avancées pour des applications aéronautiques et spatiales. La recherche vise à améliorer la surveillance de l'intégrité structurelle (SHM) et les capacités de récupération d'énergie grâce aux propriétés des matériaux piézoélectriques pour la détection, l'actionnement et la récupération d'énergie. L'étude couvre de manière exhaustive la sélection des matériaux, les processus de fabrication, la caractérisation expérimentale de ces composites multifonctionnels et l'exploration de leurs applications potentielles. La motivation provient de la transition de l'industrie aéronautique vers des matériaux composites tels que les polymères renforcés de fibres de carbone (PRFC) pour leurs propriétés mécaniques spécifiques supérieures et leur rentabilité. Malgré ces avantages, les composites sont susceptibles d'être endommagés par des défauts de fabrication et des conditions d'exploitation ou de service, ce qui nécessite des techniques de surveillance innovantes. L'introduction de méthodes de contrôle non destructif (CND) a amélioré la détection des défauts, mais ces techniques ont des limites, ce qui incite à explorer des stratégies SHM. Cette thèse contribue au domaine en développant en validant des structures composites intelligentes incorporant du fluorure de polyvinylidène (PVDF) comme matériau piézoélectrique. La recherche démontre l'intégration réussie du PVDF avec un impact minimal sur l'intégrité mécanique des structures composites. La plage d'utilisation de ces composites intelligents avec des performances thermoélectromécaniques stables, ce qui est crucial pour les applications pratiques en SHM et en récupération d'énergie à également été déterminée. Le potentiel des fibres naturelles dans les structures aérospatiales secondaires est également exploré, en soulignant leurs avantages fonctionnels malgré leurs propriétés mécaniques inférieures à celles des fibres de carbone. Les applications avancées de ces composites intelligents sont étudiées, notamment leurs capacités de récupération d'énergie et leurs performances SHM dans des conditions de charge dynamique. Des analyses empiriques et numériques confirment l'efficacité des capteurs PVDF intégrés dans la détection des anomalies structurelles, offrant ainsi une solution potentielle durable pour les systèmes SHM autonomes. Une étude de cas utilisant des techniques d'apprentissage automatique pour la détection et l'identification des défauts démontre en outre le potentiel de ces composites intelligents dans l'amélioration de la fiabilité et de la performance des systèmes SHM via une approche de détection in situ. Par conséquent, cette thèse établit une base solide pour le développement de composites intelligents avec des capteurs piézoélectriques intégrés, mettant en évidence leur potentiel de transformation pour améliorer la sécurité, l'efficacité et la durabilité des aérostructures modernes. Les résultats ouvrent la voie à de futures recherches sur l'optimisation des dimensions et du positionnement des éléments actifs, l'évaluation de la durabilité à long terme et l'amélioration des systèmes SHM grâce à des réseaux de capteurs distribués et à des capacités de transmission de données sans fil.

**Title:** Investigation of the Piezoelectric Functionalization Potential of Aeronautical Composite Parts

**Key words:** Piezoelectric, Composites, Functionalization, Structures, Sensors, Actuators

**Abstract:** This thesis investigates integrating piezoelectric materials into long fiber-reinforced composite structures to develop smart composites with advanced functionalities for aeronautics and space applications. The research aims to enhance structural health monitoring (SHM) and energy harvesting capabilities through piezoelectric materials' direct and inverse properties for sensing, actuation, and energy recovery. The study comprehensively covers material selection, manufacturing processes, the experimental characterization of these multifunctional composites, and the exploration of their potential applications. The motivation stems from the aviation industry's transition to composite materials like carbon fiber reinforced polymers (CFRP) for their superior mechanical properties and cost effectiveness. Despite these advantages, composites are prone to damage from fabrication flaws and operation/service conditions, necessitating innovative monitoring techniques. Introducing non-destructive testing (NDT) methods have improved defect detection, but these techniques have limitations, prompting exploring SHM strategies. The thesis contributes to the field by developing and validating smart composite structures incorporating polyvinylidene fluoride (PVDF) as the piezoelectric material. The research demonstrates the successful integration of PVDF with minimal impact on the mechanical integrity of the composites. The usage range of these smart composites with stable thermoelectromechanical performance, which is crucial for practical applications in SHM and energy harvesting, was also determined. The potential for natural fibers in secondary aerospace structures is also explored, emphasizing their functional benefits despite their lower mechanical properties compared to carbon fibers. Advanced applications of these smart composites are investigated, including their energy harvesting capabilities and SHM performance under dynamic loading conditions. Empirical and numerical analyses confirm the effectiveness of embedded PVDF sensors in detecting structural anomalies, offering a sustainable potential solution for autonomous SHM systems. A case study employing machine learning techniques for fault detection and identification further demonstrates the potential of smart composites in enhancing the reliability and performance of SHM systems via an in-situ sensing approach. Therefore, this thesis establishes a robust foundation for developing smart composites with embedded piezoelectric sensors, highlighting their transformative potential in improving modern aerostructure safety, efficiency, and sustainability. The findings pave the way for future research into optimizing the dimensions and positioning of active embeds, assessing long-term durability, and advancing SHM systems through distributed sensor networks and wireless data streaming capabilities.